

Second specimen of the Late Cretaceous Australian sauropod dinosaur *Diamantinasaurus matildae* provides new anatomical information on the skull and neck of early titanosaurs

STEPHEN F. POROPAT^{1,2,*}, MARTIN KUNDRÁT³, PHILIP D. MANNION⁴,
PAUL UPCHURCH⁴, TRAVIS R. TISCHLER² and DAVID A. ELLIOTT²

¹Faculty of Science, Engineering and Technology, Swinburne University of Technology, John Street, Hawthorn, VIC 3122, Australia

²Australian Age of Dinosaurs Museum of Natural History, The Jump-Up, Winton, QLD 4735, Australia

³Center for Interdisciplinary Biosciences, Technology and Innovation Park, University of Pavol Jozef Šafárik, Košice 04154, Slovakia

⁴Department of Earth Sciences, University College London, Gower Street, London WC1E 6BT, UK

Received 13 September 2020; revised 30 October 2020; accepted for publication 10 November 2020

The titanosaurian sauropod dinosaur *Diamantinasaurus matildae* is represented by two individuals from the Cenomanian–lower Turonian ‘upper’ Winton Formation of central Queensland, north-eastern Australia. The type specimen has been described in detail, whereas the referred specimen, which includes several elements not present in the type series (partial skull, atlas, axis and postaxial cervical vertebrae), has only been described briefly. Herein, we provide a comprehensive description of this referred specimen, including a thorough assessment of the external and internal anatomy of the braincase, and identify several new autapomorphies of *D. matildae*. Via an expanded data matrix consisting of 125 taxa scored for 552 characters, we recover a close, well-supported relationship between *Diamantinasaurus* and its contemporary, *Savannasaurus elliottorum*. Unlike previous iterations of this data matrix, under a parsimony framework we consistently recover *Diamantinasaurus* and *Savannasaurus* as early-diverging members of Titanosauria using both equal weighting and extended implied weighting, with the overall topology largely consistent between analyses. We erect a new clade, named Diamantinasauria herein, that also includes the contemporaneous *Sarmientosaurus musacchioi* from southern Argentina, which shares several cranial features with the referred *Diamantinasaurus* specimen. Thus, Diamantinasauria is represented in the mid-Cretaceous of both South America and Australia, supporting the hypothesis that some titanosaurians, in addition to megaraptoran theropods and possibly some ornithopods, were able to disperse between these two continents via Antarctica. Conversely, there is no evidence for rebbachisaurids in Australia, which might indicate that they were unable to expand into high latitudes before their extinction in the Cenomanian–Turonian. Likewise, there is no evidence for titanosaurs with procoelous caudal vertebrae in the mid-Cretaceous Australian record, despite scarce but compelling evidence for their presence in both Antarctica and New Zealand during the Campanian–Maastrichtian. These later titanosaurs presumably dispersed into these landmasses from South America before the Campanian (~85 Mya), when seafloor spreading between Zealandia and Australia commenced. Although Australian mid-Cretaceous dinosaur faunas appear to be cosmopolitan at higher taxonomic levels, closer affinities with South America at finer scales are becoming better supported for sauropods, theropods and ornithopods.

ADDITIONAL KEYWORDS: Australia – Cretaceous – Dinosauria – Gondwana – Mesozoic – palaeobiogeography – palaeontology – parsimony analysis – phylogenetic systematics – Sauropodomorpha.

*Corresponding author. E-mail: stephenporopat@gmail.com

INTRODUCTION

Sauropod dinosaur skulls are relatively rare in the fossil record, especially those of titanosaurs (Poropat & Kear, 2013; Wilson et al., 2016). Only seven titanosaur species are known from reasonably complete cranial material: (1) *Tapuiasaurus macedoi* Zaher et al., 2011] from the Aptian of Brazil (Wilson et al., 2016); (2) *Malawisaurus dixeyi* (Haughton, 1928) from the Aptian of Malawi (Jacobs et al., 1993; Gomani, 2005; Andrzejewski et al., 2019); (3) *Sarmientosaurus musacchioi* Martínez et al., 2016 from the Cenomanian–Turonian of Argentina (Martínez et al., 2016); (4) *Antarctosaurus wichmannianus* Huene, 1929 from the Campanian of Argentina (Huene, 1929; Powell, 2003; Paulina Carabajal, 2012); (5) *Quaesitosaurus orientalis* Kurzanov & Bannikov, 1983 from the Campanian–Maastrichtian of Mongolia (Wilson, 2005); (6) *Nemegtosaurus mongoliensis* Nowiński, 1971 from the Maastrichtian of Mongolia (Wilson, 2005); and (7) *Rapetosaurus krausei* Curry Rogers & Forster, 2001 from the Maastrichtian of Madagascar. In addition, virtually complete skulls pertaining to embryonic titanosaurs have been discovered at the Campanian Auca Mahuevo site in Neuquén Province, Argentina (Chiappe et al., 2001; Salgado et al., 2005; García, 2007a, b; García & Cerda, 2010; García et al., 2010), and in probably contemporaneous deposits nearby (Kundrát et al., 2020). Although several other titanosaurian taxa are represented by cranial remains, these are often fragmentary (see Díez Díaz et al., 2011: table 1; Poropat & Kear, 2013: table S1). Nevertheless, several titanosaur braincases have been described, with exemplars known from every continent except Antarctica (Table 1). Unfortunately, the temporal coverage of the record is patchy: most titanosaur braincases date to the Santonian–Maastrichtian (86.3–66.0 Mya), with only seven known from stratigraphically older deposits, spanning the Aptian–Coniacian (~125–86.3 Mya). Sauropod skulls are highly informative from a phylogenetic standpoint, as demonstrated by the impact of the discovery of *Rapetosaurus* Curry Rogers & Forster, 2001 on our understanding of sauropod evolutionary relationships. Therefore, the discovery and description of new specimens has great potential to shed further light on our understanding of titanosaur evolution.

To date, only one sauropod skull has been reported from Australia: AODF 836, from the Upper Cretaceous (Cenomanian–lower Turonian) ‘upper’ Winton Formation of Queensland. This specimen was attributed to the titanosaur *Diamantinasaurus matildae* Hocknull et al., 2009 (Poropat et al., 2015b) on the basis of features observed in the associated postcranial remains (Poropat et al., 2016), but at the time of its announcement, it was only described

briefly. Moreover, the only cranial elements specifically reported were the left squamosal, braincase and right surangular (Poropat et al., 2016). Other skull elements were known to be preserved (and were alluded to by Poropat et al., 2016), but determining their identity proved difficult. It was not until 2019 that the quadrates and parietals of AODF 836 were identified with confidence.

Although it has never been described in full, AODF 836 has been included in several iterations of the Mannion et al. (2013) phylogenetic data matrix, in which it has been treated as a separate operational taxonomic unit from the type specimen (AODF 603) of *D. matildae* (Poropat et al., 2016). In almost all of these analyses, AODF 836 and the type specimen of *Diamantinasaurus* Hocknull et al., 2009 were resolved as sister taxa, with *Savannasaurus elliottorum* Poropat et al., 2016 (AODF 660, also from the Winton Formation; Poropat et al., 2020a) as the sister taxon to that clade. However, the position of this Australian clade within Somphospondyli has varied between analyses. In some, it occupies an early-branching position within Titanosauria (Poropat et al., 2016). In others, it occupies a position within Somphospondyli but outside Lithostrotia (Mannion et al., 2017; Royo-Torres et al., 2017; Averianov & Efimov, 2018; Mocho et al., 2019; Moore et al., 2020); the uncertain phylogenetic position of the clade specifier *Andesaurus* Calvo & Bonaparte, 1991 in each of these analyses makes it difficult to label the node Titanosauria consistently. Most recently, Mannion et al. (2019a, b) resolved the Australian clade within Saltasauridae under an equal weights analysis. In an extended implied weight analysis [with concavity (k)-value = 9], Mannion et al. (2019a) found the clade to be highly nested within an inclusive Titanosauria; but with k -value = 3, the clade was not resolved [*Diamantinasaurus* + AODF 836 clustered with *Isisaurus* Wilson & Upchurch, 2003 + Saltasauridae, whereas *Savannasaurus* Poropat et al., 2016 occupied a position outside Lithostrotia (Mannion et al., 2019a)]. Likewise, Mannion et al. (2019b) did not resolve the clade in their extended implied weights analysis, with *Savannasaurus* instead placed as sister taxon to a polytomy comprising *Diamantinasaurus*, AODF 836 and *Baotianmansaurus* Zhang et al., 2009 + *Dongyangosaurus* Lü et al., 2008.

In this study, we provide a complete description of AODF 836. In so doing, we fortify the case for its referral to *D. matildae*. AODF 836 greatly enhances our understanding of the anatomy of *Diamantinasaurus* and sheds light on the cranial and cervical vertebral morphology of early titanosaurs in general. By incorporating new observations of AODF 836 in a revised phylogenetic analysis, we provide increased support for the placement of *Diamantinasaurus* and *Savannasaurus* as members of a new clade of early-diverging titanosaurs.

Table 1. List of titanosauriform braincases (not including isolated frontals or parietals)

Designation	Specimen number	Formation	Stage	Country	Classification	Reference(s)
<i>Jainosaurus septentrionalis</i>	GSI K27/497	Lameta	Maastrichtian	India	Titanosauria	Huene & Matley (1933); Wilson <i>et al.</i> (2009)
<i>Jainosaurus septentrionalis</i>	ISI R162	Lameta	Maastrichtian	India	Titanosauria	Chatterjee & Rudra (1996); Wilson <i>et al.</i> (2009)
<i>Isisaurus colberti</i>	ISI R199	Lameta	Maastrichtian	India	Titanosauria	Berman & Jain (1982); Chatterjee & Rudra (1996); Wilson <i>et al.</i> (2009)
<i>Isisaurus colberti</i>	ISI R467	Lameta	Maastrichtian	India	Titanosauria	Chatterjee & Rudra (1996); Wilson <i>et al.</i> (2009)
<i>Isisaurus colberti</i>	GSP-UM 7000	Pab	Maastrichtian	Pakistan	Titanosauria	Wilson <i>et al.</i> (2005, 2009)
<i>Rapetosaurus krausei</i>	FMNH PR 2184	Maevvarano	Maastrichtian	Madagascar	Titanosauria	Curry Rogers & Forster (2004)
<i>Rapetosaurus krausei</i>	FMNH PR 2192	Maevvarano	Maastrichtian	Madagascar	Titanosauria	Curry Rogers & Forster (2004)
<i>Rapetosaurus krausei</i>	FMNH PR 2197	Maevvarano	Maastrichtian	Madagascar	Titanosauria	Curry Rogers & Forster (2004)
<i>Rapetosaurus krausei</i>	UA 8698	Maevvarano	Maastrichtian	Madagascar	Titanosauria	Curry Rogers & Forster (2004)
<i>Vahiny depereti</i>	UA 9940	Maevvarano	Maastrichtian	Madagascar	Titanosauria	Curry Rogers & Wilson (2014)
<i>Vahiny depereti</i>	FMNH PR 3046	Maevvarano	Maastrichtian	Madagascar	Titanosauria	Curry Rogers & Wilson (2014)
? <i>Magyarosaurus dacus</i>	FGGUB 1007	Sinpetru	Maastrichtian	Romania	Titanosauria	Weishampel <i>et al.</i> (1991)
<i>Nemegtosaurus mongoliensis</i>	Z. PAL_MgD-J/9	Nemegt	Maastrichtian	Mongolia	Titanosauria	Nowinski (1971); Upchurch (1999); Wilson (2005)
<i>Ampelosaurus atacis</i>	MDE-C3-761	Marnes Rouges Inférieures	Maastrichtian	France	Titanosauria	Le Loeuff (2005)
<i>Saltasaurus loricatus</i>	PVL 4017/161	Lecho	Campanian–Maastrichtian	Argentina	Titanosauria	Powell (1986, 1992, 2003); S.F.P., P.D.M. & P.U., pers. obs., 2013
<i>Saltasaurus loricatus</i>	PVL 4017/162	Lecho	Campanian–Maastrichtian	Argentina	Titanosauria	Powell (1986, 1992, 2003); S.F.P., P.D.M. & P.U., pers. obs., 2013
<i>Bonatitan reigi</i>	MACN-PV RN 821	Allen	Campanian–Maastrichtian	Argentina	Titanosauria	Martinelli & Forasiepi (2004); Paulina Carabajal (2012); Salgado <i>et al.</i> (2015a); S.F.P., P.D.M. & P.U., pers. obs., 2013
<i>Bonatitan reigi</i>	MACN-PV RN 1061	Allen	Campanian–Maastrichtian	Argentina	Titanosauria	Martinelli & Forasiepi (2004); Paulina Carabajal (2012); Salgado <i>et al.</i> (2015a); S.F.P., P.D.M. & P.U., pers. obs., 2013
Titanosauria indet.	MGPIFD-GR 118	Allen	Campanian–Maastrichtian	Argentina	Titanosauria	Paulina Carabajal & Salgado (2007); Paulina Carabajal (2012)
Titanosauria indet.	MMI-194	Allen	Campanian–Maastrichtian	Argentina	Titanosauria	García <i>et al.</i> (2008)
Titanosauria indet.	MPCA-PV 80	Allen	Campanian–Maastrichtian	Argentina	Titanosauria	Coria & Salgado (2005); Paulina Carabajal & Salgado (2007)

Table 1. Continued

Designation	Specimen number	Formation	Stage	Country	Classification	Reference(s)
<i>Lithostrotia</i> indet.	MPCM-HUE-8741	Villalba de la Sierra	Campanian–Maastrichtian	Spain	Titanosauria	Knoll <i>et al.</i> (2013) as <i>Ampelosaurus</i> sp.; Knoll <i>et al.</i> (2019) as cf. <i>Lohuecoticus pandaiflandi</i>
<i>Lithostrotia</i> indet.	MPCM-HUE-1667	Villalba de la Sierra	Campanian–Maastrichtian	Spain	Titanosauria	Knoll <i>et al.</i> (2015)
<i>Titanosauria</i> indet.	Mechin Collection 225 (cast in MDE)		Campanian / Maastrichtian	France	Titanosauria	Le Loeuff <i>et al.</i> (1989)
<i>Quaesitosaurus orientalis</i>	PIN 3906/2	Baruungoyot	Campanian–Maastrichtian	Mongolia	Titanosauria	Kurzanov & Bannikov (1983); Upchurch (1999); Wilson (2005)
<i>Atsinganosaurus velauciensis</i>	MMS/VBN.09.41	Argiles et Grès à Reptiles	Campanian–Maastrichtian	France	Titanosauria	Diez Díaz <i>et al.</i> (2018)
<i>Atsinganosaurus velauciensis</i>	MMS/VBN.09.167	Argiles et Grès à Reptiles	Campanian–Maastrichtian	France	Titanosauria	Diez Díaz <i>et al.</i> (2012); Knoll <i>et al.</i> (2019)
<i>Titanosauria</i> indet.	FAM 03.064	Grès à Reptiles	Campanian	France	Titanosauria	Allain (1998)
<i>Titanosauria</i> indet.	MNHN (uncatalogued)	Grès à Reptiles	Campanian	France	Titanosauria	Sanz <i>et al.</i> (1999); Diez Díaz <i>et al.</i> (2011)
<i>Lirainosaurus astibiae</i>	MCNA 7439	Sierra Perenchiza	Campanian	Spain	Titanosauria	Diez Díaz <i>et al.</i> (2011)
<i>Mansourasaurus shahinae</i>	MCNA 13913	Sierra Perenchiza	Campanian	Spain	Titanosauria	Sallam <i>et al.</i> (2018)
<i>Antarctosaurus wichmannianus</i>	MUVP 2000 MACN 6904	Quseir Anacleto	Campanian Campanian	Egypt Argentina	Titanosauria Titanosauria	Huene (1929); Powell (2003); Paulina Carabajal (2012); S.F.P., P.D.M. & P.U., pers. obs., 2013
<i>Narambuenatitan palomoi</i>	MAU-Pv-N-425	Anacleto	Campanian	Argentina	Titanosauria	Filippi <i>et al.</i> (2011); Paulina-Carabajal <i>et al.</i> (2020)
<i>Pitekunsaurus macayai</i>	MAU-Pv-AG-446/5	Anacleto	Campanian	Argentina	Titanosauria	Filippi & Garrido (2008); P.D.M., pers. obs., 2014
<i>Titanosauria</i> indet.	MAU-Pv-AC-01	Rio Colorado Subgroup	Santonian–Campanian	Argentina	Titanosauria	Calvo <i>et al.</i> (1997); Coria & Salgado (1999)
<i>Titanosauria</i> indet.	MUCPv-334	Bajo de la Carpa	Santonian	Argentina	Titanosauria	Calvo & Kellner (2006a, b)
<i>Kajititan maii</i>	MAU-Pv-CM-522	Sierra Barrosa	Coniacian	Argentina	Titanosauria	Filippi <i>et al.</i> (2019)
<i>Titanosauria</i> indet.	MCF-PVPH-765	Portezuelo	Turonian–Coniacian	Argentina	Titanosauria	Paulina Carabajal <i>et al.</i> (2008); Paulina Carabajal (2012)
<i>Muyelensaurus pecheni</i>	MRS-PV 207	Portezuelo	Turonian–Coniacian	Argentina	Titanosauria	Calvo <i>et al.</i> (2007a)
<i>Titanosauria</i> indet.	CCMGE 628/12457	Bissekty	Turonian	Uzbekistan	Titanosauria	Sues <i>et al.</i> (2015)
<i>Diamantinosaurus matildae</i>	AODF 836	Winton	Cenomanian–Turonian	Australia	Titanosauria	Poropat <i>et al.</i> (2016); this paper
<i>Sarmientosaurus musacchioi</i>	MDT-PV 2	Bajo Barreal	Cenomanian–Turonian	Argentina	Titanosauria	Martínez <i>et al.</i> (2016)

Table 1. Continued

Designation	Specimen number	Formation	Stage	Country	Classification	Reference(s)
<i>Abydosaurus mcintoshii</i>	DINO 16488	Cedar Mountain	Albian–Cenomanian	USA	Brachiosauridae	Chure <i>et al.</i> (2010)
<i>Abydosaurus mcintoshii</i>	DINO 17849	Cedar Mountain	Albian–Cenomanian	USA	Brachiosauridae	Chure <i>et al.</i> (2010)
<i>Abydosaurus mcintoshii</i>	DINO 39727	Cedar Mountain	Albian–Cenomanian	USA	Brachiosauridae	Chure <i>et al.</i> (2010)
<i>Tambatitanis amacitiae</i>	MNHAAH D-1029280	Sasayama Group	Albian	Japan	Somphospondyli	Saegusa & Ikeda (2014)
Titanosauriformes indet.	TMM 40435	Glen Rose	Aptian–Albian	USA	Titanosauriformes	Tidwell & Carpenter (2003)
<i>Mongolosaurus haplodon</i>	AMNH 6710	On Gong	Aptian–Albian	China	Somphospondyli	Gilmore (1933); Mannion (2011)
<i>Tapuiasaurus macedoi</i>	MZSP-PV 807	Quiriricó	Aptian	Brazil	Titanosauria	Zaher <i>et al.</i> (2011); Wilson <i>et al.</i> (2016)
<i>Malawisaurus dixeyi</i>	Mal-202-1	Dinosaur Beds	Aptian	Malawi	Titanosauria	Gomani (2005); Andrzejewski <i>et al.</i> (2019)
<i>Phuwangosaurus sirindhornae</i>	SM K11-0006	Sao Khua	Barremian–Aptian	Thailand	Somphospondyli	Suteethorn <i>et al.</i> (2009)
<i>Giraffatitan brancai</i>	MfN 2223.1 (HMN t 1)	Tendaguru	Kimmeridgian–Tithonian	Tanzania	Brachiosauridae	Janensch (1935–1936, 1936); Knoll & Schwarz-Wings (2009)
<i>Giraffatitan brancai</i>	MfN 2180.22.1–4 (HMN Tendaguru S 66)	Tendaguru	Kimmeridgian–Tithonian	Tanzania	Brachiosauridae	Janensch (1935–1936, 1936); Clarke (2005); Knoll & Schwarz-Wings (2009)
<i>Giraffatitan brancai</i>	MfN 2384 (HMN Y 1)	Tendaguru	Kimmeridgian–Tithonian	Tanzania	Brachiosauridae	Janensch (1935–1936, 1936); Knoll & Schwarz-Wings (2009)
<i>Brachiosaurus</i> sp.	USNM 5730 (YPM 1986)	Morrison	Kimmeridgian–Tithonian	USA	Brachiosauridae	Carpenter & Tidwell (1998); D’Emic & Carrano (2020)

Somphospondyli = non-titanosaurian somphospondylan.

MATERIAL AND METHODS

GEOLOGICAL SETTING

AODF 836 was found on Belmont Station, ~60 km north-east of Winton, Queensland, Australia (Fig. 1). Specifically, it was discovered in the westernmost subsite of the ‘Elliot’ site (QM L1333/AODL 001), which was excavated between 2001 and 2005 (Salisbury, 2003, 2004, 2005; Hocknull, 2005; Salisbury *et al.*, 2006, 2007). This site yielded the remains of several sauropod individuals (spanning a significant size range), in addition to isolated elements pertaining to Theropoda, Ankylosauria (Leahey & Salisbury, 2013), Pterosauria, Crocodyliformes, ?Plesiosauria and Testudines (S.F.P. & D.A.E., pers. obs., 2019). The ‘Elliot’ site was divided into 10 m × 10 m quadrats, with letters assigned to each from south to north, and numbers assigned from west to east. The site was then divided into three subsites based on localized concentrations of the fossils. The most easterly subsite is the original ‘Elliot’ site (AODL 001; quadrats A22–K35; 110 m × 140 m), which produced elements pertaining to at least two sauropods of different sizes, including a large femur. Immediately west of this subsite lies ‘Kylie’s Corner’ (AODL 126; quadrats A12–K21; 110 m × 100 m), which also yielded remains from at least two sauropods of different sizes. Finally, the most westerly subsite, ‘Alex’ (AODL 127; quadrats A1–K11; 110 m × 110 m), produced an abundance of sauropod cranial and postcranial elements, localized in an area of < 40 m². Most of this material derived from two main concentrations: (1) a south-west one, from which dorsal vertebrae, ribs and pelvic elements were collected; and (2) a north-east one that produced cranial elements, cervical vertebrae and ribs, dorsal ribs and a right scapula (Supporting Information, Fig. S1). No elements are duplicated between these two concentrations of skeletal remains, all appear to be size congruent, and several fragments have been shown to connect to others found several metres distant. Consequently, all of the sauropod bones found at AODL 127 are thought to pertain to a single individual and have been registered as AODF 836.

The association of the material from the other subsites of the ‘Elliot’ site (AODL 001 and AODL 126) with AODF 836 is highly unlikely based on the size of the preserved elements and their distance from AODL 127. The material recovered from AODL 001, which was situated > 110 m from AODL 127, includes three cervical vertebrae, two dorsal vertebrae, a radius, a metacarpal IV, a femur (QM F43302) and a tibia (QM F44573). Based on their relative sizes, these remains derive from more than one individual: the femur (1685 mm) is longer than the holotype femur (1345 mm) of *Diamantinasaurus*, whereas the fourth metacarpal is shorter (270 vs. 352 mm), as is the tibia

(668 vs. 769 mm). Although the tibia and metacarpal are approximately size congruent, they cannot be attributed unequivocally to a single individual. The material recovered from AODL 126, which lies 40 m to the east of the easternmost specimens from AODL 127, includes a large cervical centrum, two incomplete dorsal vertebrae (including QM F43332) and a radius. Based on the dimensions of these remains, they cannot pertain to the AODF 836 individual: for example, the radius from AODL 126 is longer than the paratype radius of *Diamantinasaurus* (689 vs. 675 mm), despite being incomplete.

The bones of AODF 836 were disarticulated (Supporting Information, Fig. S1), transported and weathered before fossilization. The preservation of some elements implies that the carcass was (or parts thereof were) transported and damaged before its disarticulation. A specific example of this is the axis and cervical vertebra III. The right postzygapophysis and spinopostzygapophyseal lamina (SPOL) of the axis and the right prezygapophysis and centroprezygapophyseal lamina (CPRL) of cervical vertebra III have been compressed under pressure from the right lateral side. This distortion is readily explicable if the bones were crushed while still in articulation. However, these elements were found several metres apart (Supporting Information, Fig. S1). It is likely that the carcass was impacted by flowing water, as evinced by the fine sandstones that host the specimen, but ultimately split into two sections: a north-east one, preserving the skull, cervical series and the anterior thorax; and a south-west one, preserving the posterior thorax and pelvis. However, most of the post-mortem disturbance, which resulted in the disarticulation of the specimen and the fragmentation of some elements, was probably caused by scavenging activity: small crocodyliform teeth were found throughout the site, and a small theropod tooth (AODF 894; Fig. 2) was found in the same section of the site as the braincase. Furthermore, a large puncture on the ventral surface of the braincase, within which displaced external bone can be observed, is consistent with a bite mark. Before burial, several of the sauropod bones were weathered. This is especially evident in the dorsal vertebrae, wherein one side (the right in dorsal vertebra VII, the left in dorsal vertebra VIII) is far better preserved than the other.

COMPUTED TOMOGRAPHY SCANNING

Multiple elements of AODF 836 (including the braincase) were imaged by X-ray computed tomography (CT) at the radiology unit of Queensland X-Ray, Mater Mackay Hospital (Queensland, Australia) on a Philips Brilliance CT 64-slice scanner. The spacing between slices was 0.9 mm. The commercial software VG

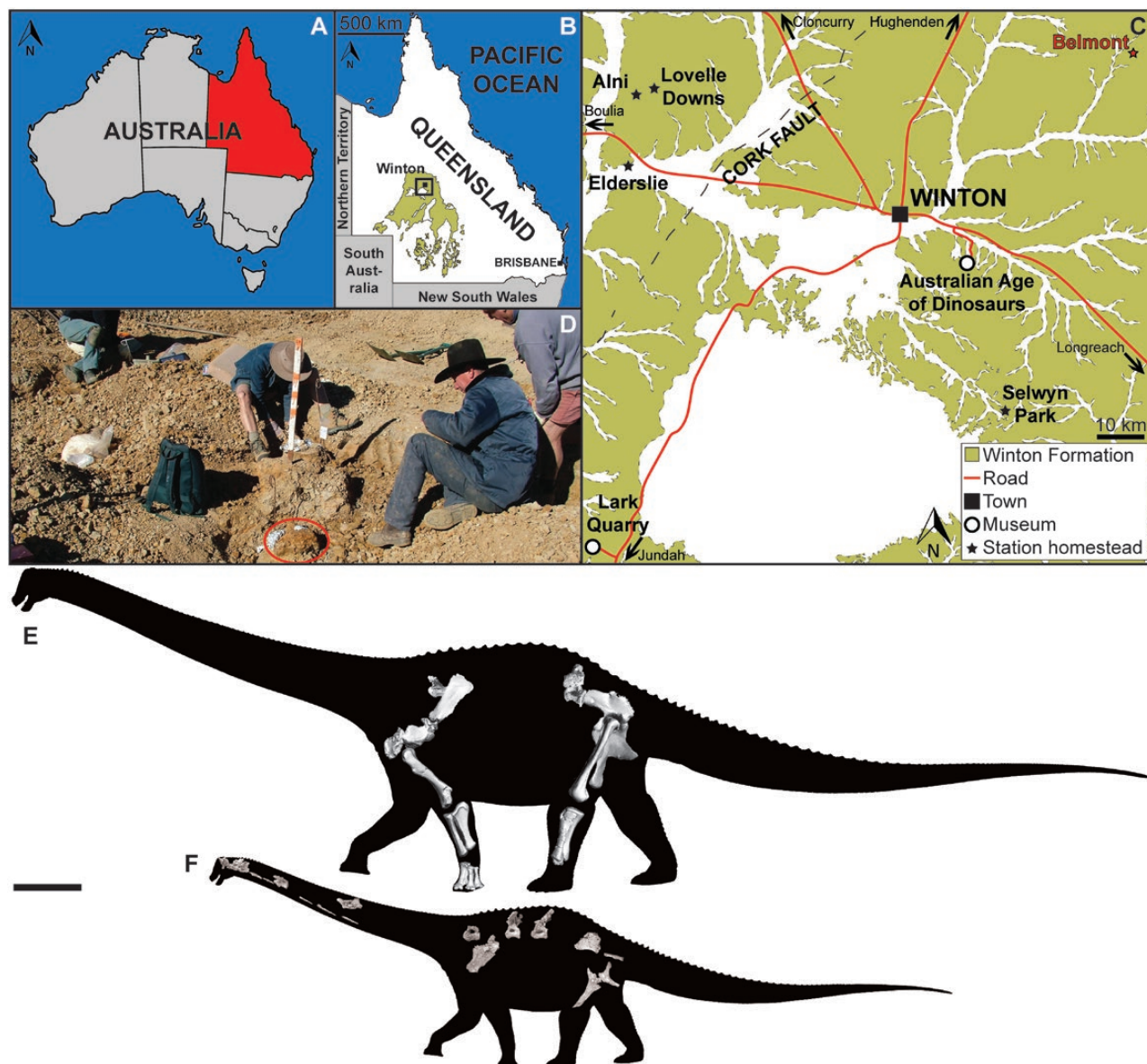


Figure 1. Locality maps for the referred specimen (AODF 836) of *Diamantinasaurus matildae* (modified from Poropat *et al.*, 2016; Pentland *et al.*, 2019) and skeletal reconstructions of *D. matildae*. A, map of Australia, showing the location of Queensland. B, map of Queensland, showing the distribution of Winton Formation outcrop. C, map of the Winton area, showing Winton Formation outcrop, the location of Belmont Station and other stations on which sauropod body fossils have been recovered, and museums in the region. This map incorporates geological information from Vine (1964) and Vine & Casey (1967) [© Commonwealth of Australia (Geoscience Australia) 2019. This product is released under the Creative Commons Attribution 4.0 International Licence. <http://creativecommons.org/licenses/by/4.0/legalcode>]. D, photograph from the September 2004 dig, showing one of the authors (D.A.E., right, seated) with the braincase *in situ* (circled). E, skeletal reconstruction of the *D. matildae* holotype and paratype specimens (AODF 603), incorporating data from Klinkhamer *et al.* (2018, 2019). F, skeletal reconstruction of the referred specimen of *D. matildae* (AODF 836). Scale bar: 1 m in E, F.

STUDIOMAX v.2.2 (Volume Graphics Inc., Heidelberg, Germany) and the freeware IMAGEJ (Schneider *et al.*, 2012) were used for three-dimensional segmentation to restore the endoneurocranial and inner ear morphology, and for rendering, animation and collecting

volumetric data and linear measurements of the *Diamantinasaurus* endocast and associated structures. Angular measurements were made through two-dimensional projections generated from the rendered three-dimensional models using ADOBE PHOTOSHOP.



Figure 2. Theropod tooth (AODF 894), found in association with *Diamantinasaurus matildae* referred cranial elements (AODF 836), in basal (A), lingual (B), distal (C), apical (D), labial (E) and mesial (F) views. Scale bar: 10 mm.

Plates of figures were assembled and labelled in the graphic environment of CORELDRAW X5.

INSTITUTIONAL ABBREVIATIONS

AAOD, Australian Age of Dinosaurs Natural History Museum, Winton, Queensland, Australia; AMNH, American Museum of Natural History, New York, NY, USA; AODF, Australian Age of Dinosaurs Fossil; AODL, Australian Age of Dinosaurs Locality; BYU, Brigham Young University, Earth Science Museum, Provo, UT, USA; CCMGE, Chernyshev's Central Museum of Geological Exploration, Saint Petersburg, Russia; CM, Carnegie Museum of Natural History, Pittsburgh, PA, USA; DINO, Dinosaur National Monument, Colorado and Utah, USA; FAM, Fox-Amphoux-Métisson, Mairie de Fox-Amphoux, France; FGGUB, Faculty of Geology and Geophysics of the University of Bucharest, Bucharest, Romania; FMNH, Field Museum of Natural History, Chicago, IL, USA; GCP, Grupo Cultural Paleontológico de Elche, Museo Paleontológico de Elche, Elche, Spain; GSI, Geological Survey of India, Kolkata, India; ISI, Indian Statistical Institute, Kolkata, India; GSP, Geological Survey of Pakistan, Quetta, Pakistan; MACN, Museo Argentino de Ciencias Naturales 'Bernardino Rivadavia', Buenos Aires, Argentina; MAL, Malawi Department of Antiquities Collection, Lilongwe and Nguludi,

Malawi; MAU, Museo Municipal 'Argentina Urquiza', Rincón de los Sauces, Argentina; MCF-PVPH, Museo Carmen Funes, Plaza Huincul, Neuquén, Argentina; MCNA, Museo de Ciencias Naturales de Álava/Arabako Natur Zientzien Museoa, Vitoria-Gasteiz, Spain; MDE, Musée des Dinosaures, Espéraza, France; MfN, Museum für Naturkunde, Berlin, Germany (formerly HMN, Humboldt Museum für Naturkunde); MGPIFD-GR, Museo de Geología y Paleontología del Instituto de Formación Docente Continua de General Roca, Río Negro, Argentina; MML, Museo Municipal de Lamarque, Río Negro, Argentina; MMS/VBN, Musée Moulin Seigneurial/Velaux-La Bastide Neuve, Bouches-du-Rhône, France; MNHAH, Museum of Nature and Human Activities, Hyogo, Japan; MNHN, Muséum National d'Histoire Naturelle, Paris, France; MNN, Musée National du Niger, Niamey, Niger (currently stored at the University of Chicago); MPCA-PV, Museo Provincial 'Carlos Ameghino', Cipolletti, Río Negro, Argentina; MPCM, Museo de Paleontología de Castilla-La Mancha, Cuenca, Spain; MRS-PV, Museo de Rincón de los Sauces, Neuquén, Argentina; MUCPv, Museo de Geología y Paleontología de la Universidad Nacional del Comahue, Argentina; MZSP, Museu de Zoologia da Universidade de São Paulo, São Paulo, Brazil; PIN, Russian Academy of Sciences, Moscow, Russia; PVL, Fundación Miguel Lillo, Universidad Nacional de Tucuman, San Miguel

de Tucuman, Argentina; QM, Queensland Museum, Brisbane, Queensland, Australia; SM, Sirindhorn Museum, Changwat Kalasin, Thailand; TMM, Texas Memorial Museum, Austin, TX, USA; UNPSJB-PV, Universidad Nacional de la Patagonia ‘San Juan Bosco’ – Paleovertebrados, Comodoro Rivadavia, Argentina; UA, Université d’Antananarivo, Antananarivo, Madagascar; UQ, University of Queensland, Brisbane, Australia; USNM, National Museum of Natural History, Smithsonian Institution, Washington, DC, USA; YPM, Yale Peabody Museum, New Haven, CT, USA; Z. PAL, Instytut of Paleobiologii, Polish Academy of Sciences, Warsaw, Poland; ZG, Zigong Dinosaur Museum, Zigong, China.

ANATOMICAL ABBREVIATIONS

ACDL, anterior centrodiapophyseal lamina; ACPL, anterior centroparapophyseal lamina; asc, anterior semicircular canal; asca, ampulla of anterior semicircular canal; aSPDL, anterior spinodiapophyseal lamina; bcp, base of cultriform process; BO, basioccipital; bors, basioccipital recess; bp, basipterygoid process; brst, brainstem; bt, basal tuber; cc, crus commune; cca, internal carotid artery; CDF, centrodiapophyseal fossa; CN, cranial nerve; coch, cochlea; con, constriction; CPAF, centroparapophyseal fossa; cphf, craniopharyngeal foramen; cpo, crista prootica; CPOF, centropostzygapophyseal fossa; CPOL, centropostzygapophyseal lamina; CPRF, centroprezygapophyseal fossa; CPRL, centroprezygapophyseal lamina; crb, cerebral hemisphere; crbl, cerebellum; dds, dorsal dural sinus; dose, dorsum sellae; dp, diapophysis; EO, exoccipital; f, foramen; fecoch, fenestra cochleae; fm, foramen magnum; (fp+fo)p, placement of foramen perilymphaticum and foramen ovale; FR, frontal; frpafp, placement of frontoparietal foramen; gVII_{hm}, groove transmitting hyomandibular branch of the facial nerve; gVII_{pal}, groove transmitting palatine branch of the facial nerve; hfp, hypophyseal fossa placement; is, infundibular stalk; jug, jugular vein; lbr, endosseous labyrinth; lCPRL, lateral centroprezygapophyseal lamina; le-dds, lateral expansion of the dorsal dural sinus; lmds, lateral middle dural sinus; lsc, lateral semicircular canal; LTS, laterosphenoid; mCPRL, medial centroprezygapophyseal lamina; midb, midbrain; mo, medulla oblongata; occ, occipital condyle; ofb, olfactory bulb; offip, olfactory filaments placement; oft, olfactory tract; OPO, opisthotic; ORS, orbitosphenoid; PACDF, parapophyseal centrodiapophyseal fossa; PACPRF, parapophyseal centroprezygapophyseal fossa; PAR, parietal; PBS, parabasisphenoid; PCDL, posterior centrodiapophyseal lamina; PCPL, posterior centroparapophyseal lamina; pdse, pontine dural sinus extension; POCDF, postzygapophyseal

centrodiapophyseal fossa; PODL, postzygodiapophyseal lamina; POSDF, postzygapophyseal spinodiapophyseal fossa; POSL, postspinal lamina; poz, postzygapophysis; pp, parapophysis; PPDL, parapodiapophyseal lamina; ppf, postparietal foramen; ppr, paroccipital process; PRDL, prezygodiapophyseal lamina; PRO, prootic; PRPADF, prezygapophyseal parapodiapophyseal fossa; PRPL, prezygoparapophyseal lamina; PRSDF, prezygapophyseal spinodiapophyseal fossa; PRSL, prespinal lamina; prz, prezygapophysis; psc, posterior semicircular canal; pSPDL, posterior spinodiapophyseal lamina; SDF, spinodiapophyseal fossa; SO, supraoccipital; SPDL, spinodiapophyseal lamina; SPDL-F, spinodiapophyseal lamina fossa; spha, sphenopalatine artery canal; SPOF, spinopostzygapophyseal fossa; SPOL, spinopostzygapophyseal lamina; SPRF, spinoprezygapophyseal fossa; SPRL, spinoprezygapophyseal lamina; TPOL, interpostzygapophyseal lamina; TPRL, interprezygapophyseal lamina; ves, vestibule; II, optic tract; III, oculomotor nerve; IV, trochlear nerve; V, trigeminal nerve; V₁, ophthalmic branch of the trigeminal nerve; V₂₊₃, maxillomandibular branch of the trigeminal nerve; VI, abducens nerve; VII, facial nerve; IX, glossopharyngeal nerve; X, vagus nerve; XI, accessory nerve; XII, hypoglossal nerve; ?, structure of unknown or disputable identity/placement.

RESULTS

SYSTEMATIC PALAEOLOGY

DINOSAURIA OWEN, 1842

SAUROPODA MARSH, 1878

TITANOSAURIFORMES SALGADO *ET AL.*, 1997

SOMPHOSPONDYLI WILSON & SERENO, 1998

TITANOSAURIA BONAPARTE & CORIA, 1993

DIAMANTINASAURIA CLADE NOV.

Definition: The most inclusive clade that includes *D. matildae* but not *Saltasaurus loricatus* Bonaparte & Powell, 1980.

Characteristics: (1) Supratemporal fenestrae wider mediolaterally than the intervening space between them (plesiomorphic); (2) laterosphenoid–prootic with ossified canals for at least two branches of CN V (trigeminal); (3) cervical centra with prominent lateral pneumatic foramina (plesiomorphic); (4) TPOLs absent in dorsal vertebrae, resulting in confluence of the SPOF and CPOF; (5) hyosphene–hypantrum articulations absent throughout dorsal vertebral series; (6) caudal

centra amphicoelous (plesiomorphic); (7) sternal plate D-shaped rather than reniform (plesiomorphic); and (8) manual phalanges present (plesiomorphic).

Included taxa: *Diamantinasaurus matildae*, *Savannasaurus elliottorum* and *Sarmientosaurus musacchioi*.

DIAMANTINASAUROS MATILDAE
HOCKNULL *ET AL.*, 2009

Holotype (including paratype specimens from the same individual): AODF 603 (AODL 85): several cervical ribs; three incomplete dorsal vertebrae; numerous dorsal ribs; fragmentary gastralia; five coalesced sacral vertebrae; isolated sacral processes; right scapula; right coracoid; partial sternal plate; right and left humeri; right and left ulnae; right radius; right and left metacarpals I–V; three right and five left manual phalanges (including manual ungual I-2); left ilium; right and left pubes; right and left ischia; right femur; right tibia; right fibula; right astragalus.

Referred specimen: AODF 836: left squamosal; right and left quadrates; braincase [including left frontal, both parietals, supraoccipital, otoccipitals (exoccipital-opisthotics), basioccipital, partial basisphenoid, prootics, laterosphenoids and orbitosphenoids]; right surangular; atlas intercentrum; axis; cervical vertebrae III–VI (IV and V fragmentary); middle cervical neural arch; four dorsal vertebrae; dorsal ribs; two co-ossified sacral centra; partial right scapula; right and left iliac preacetabular processes; right and left pubes; right and left ischia; and abundant associated fragments, many constituting partial ribs or vertebrae.

Diagnosis (modified from Poropat et al., 2015b): *Diamantinasaurus matildae* can be diagnosed by 14 autapomorphies (marked with an asterisk), in addition to two local autapomorphies: (1) parietal dorsal surface with anteriorly crescentic concave medial half and anteroposteriorly convex lateral half*; (2) otoccipital with small depression situated lateral to proatlantal facet*; (3) endosseous labyrinth with lateral and posterior semicircular canals defining an angle of 130°*; (4) cervical axis with average elongation index < 1.5*; (5) cervical rib distal shaft dorsal surface with laterodistally directed ridge and without dorsal midline trough*; (6) middle–posterior dorsal vertebrae with dorsally bifurcated PCPL*; (7) scapular blade lateral surface with accessory longitudinal ridge and fossa at midlength, situated dorsal to main lateral ridge*; (8) humerus proximal shaft posterolateral margin formed by stout vertical ridge that increases depth of lateral triceps fossa*; (9) humerus with ridge

that extends medially from deltopectoral crest, then turns to extend proximally, creating a fossa lying medial to the dorsal part of the deltopectoral crest on the anterior face*; (10) femur with shelf linking posterior ridges of fibular condyle*; (11) tibia proximal lateral face with double ridge extending distally from lateral projection of proximal articular area*; (12) tibia with posterolateral fossa posterior to the double ridge, containing a lower tuberosity and an upper deep pit*; (13) tibial shaft anterolateral margin, distal to cnemial crest, forms a thin flange-like projection extending proximodistally along the central region of the element*; (14) fibular shaft medial surface, between proximal triangular scar and midlength, with vertical ridge separating anterior and posterior grooves*; (15) astragalus lateral fossa divided into upper and lower portions by anteroposteriorly directed ridge*; and (16) astragalus posteroventral margin, below and medial to the ascending process, with well-developed, ventrally projecting rounded process visible in posterior, lateral and ventral views*.

Locality of referred specimen AODF 836: AODL 127 (the ‘Alex’ Site), Belmont Station, ~60 km north-east of Winton, Central West Queensland, Australia.

Horizon and age: Winton Formation (Rolling Downs Group, Eromanga Basin; Cenomanian–earliest Turonian (Bryan *et al.*, 2012; Tucker *et al.*, 2013).

DESCRIPTION AND COMPARISONS

AODF 836 overlaps anatomically with the type specimens of all four named sauropod taxa from the Eromanga Basin of Australia: *Austrosaurus mckillopi* Longman, 1933 from the upper Albian Allaru Mudstone (Poropat *et al.*, 2017); and *Wintonotitan watsi* Hocknull *et al.*, 2009 (Poropat *et al.*, 2015a), *D. matildae* (Hocknull *et al.*, 2009; Poropat *et al.*, 2015b) and *Savannasaurus elliottorum* (Poropat *et al.*, 2016, 2020a) from the Winton Formation. Based on the close similarity of postcranial elements that overlap with the type specimen of *Diamantinasaurus*, in addition to a number of shared autapomorphies, AODF 836 was referred to that taxon when it was first described (Poropat *et al.*, 2016), and this referral is supported herein. Based on the proportions of the pubes, AODF 836 represents an individual $\geq 20\%$ smaller than the type specimen of *D. matildae* (AODF 603); the nearly complete pubis from AODF 836 is 779 mm long proximodistally, whereas that of AODF 603 is 1000 mm long proximodistally.

Skull

Squamosal: The left squamosal (Fig. 3A–D) is incomplete anteriorly, medially and ventrally;

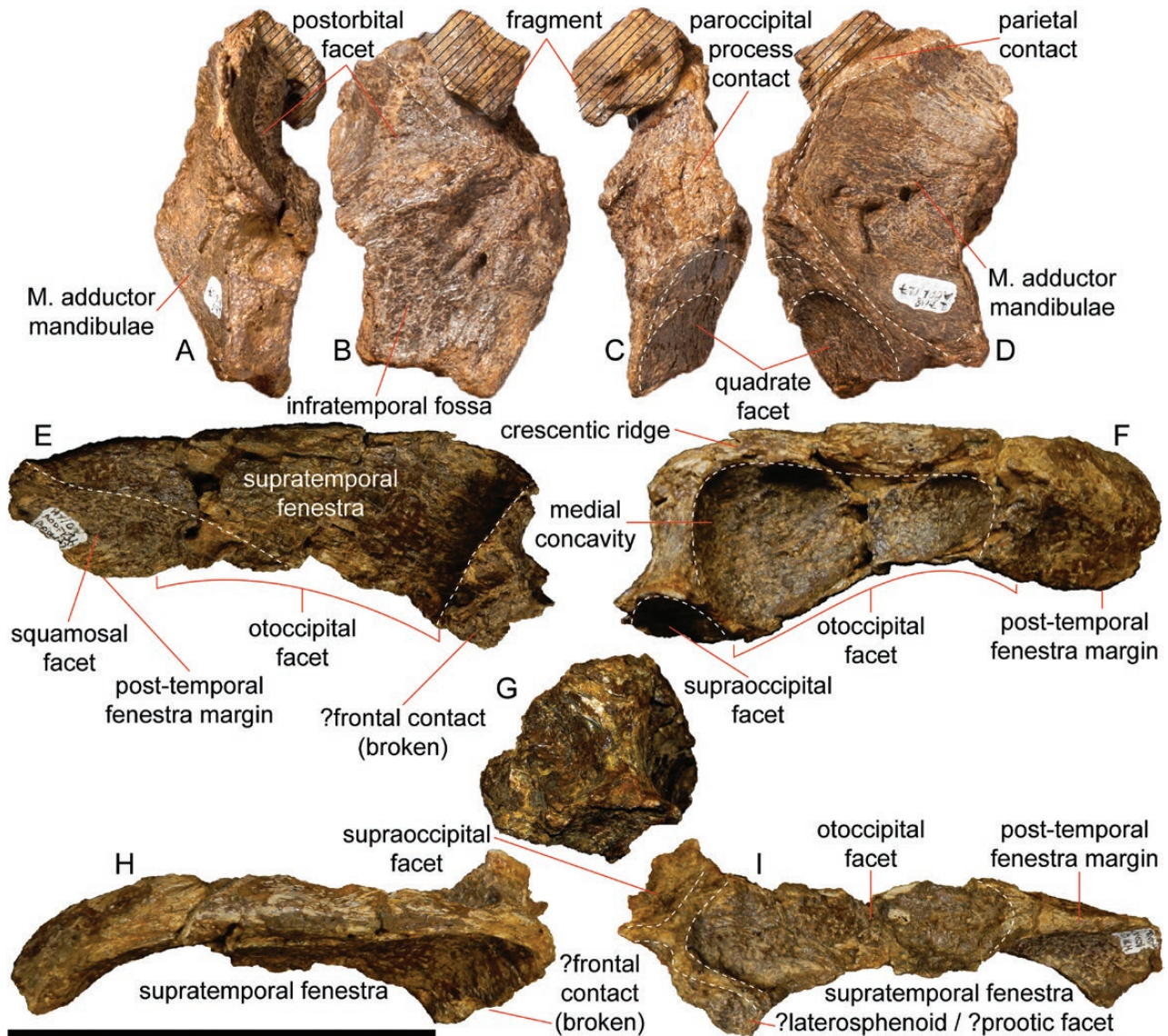


Figure 3. *Diamantinasaurus matildae* referred left squamosal and right parietal (AODF 836). A–D, left squamosal in anterior (A), lateral (B), posterior (C) and medial (D) views. E–I, right parietal in anterior (E), posterior (F), medial (G), dorsal (H) and ventral (I) views. Dorsal is towards top of page in E–G; anterior is towards bottom of page in H–I. Scale bar: 100 mm.

nevertheless, it is still anatomically informative. The lateral surface (Fig. 3B) of the incomplete anterior process bears a shallow concavity, which accommodated the posterior process of the postorbital. This triangular concavity flares anteriorly (such that it can be seen in anterior view; Fig. 3A) and tapers posteriorly. A subtle ridge delineates the ventral margin of this concavity, and ventral to this the lateral surface hosts a shallowly concave infratemporal fossa. In posterior view (Fig. 3C), the squamosal can be divided broadly into three sections. The dorsalmost of these is non-articular and poorly preserved. Ventral to this is the shallowly concave facet for the

otoccipital portion of the paroccipital process. The long axis of this parallelogram-shaped facet is inclined dorsomedially–ventrolaterally. It is separated from the quadrate facet below by a subtle ridge, also inclined dorsomedially–ventrolaterally. The quadrate facet, which occupies the ventral portion of the posterior surface, is bilobate, with a shallow, dorsally situated sulcus offset from a slightly deeper (and, as preserved, subcircular) sulcus by a very weak, horseshoe-shaped ridge. Bilobate quadrate facets have also been observed on the squamosal of *Camarasaurus* Cope, 1877 (Madsen *et al.*, 1995), ‘*Brachiosaurus*’ (D’Emic & Carrano, 2020), *Euhelopus* Romer, 1956 (Poropat

& Kear, 2013; fig. 9F) and *Antarctosaurus* Huene, 1929 (MACN 6904; S.F.P., P.D.M. and P.U., pers. obs., 2013), although the last of these almost appears to be trilobate, with the dorsalmost 'lobe' (equivalent to the same in '*Brachiosaurus*' and *Diamantinasaurus*) not in articulation with the quadrate as preserved. By contrast, the quadrate facets of *Rapetosaurus* and an indeterminate titanosaur specimen from the latest Cretaceous of Brazil (CPPLIP 247) do not comprise multiple 'lobes' (Curry Rogers & Forster, 2004; Martinelli *et al.*, 2015), retaining the plesiomorphic state seen in non-neosauropodan sauropods [e.g. *Tazoudasaurus* Allain *et al.*, 2004 (Allain & Aquesbi, 2008), *Bellusaurus* Dong, 1990 (Moore *et al.*, 2018) and *Turiasaurus* Royo-Torres *et al.*, 2006 (Royo-Torres & Upchurch, 2012)] and diplodocoids (Holland, 1906; Janensch, 1935–1936; Berman & McIntosh, 1978). The medial surface of the squamosal is broadly concave to accommodate the muscle adductor mandibulae (Fig. 3D). The posterior margin of this sulcus is separated from the quadrate facet by a narrow, anteroventrally–posterodorsally inclined ridge. In dorsal view, the squamosal rises dorsomedially to a ridge, separating the dorsal surface from the medial one. A small fragment of bone (possibly representing part of the parietal) remains adhered to the squamosal on this margin.

Quadrate: The left quadrate is almost complete (Fig. 4A–E), whereas the right quadrate is represented by only the ventral third (Fig. 4F–I). Consequently, the description below is based mostly on the left quadrate. When complete, the dorsal process would have been clasped between the squamosal laterally and the otoccipital medially. Ventral to this, the shaft of the quadrate expands anteriorly to form a wedge-shaped, mediolaterally thin pterygoid process (Fig. 4B, E). The lateral surface of the quadrate process of the pterygoid would have articulated with the medial surface of the pterygoid process of the quadrate (Fig. 4E). The posterior surface of the quadrate is invaded by a deep quadrate fossa (Fig. 4D), as in most non-diplodocoid eusauropods (Wilson & Sereno, 1998; Upchurch *et al.*, 2004). The medial wall of this fossa is intact in the left quadrate, whereas the lateral wall is not preserved in either the left or right quadrate. However, the ventral divergence of the medial and lateral walls can be seen in both (Fig. 4D, H). The quadrate fossa in *Diamantinasaurus* faces posterolaterally; among sauropods, this is otherwise true only of the titanosaurs *Nemegtosaurus* Nowiński, 1971, *Quaesitosaurus* Kurzanov & Bannikov, 1983, *Rapetosaurus*, *Sarmientosaurus* Martínez *et al.*, 2016 and *Tapuiasaurus* Zaher *et al.*, 2011 (Wilson, 2002, 2005; Curry Rogers & Forster, 2004; Martínez *et al.*, 2016; Wilson *et al.*, 2016). In other sauropods,

including the titanosaurs *Antarctosaurus* (MACN 6904; S.F.P., P.D.M. and P.U., pers. obs., 2013), *Malawisaurus* Jacobs *et al.*, 1993 (Gomani, 2005), *Muyelensaurus* Calvo *et al.*, 2007 (MAU-Pv-LL-207; P.D.M., pers. obs., 2014) and *Narambuenatitan* Filippi *et al.*, 2011 (MAU-Pv-N-425; P.D.M., pers. obs., 2014), the quadrate fossa faces posteriorly (Wilson, 2002). Ventral to the pterygoid process and quadrate fossa, on the lateral surface, lies the quadratojugal articulation. This facet is incompletely preserved on both quadrates, but more complete on the right one (Fig. 4G, H). It appears to have constituted a laterally concave, anteroposteriorly convex, very thin ridge. The ventral process is mediolaterally expanded and bevelled laterally at ~45°. In distal view, the quadrate condyle is crescentic, with the concave surface facing anterolaterally and the convex one posteromedially (Fig. 4C). This morphology is similar to that seen in *Giraffatitan* Paul, 1988 (Janensch, 1935–1936; Wilson & Sereno, 1998), *Euhelopus* (Wiman, 1929; Wilson & Upchurch, 2009; Poropat & Kear, 2013) and *Sarmientosaurus* (Martínez *et al.*, 2016), but intermediate between that seen in *Camarasaurus*, *Nemegtosaurus*, *Phuwiangosaurus* Martin *et al.*, 1994 and *Quaesitosaurus*, wherein the concave surface is anterior and the convex one posterior (Madsen *et al.*, 1995; Wilson, 2005; Suteethorn *et al.*, 2009), and *Narambuenatitan*, wherein the concave surface faces laterally and the convex one medially (Filippi *et al.*, 2011). In complete contrast, the quadrate condyle of *Tapuiasaurus* is convex posterolaterally and concave anteromedially (Wilson *et al.*, 2016), whereas those of *Malawisaurus* and *Bonitasaura* Apesteguía, 2004 are ovoid (Gomani, 2005; Gallina & Apesteguía, 2011).

Braincase: The ventral and posterior portions of the braincase of *Diamantinasaurus* (Figs 5–7) are completely ossified, as in all adult sauropods (Upchurch *et al.*, 2004). Although the sutures between many of the elements are indistinct, determination of the approximate limits of each was achieved through comparison with other sauropod braincases (e.g. Table 1).

Frontal: Only the left frontal is present, firmly adhered to the roof of the braincase. Despite its incompleteness, the frontal is clearly shorter anteroposteriorly (61 mm) than it is wide mediolaterally (92 mm), with a ratio of anteroposterior length to mediolateral width of ~0.7. This is within the range for this ratio (> 0.5 to < 1.0) seen in nearly all titanosauriforms (Poropat *et al.*, 2016) and many other sauropods (Whitlock, 2011b; Mannion *et al.*, 2019b), with the exception of the euhelopodid somphospondylan *Phuwiangosaurus* (Suteethorn *et al.*, 2009) and an indeterminate titanosaur specimen (FAM 03.175) from the latest

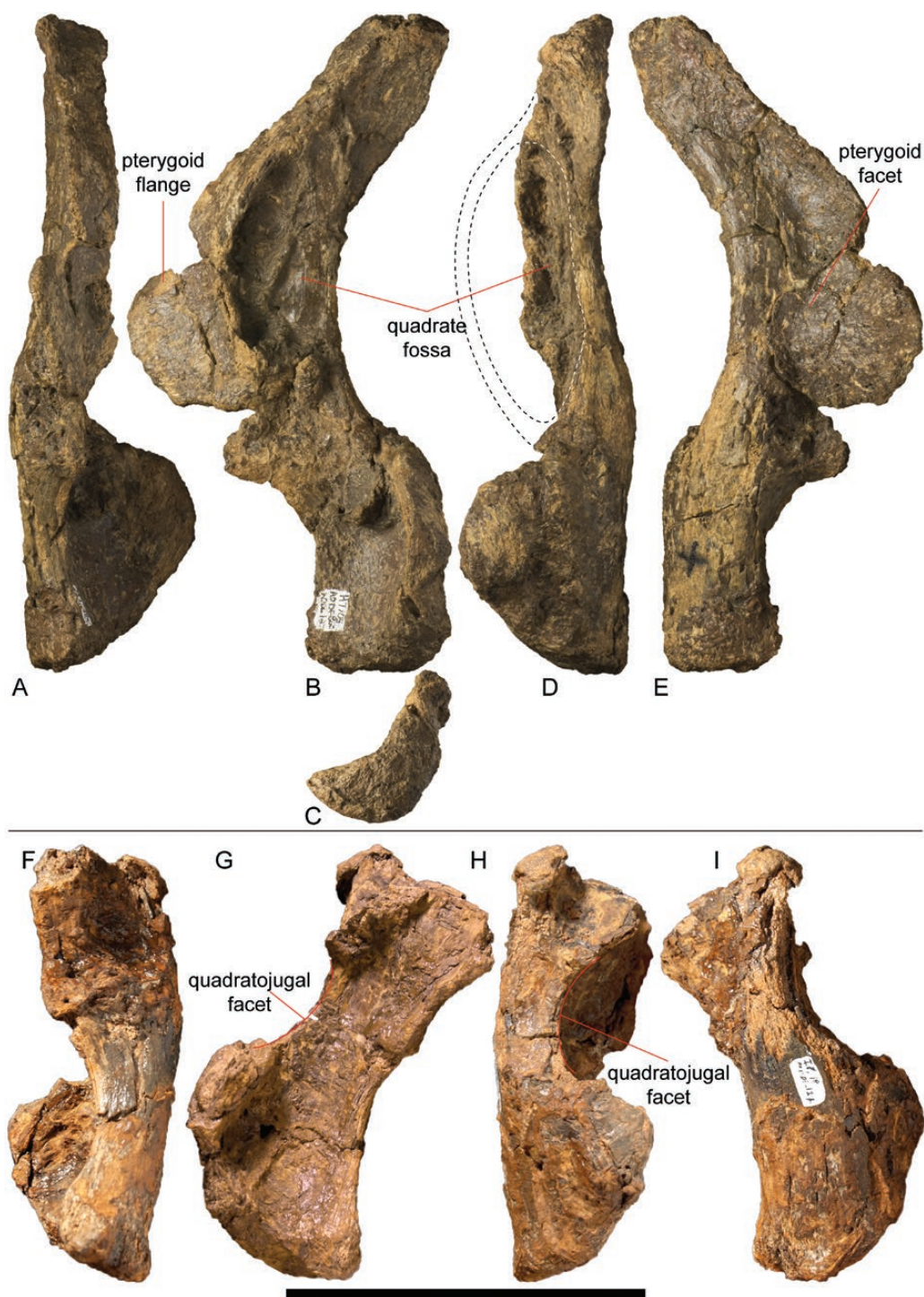


Figure 4. *Diamantinasaurus matildae* referred left and right quadrates (AODF 836). A–E, left quadrate in anterior (A), lateral (B), ventral (C), posterior (D) and medial (E) views. F–I, right quadrate in anterior (F), lateral (G), posterior (H) and medial (I) views. Scale bar: 100 mm.

Cretaceous of France (Díez Díaz *et al.*, 2012). In dorsal view, the frontal is hemi-hexagonal (Fig. 5A), similar to that of *Nemegtosaurus* (Wilson, 2005). The preserved dorsal surface undulates, such that it is mediolaterally

convex towards the orbital margin (lateral), deeply and doubly concave centrally, and mediolaterally convex near the midline frontal articulation. A similar median convexity is observed in ‘*Brachiosaurus*’ (D’Emic &

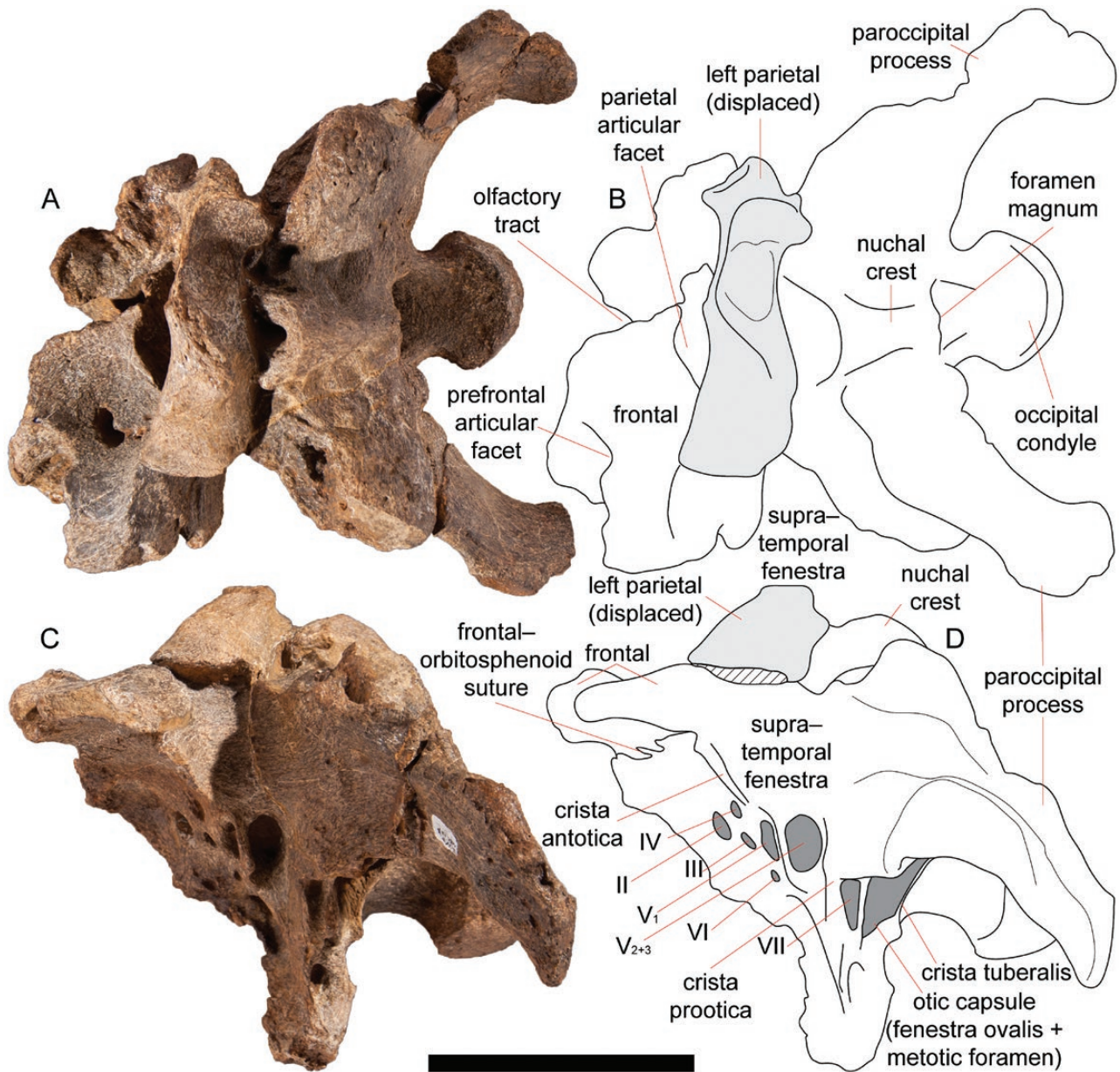


Figure 5. *Diamantinasaurus matildae* referred braincase (AODF 836) in dorsal (A, B) and left lateral (C, D) views. Scale bar: 100 mm.

Carrano, 2020), *Phuwiangosaurus* (Suteethorn *et al.*, 2009) and most titanosaurs (Curry Rogers, 2005; Mannion *et al.*, 2013; Martínez *et al.*, 2016), including *Ampelosaurus* Le Loeuff, 1995 (Le Loeuff, 2005), *Antarctosaurus* (Huene, 1929), *Rapetosaurus* (Curry Rogers & Forster, 2004) and *Saltasaurus* Bonaparte & Powell, 1980; (Powell, 1992, 2003). By contrast, no median convexity is present in the titanosaurs *Sarmientosaurus* (Martínez *et al.*, 2016), *Pitekunsaurus* Filippi & Garrido, 2008 (MAU-Pv-AG-446/5; P.D.M., pers. obs., 2014), *Jainosaurus* Hunt *et al.*, 1994 (Wilson *et al.*, 2009) or *Nemegtosaurus* (Wilson, 2005). The

raised lateral margin, which characterizes the frontals of *Antarctosaurus*, *Bonitasaura* and *Jainosaurus* (Wilson *et al.*, 2009; Gallina & Apesteguía, 2015; Mannion *et al.*, 2019a), is absent in *Diamantinasaurus*. In *Nemegtosaurus*, *Quaesitosaurus* and *Saltasaurus*, there is an anteromedial concavity on the dorsal surface of each frontal, near the nasal articulation (Wilson, 2005); however, the presence of this feature cannot be determined on the frontal of *Diamantinasaurus* because of its incomplete preservation. The grooves present on the dorsal surface of the frontal of *Saltasaurus* (Powell, 1992, 2003) are absent in *Diamantinasaurus*.

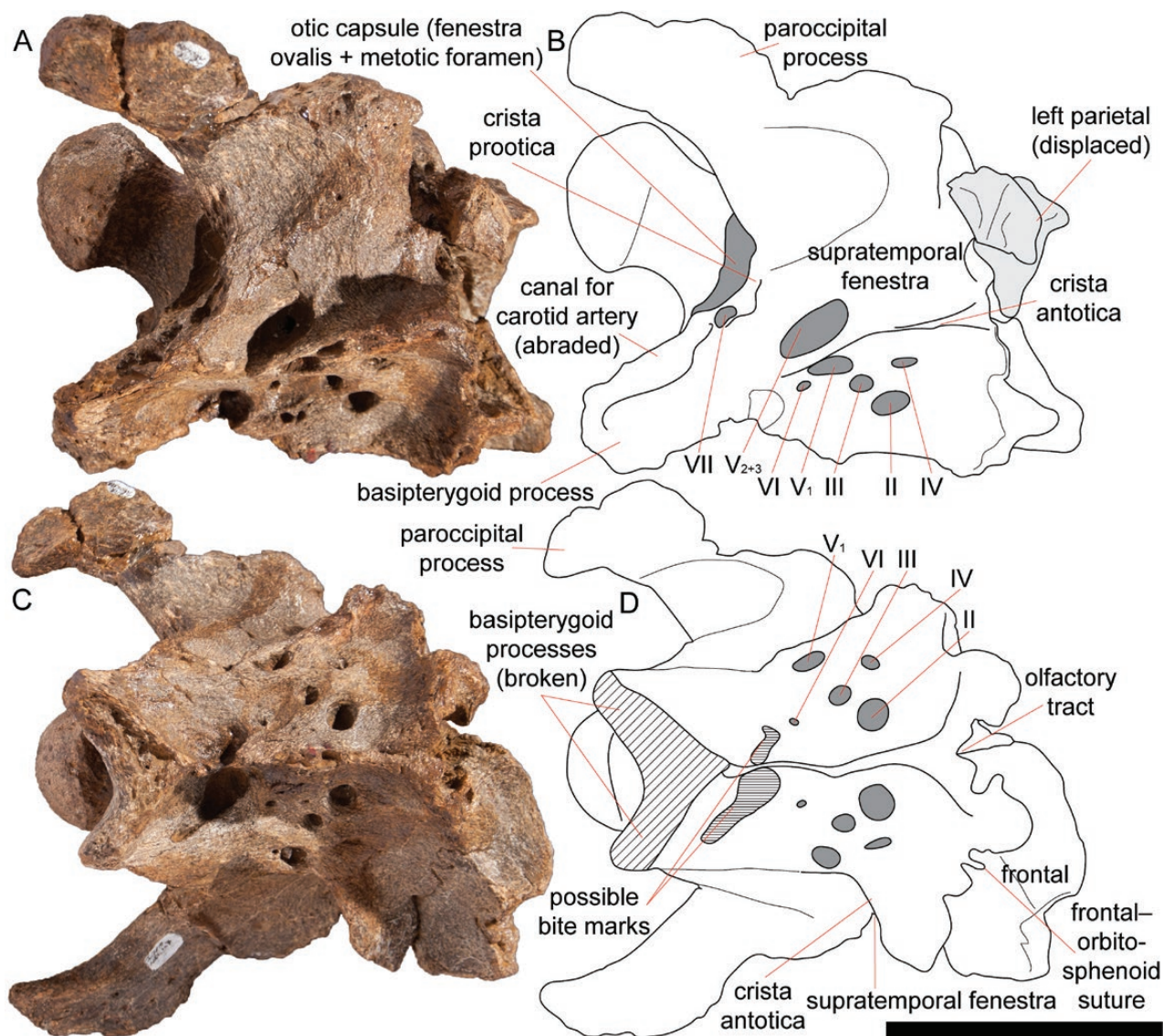


Figure 6. *Diamantinasaurus matildae* referred braincase (AODF 836) in right ventrolateral (A, B) and anteroventral (C, D) views. Scale bar: 100 mm.

The parietal articular surface is largely unobservable because the left parietal, which has been displaced from articulation, remains attached to the relevant region via matrix (Fig. 5A). The posteromedial margin of the frontal is visible in dorsal view (Fig. 5A, B), and it presents an anteriorly concave surface that is interpreted as the articulation point for the parietal. The poorly preserved sutural surface for the right frontal appears to be jagged, as in *Rapetosaurus* (Curry Rogers & Forster, 2004). This suggests that the frontals were not fused in *Diamantinasaurus*, as is the case in nearly all sauropods, with the exception of dicraeosaurids (Salgado & Calvo, 1992) and a small number of titanosaurs, consisting of a braincase from the latest Cretaceous of Spain [MPCM-HUE-8741, from

the Lo Hueco site, referred to in the literature as either *Ampelosaurus* sp. (Knoll *et al.*, 2013) or *Lohuecotitan pandafilandi* Diez Díaz *et al.*, 2016 (Knoll *et al.*, 2019)], *Narambuenatitan* (Filippi *et al.*, 2011), an unnamed form (MGPIFD-GR 118) from the latest Cretaceous of Argentina (Paulina-Carabajal & Salgado, 2007) and, possibly, *Antarctosaurus* (MACN 6904; S.F.P., P.D.M. and P.U., pers. obs. 2013). Anteriorly, the frontal would have articulated with the nasal medially and the prefrontal laterally. Neither articular surface appears to be complete, although in anterior view a distinct step is present between the two articular surfaces, with the medial surface (nasal) higher than the lateral (prefrontal) one; thus, the medial edge of the prefrontal would have overlapped the nasal. In dorsal view, the

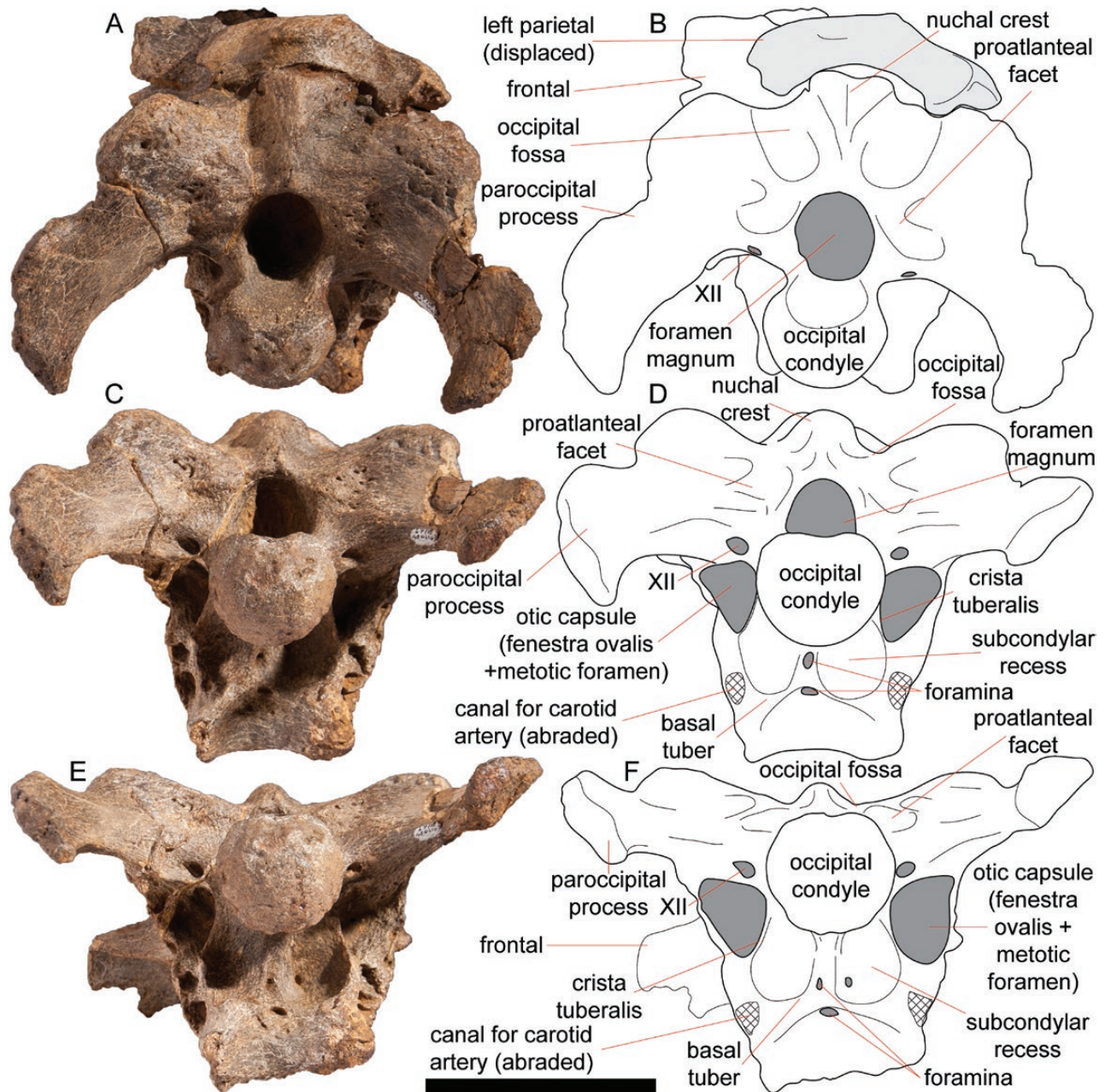


Figure 7. *Diamantinasaurus matildae* referred braincase (AODF 836) in posterodorsal (A, B), posterior (C, D) and posteroventral (E, F) views. Scale bar: 100 mm.

prefrontal contact is anteriorly concave (Fig. 5A), whereas the nasal contact (as preserved) is anteriorly convex, as is typical of macronarians (Whitlock, 2011b). The orbital (lateral) margin of the frontal curves posteroventrally to form the posterodorsal margin of the orbit (Fig. 5C, D). Unfortunately, the lateral margin is insufficiently complete to enable assessment of its shape in dorsal view or whether or not it was ornamented. The posterior surface of the frontal appears to have formed the anterior margin of the supratemporal fenestra,

as in *Ampelosaurus*, *Antarctosaurus*, *Bonatitan* Martinelli & Forasiepi, 2004, *Rapetosaurus* and *Saltasaurus* (Huene, 1929; Powell, 1992, 2003; Curry Rogers & Forster, 2004; Le Loeuff, 2005; Salgado *et al.*, 2015a). However, it is plausible that each parietal (both of which are incomplete anteromedially) possessed an anterior extension that ran along the posterior margin of the frontal and excluded it from the supratemporal fenestra, as in most neosauropods, including the titanosaurs *Nemegtosaurus*, *Sarmientosaurus* and

Tapuiasaurus (Wilson & Sereno, 1998; Wilson, 2005; Martínez *et al.*, 2016; Wilson *et al.*, 2016). Anteroventrally, the frontal is firmly adhered to the orbitosphenoid via an interdigitating suture that is still clearly visible (Figs 5C, D, 6C, D). By contrast, its posteroventral suture with the laterosphenoid is indiscernible. A similar distinction between these two suture margins is evident in *Nemegtosaurus* (Wilson, 2005) and would also have been the case in *Rapetosaurus* based on the morphology of the disarticulated frontals (Curry Rogers & Forster, 2004). The lateral half of the ventral surface of the frontal of *Diamantinasaurus* is deeply concave to accommodate the eyeball (Fig. 6C, D).

Parietal: Both parietals are preserved, but neither was found sutured to the braincase: the left parietal was found atop the braincase, adhered via matrix (Fig. 5A, B), whereas the right parietal was found isolated (Fig. 3E–I). Despite their dissociation, it seems likely that the parietals were fused to the top of the braincase *in vivo*. This is inferred because the right parietal appears to be broken along its otoccipital articular facet. This description, unless otherwise indicated, is based on the right parietal.

Both parietals appear to be incomplete medially (the right more so than the left), and anteromedially, where they would have been fused to the frontals. Each parietal is essentially quadrangular in anterior (Fig. 3E) and posterior views (Fig. 3F), being substantially wider mediolaterally (129 mm) than tall dorsoventrally (44 mm). The dorsoventral height of the occipital process of the parietal is slightly greater than that of the foramen magnum (42 mm). In nearly all other titanosaurs, the reverse is true (Wilson, 2002; Mannion *et al.*, 2013), although *Sarmientosaurus* is also characterized by a relatively taller occipital process (Martínez *et al.*, 2016). The medial half of the posterior surface is dominated by the occipital fossa, which is deepest medially and is demarcated along its medial, dorsal and lateral borders by a crescentic ridge. This ridge characterizes the parietal of all titanosaurs (Salgado & Calvo, 1997; Curry Rogers & Forster, 2004; Curry Rogers, 2005; Poropat *et al.*, 2016). However, the occipital fossa occupies only the medial half of the parietal of *Diamantinasaurus*; the lateral half of the parietal is dorsoventrally convex. Potentially, this feature is locally autapomorphic for *Diamantinasaurus* within Titanosauria, given that in most titanosaurs [aside, perhaps, from *Sarmientosaurus* (Martínez *et al.*, 2016)] almost the entire posterior surface of the parietal is occupied by the occipital fossa. The parietal occipital fossa of *Rapetosaurus* is shallow (Curry Rogers, 2009), but this might be an ontogenetic feature. In this regard, the parietal of *Diamantinasaurus* is morphologically most

similar to those of early-branching titanosauriforms (D'Emic & Carrano, 2020). The ventral surface of the parietal (Fig. 3I) comprises: (1) a small, flat, rhomboidal surface that would have abutted the supraoccipital (situated posteromedially); (2) a small, deeply concave, teardrop-shaped (anterolaterally tapered), broken surface that presumably contacted the laterosphenoid and/or prootic (situated anteromedially); and (3) a mediolaterally broad but shallow articular facet across much of the rest of the surface, which would have articulated with the otoccipital. Laterally, the ventral surface tapers to form a thin, non-articular ridge. This would have formed the anterior margin of the post-temporal fenestra, as in most non-diplodocoid eusauropods other than *Nemegtosaurus*, *Quaesitosaurus* and *Rapetosaurus*, wherein the parietal is excluded from this fenestra (Curry Rogers & Forster, 2001; Wilson, 2002, 2005), and *Tapuiasaurus*, in which this fenestra is absent (Wilson *et al.*, 2016). The anterior margin of the ventral surface of the parietal is manifested as a ridge. The majority of the anterior surface is shallowly concave where it forms the posterior margin of the supratemporal fenestra (Fig. 3E). Ventrolateral to this concave surface lies the ventromedially tapering facet that receives the squamosal. In lateral view, the squamosal facet of the parietal is anteriorly concave. The medial surface of the parietal comprises a dorsoventrally concave, anteroposteriorly convex, saddle-shaped and apparently non-articular surface (Fig. 3G). Anterior to this lies a broken facet, which is triangular (tapering dorsally) and jagged, and presumably contacted the frontal or an anterior continuation of the parietal. There was almost certainly no postparietal foramen. The dorsal surface is manifested as a smooth ridge. The overall morphology of the parietal implies that the supratemporal fenestrae were wider mediolaterally than was the space between them, distinguishing *Diamantinasaurus* from all titanosaurs, with the exception of *Sarmientosaurus* (Martínez *et al.*, 2016).

Supraoccipital: The subhexagonal supraoccipital is firmly sutured to the otoccipitals and would also have contacted the parietals. It forms the dorsal margin of the foramen magnum and makes a substantial contribution to the occipital fossae. Although the sutures between the supraoccipital and the otoccipitals have been obliterated, their position can be inferred based on directional changes in the surficial bone and on comparisons with other sauropod taxa, especially *Rapetosaurus*, which preserves a disarticulated, morphologically similar supraoccipital (Curry Rogers & Forster, 2004). The middle portion of the supraoccipital of *Diamantinasaurus* rises to form a low, anterodorsally–posteroventrally elongate nuchal crest. This structure is transversely flared dorsally

and narrow ventrally, fading out before reaching the dorsal margin of the foramen magnum. The presence of a nuchal crest distinguishes *Diamantinasaurus* from a small number of titanosaurs [*Antarctosaurus*, *Narambuenatitan* and *Pitekunsaurus* (MAU-Pv-AG-446/5; P.D.M., pers. obs., 2014)] in which the posterior surface of the supraoccipital is smooth, lacking any distinct midline ridge. *Diamantinasaurus* also lacks the midline groove that extends along the supraoccipital of *Muyelensaurus* (Calvo *et al.*, 2007a), *Bonatitan* (Martinelli & Forasiepi, 2004; Salgado *et al.*, 2015a), *Saltasaurus* (Powell, 1992, 2003), *Rapetosaurus* (Curry Rogers & Forster, 2004) and an indeterminate titanosaur specimen (MML-194) from the latest Cretaceous of Argentina (García *et al.*, 2008). The anterior end of the nuchal crest preserves a dorsally tapered, triangular opening that was probably overlapped by the paired parietals anteriorly. Either side of the nuchal crest, the supraoccipital hosts an occipital fossa, and each fossa rises laterally towards the base of its ipsilateral paroccipital process. The supraoccipital is taller dorsoventrally (55 mm) than the foramen magnum (42 mm), as in most sauropods (Wilson, 2002; Mannion *et al.*, 2013), including *Nemegtosaurus* (Wilson, 2005), *Saltasaurus* (Powell, 1992, 2003), *Sarmientosaurus* (Martínez *et al.*, 2016) and *Tapuiasaurus* (MZSP-PV 807; P.D.M., pers. obs., 2019). However, in a small number of titanosaurs [*Malawisaurus* (Gomani, 2005), *Pitekunsaurus* (Filippi & Garrido, 2008) and *Rapetosaurus* (Curry Rogers & Forster, 2004)] the foramen magnum is taller than the supraoccipital. In *Diamantinasaurus*, the nuchal crest is also 1.2 times taller than the occipital condyle.

Otoccipital: The exoccipital and opisthotic of sauropods are often fused, with their line of suture indistinct, presumably because these two elements coalesced at an early stage of development (Janensch, 1935–1936; Berman & Jain, 1982; Madsen *et al.*, 1995); consequently, they are referred to herein as the otoccipital. The exoccipital portions of the otoccipitals form the majority of the margins of the foramen magnum (with the exception of the dorsal margin, which is formed by the supraoccipital) and also the dorsolateral portions of the occipital condyle (Fig. 7A–D). The foramen magnum is taller dorsoventrally (42 mm) than it is wide transversely (36 mm), as in many, but not all, macronarians (Martínez *et al.*, 2016). Among titanosaurs, the foramen magnum is taller than wide in *Sarmientosaurus* (Martínez *et al.*, 2016), *Pitekunsaurus* (Filippi & Garrido, 2008), *Antarctosaurus* (Powell, 2003), *Bonatitan* (Martinelli & Forasiepi, 2004; Salgado *et al.*, 2015a), *Quaesitosaurus* and *Nemegtosaurus* (Wilson, 2005), *Jainosaurus* (Wilson *et al.*, 2009) and *Vahiny* (Curry Rogers & Wilson, 2014; by contrast, the foramen magnum is subcircular

in *Malawisaurus* (Gomani, 2005), *Kaijutitan* (Filippi *et al.*, 2019), *Narambuenatitan* (Filippi *et al.*, 2011), *Muyelensaurus* (Calvo *et al.*, 2007a), *Saltasaurus* (Powell, 1992, 2003), *Rapetosaurus* (Curry Rogers & Forster, 2004) and MPCM-HUE-8741 (Knoll *et al.*, 2013). Each ventrolateral margin of the foramen magnum bears a small opening that communicates with another opening at the base (medial) of the paroccipital processes; this represents the passage of CN XII (hypoglossal). Therefore, in *Diamantinasaurus*, CN XII passes through the exoccipital portion of the otoccipital only (not the basioccipital). The presence of a single exit for CN XII on each side of the occipital condyle aligns *Diamantinasaurus* with most titanosauriforms (Paulina Carabajal, 2012), including the titanosaurs *Bonatitan* (Martinelli & Forasiepi, 2004), *Rapetosaurus* (Curry Rogers & Forster, 2004), MPCM-HUE-8741 (Knoll *et al.*, 2013) and *Malawisaurus* (Gomani, 2005; Andrzejewski *et al.*, 2019). By contrast, there are two openings for CN XII per side in *Sarmientosaurus* (Martínez *et al.*, 2016) and a probable titanosaur specimen (CCMGE 628/12457) from the early Late Cretaceous of Uzbekistan (Sues *et al.*, 2015). This is the plesiomorphic condition in sauropods, and there is variation between one and two openings in specimens referred to the early-branching macronarians *Camarasaurus* and *Giraffatitan* (Janensch, 1935–1936; Witmer *et al.*, 2008; Knoll & Schwarz-Wings, 2009; Paulina Carabajal, 2012). Immediately dorsal to the external opening for CN XII in *Diamantinasaurus*, a slight ridge extends laterally to approximately three-quarters the length of the paroccipital process (Fig. 7C, D). This ridge might represent the boundary between the opisthotic, which forms the majority of the paroccipital process, and the exoccipital, which forms the ventromedial portion. It has also been observed in *Nemegtosaurus* and *Quaesitosaurus* by Wilson (2005), who suggested that it formed the ventral boundary of the occipital fossa. Dorsal to this ridge, and immediately lateral to the foramen magnum, lies the proatlantal facet, which constitutes a raised protuberance that is accompanied slightly further laterally by a small depression (Fig. 7A–D). Similar proatlantal facets have been identified in many other titanosaurs, including *Isisaurus* (Wilson & Upchurch, 2003; Berman & Jain, 1982), *Kaijutitan* (Filippi *et al.*, 2019), *Quaesitosaurus* and *Nemegtosaurus* (Wilson, 2005), *Saltasaurus* (Powell, 1992, 2003) and *Tapuiasaurus* (Wilson *et al.*, 2016). By contrast, most non-diplodocoid sauropods lack such facets, including the titanosaurs *Ampelosaurus*, *Malawisaurus*, *Rapetosaurus* and *Sarmientosaurus* (Le Loeuff, 2005; Wilson *et al.*, 2005; Martínez *et al.*, 2016; Poropat *et al.*, 2016; Mannion *et al.*, 2019b). These facets have been interpreted as demarcating the supraoccipital–exoccipital contact in some titanosaurs (Salgado *et al.*, 2015a), and in

Diamantinasaurus a subtle ridge dorsolateral to each facet is herein interpreted as a continuation of this suture line. This suture line is indistinct in *Nemegtosaurus* (Wilson, 2005). The excavation lateral to each proatlantal facet in *Diamantinasaurus* is much less common in sauropods and is currently known only in some dicraeosaurids (Xu *et al.*, 2018), the ‘basal’ somphospondylan *Tambatitanis* Saegusa & Ikeda, 2014 and the titanosaur *Narambuenatitan* (MAU-Pv-N-425; P.D.M., pers. obs., 2014). As such, it is herein regarded as a local autapomorphy of *Diamantinasaurus*.

The paroccipital processes are formed largely by the opisthotic portions of the otoccipitals. The left paroccipital process is more completely preserved than the right, which is missing a small portion of its dorsal surface. Each paroccipital process articulated with the parietal anteromedially. The squamosal articulated with the anterodorsal surface of the dorsal notch of the paroccipital process. Immediately ventral to this, near the lateral margin of the paroccipital process, the head of the quadrate articulated with the otoccipital. The paroccipital processes project posteroventrally at ~45° relative to the occipital plane. They are thickened proximally, slightly narrower at midlength, and expand slightly near their distal terminations to form ventrally directed ‘prongs’ (Fig. 7A–D). Distoventral prongs on the paroccipital processes (‘ventral non-articular processes’), first recognized as a derived character state uniting *Antarctosaurus* and *Saltasaurus* (Powell, 1986), characterize nearly all titanosaurs (Wilson, 2002), with the exception of *Tapuiasaurus* (Wilson *et al.*, 2016). Those of *Diamantinasaurus* are not developed to the same degree as the processes of *Antarctosaurus* (Huene, 1929; Salgado & Calvo, 1997), *Quaesitosaurus* (Kurzanov & Bannikov, 1983), *Rapetosaurus* (Curry Rogers & Forster, 2004) or *Saltasaurus* (Powell, 1992, 2003), but more closely approach the condition seen in *Jainosaurus* (Wilson *et al.*, 2009) and *Narambuenatitan* (Filippi *et al.*, 2011).

Basioccipital: As in all sauropods, the basioccipital of *Diamantinasaurus* forms the majority of the occipital condyle and the dorsal part of the basal tubera. A relatively minor contribution to each dorsolateral margin of the occipital condyle is presumed to have been made by the exoccipital portion of the otoccipital, as documented in *Rapetosaurus* (Curry Rogers & Forster, 2004) and *Nemegtosaurus* (Wilson, 2005). The occipital condyle is more or less ventrally directed relative to the plane of the occiput (Fig. 5C, D), as in diplodocoids (Berman & McIntosh, 1978; Salgado & Calvo, 1992), *Isisaurus* (Wilson *et al.*, 2005, 2009) and *Saltasaurus* (Powell, 1992, 2003; Upchurch, 1998). The occipital condyle is wider transversely (52 mm) than tall dorsoventrally (46 mm; Fig. 7C, D) and is 1.1 times the height of the foramen magnum. All margins of the

occipital condyle are convex except the dorsal margin, which is slightly concave in line with the foramen magnum (Fig. 7A–D). This concavity, formed, in part, by the paired opisthotics, would have accommodated the ventral surface of the spinal cord. This corresponds well to the morphology of the occipital condyles of *Antarctosaurus* (Huene, 1929; Powell, 2003), *Isisaurus* (Berman & Jain, 1982) and *Nemegtosaurus* (Wilson, 2005). The stem of the occipital condyle separates the condylar ball from the posterior margin of the skull by 20 mm. Immediately ventral to the occipital condyle is a subtle, vertically oriented ridge, which is bordered on either side by a round subcondylar recess. The left recess is somewhat smaller than the right, because the ridge is slightly offset to the left (Fig. 7C–F). A small foramen is present, immediately to the right of the ridge dividing the paired recesses; although this might be an artefact of preparation, we consider it to be a natural feature. The ridge that forms the dorsolateral margin of the subcondylar recess also separates it from the otic capsule. At the ventromedial junction of the subcondylar recesses, a small, ventrally directed, transversely elongate foramen is present. A comparable foramen is variably present among eusauropods, including titanosaurs (Wilson, 2002; Mannion *et al.*, 2013, 2019a). For example, it is present in *Antarctosaurus*, *Saltasaurus* and *Sarmientosaurus* (Powell, 1992, 2003; Martínez *et al.*, 2016), whereas it is absent in *Jainosaurus*, *Lirainosaurus*, (Sanz *et al.*, 1999) *Malawisaurus* and *Rapetosaurus* (Gomani, 2005; Curry Rogers, 2009; Wilson *et al.*, 2009; Díez Díaz *et al.*, 2011). The combined height of the occipital condyle and basal tubera is 102 mm, with the former contributing 45% of this total height. In early-branching titanosauriforms, such as *Giraffatitan* (Janensch, 1935–1936), *Phuwiangosaurus* (Suteethorn *et al.*, 2009) and *Mongolosaurus* Gilmore, 1933 (Mannion, 2011), and in the titanosaur *Nemegtosaurus* (Wilson, 2005), this ratio is ≥ 0.6 (Mannion *et al.*, 2013), but in all other titanosaurs this ratio is < 0.6 [e.g. 0.45 in *Malawisaurus* (Gomani, 2005); 0.5 in *Saltasaurus* (Powell, 1992, 2003)], as is the case in most non-titanosauriform sauropods (Mannion *et al.*, 2013).

Basisphenoid: The basisphenoid forms the floor of the braincase, such that its dorsal margin contacts the basioccipital, prootic, laterosphenoid and orbitosphenoid. It forms the majority of the basal tubera, the ventral margin of the metotic foramen, the preserved portion of the basiptyergoid processes, and the ventral margins of several CN openings. The left basal tuber, which also preserves part of the left basiptyergoid process, was found 6 m distant from the rest of the braincase (Supporting Information, Fig. S1), but keys into the broken surface ventral to the left metotic foramen (note that this fragment is

not included in the figures). The suture between the basisphenoid and basioccipital cannot be observed, as in most sauropod braincases (Upchurch *et al.*, 2004; Wilson, 2005), other than juvenile specimens, such as *Rapetosaurus*, wherein traces of the suture remain visible (Curry Rogers & Forster, 2004). Thus, the extent to which each element contributed to the subcondylar recesses and the basal tubera cannot be determined. Nevertheless, it is presumed that the basisphenoid contributed to the basal tubera at least.

As preserved, the basal tubera (which host the subcondylar recesses) extend 50 mm below the base of the occipital condyle. The basal tubera of *Diamantinasaurus* appear to have lacked significant relief, although this is almost certainly exaggerated by their incomplete preservation. As preserved, the basal tubera of *Diamantinasaurus* resemble the anteroposteriorly compressed, sheet-like processes of many other titanosaurs (e.g. *Antarctosaurus*, *Jainosaurus*, *Muyelensaurus*, *Nemegtosaurus*, *Pitekunsaurus*, *Quaesitosaurus*, *Saltasaurus*, *Tapuiasaurus*, *Vahiny*) (Wilson, 2002). However, based on the preserved portion of the left basal tuber, their relief was substantially greater than that observed in these taxa. Thus, it is more likely that the basal tubera of *Diamantinasaurus* were anteroposteriorly thicker *in vivo*, like the basal tubera of the titanosaurs *Bonatitan*, *Lirainosaurus*, *Malawisaurus*, *Rapetosaurus* and *Sarmientosaurus* (Curry Rogers & Forster, 2004; Gomani, 2005; Díez Díaz *et al.*, 2011; Martínez *et al.*, 2016). The transverse width across the paired basal tubera is 93 mm in *Diamantinasaurus*; thus, the ratio of this value to the transverse width of the occipital condyle is 1.8. Among titanosaurs, most taxa have a comparable or even greater ratio (Mannion, 2011: table 1), but this ratio is < 1.5 in *Nemegtosaurus* (Wilson, 2005) and *Rapetosaurus* (Curry Rogers & Forster, 2004). The basal tubera are divergent from each other only at their ventral ends, with an angle of ~40° (based on the preserved portion of the left one); this distinguishes *Diamantinasaurus* from most titanosauriforms, in which this angle of divergence is > 50° (Curry Rogers, 2005; Calvo *et al.*, 2007a; Poropat *et al.*, 2016). *Sarmientosaurus* (Martínez *et al.*, 2016), *Quaesitosaurus* (Curry Rogers & Wilson, 2014: fig. 6f) and *Saltasaurus* (Curry Rogers, 2005) share a shallow divergence angle with *Diamantinasaurus*. The anterior surface of the isolated lateral rim of the left basal tuber is smoothly convex, whereas the posterior surface is relatively flat, triangular in outline, tapering dorsally to form a thin crista tuberalis (Figs 5C, D, 6A, B). The medial margin of the ventral portion of the basal tuber is slightly convex, whereas the lateral margin as a whole is concave. Its dorsomedial surface hosts two relatively deep concavities: an upper one that faces dorsomedially and a lower one that faces

anteromedially. The upper concavity appears not to correspond to a true anatomical feature, instead being the point of attachment for the basal tuber. The lower concavity is the continuation of the canal for the carotid artery, the abraded continuation of which can be seen ventrolateral to the left subcondylar recess.

A small foramen is present between the basal tubera and the basiptyergoid processes (ventral to that between the subcondylar recesses; Fig. 7E, F). The presence of this 'basiptyergoid recess' is the plesiomorphic eusauropod condition (Wilson, 2002) that is retained in the titanosaurs *Isisaurus*, *Nemegtosaurus* (Wilson, 2005) and *Rapetosaurus* (Curry Rogers & Forster, 2004) but is absent in all other titanosaurs for which this can be assessed (Poropat *et al.*, 2016; Mannion *et al.*, 2019a). The angle at which the basiptyergoid processes diverged from one another cannot be determined because only their uppermost portions are preserved.

Prootic: The prootic is a ventrally tapered element that is sutured to the laterosphenoid anteriorly. The crista prootica (otosphenoidal crest) of *Diamantinasaurus*, which is situated posterior to this suture, lacks the leaf-like process seen in some dicraeosaurids (Salgado & Calvo, 1992). The prootic is sutured to the opisthotic section of the otoccipital posteriorly, as in other sauropods (Upchurch *et al.*, 2004). It is also sutured to the basisphenoid ventrally, the basioccipital posteriorly (with the presumed boundary between the two marked by the crista tuberalis), and would have contacted the parietal dorsally. The prootic is penetrated by CN VII (facial) and the otic capsule, which houses the fenestra ovalis and the metotic foramen [CN IX (glossopharyngeal), CN X (vagus) and CN XI (accessory)]. The otic capsule of *Diamantinasaurus* is relatively large (23 mm transversely, 33 mm dorsoventrally) and is separated from the opening for CN XII dorsally and from the opening for CN VII anteriorly by very thin ridges. However, the crista interfenestralis cannot be observed. The posterior margin of the otic capsule is formed by the crista tuberalis. A shallow groove runs ventrally from the otic capsule along the posterior surface of the basal tuber. Ventral to the otic capsule, the braincase is broken on both sides.

Laterosphenoid: The laterosphenoid lies posterior to the orbitosphenoid, ventral to the frontal, anterior to the otoccipital and anterodorsal to the prootic. It forms the lateral wall of the braincase, posterior to the orbitosphenoid, and is flared laterally to form the posterior surface of the orbit (along with the posteriormost portion of the frontal). This flared portion also separates it from the supratemporal fenestra. The laterosphenoid is presumed to have been sutured to

the orbitosphenoid along a line passing through the openings for CN IV and CN III towards CN VI (which was probably hosted on the parabasisphenoid), as interpreted for *Rapetosaurus* (Curry Rogers & Forster, 2004) and *Bonatitan* (Martinelli & Forasiepi, 2004); this differs from the situation observed in *Nemegtosaurus* and *Quaesitosaurus*, wherein the suture line was interpreted to have passed through the openings for CN IV and CN V and a large opening dorsal to CN IV (Wilson, 2005). As in *Bonatitan*, a raised section of bone between the openings for CN IV and CN III indicates the position of a portion of this suture line (Martinelli & Forasiepi, 2004). The opening for the orbitocerebral vein could not be identified in *Diamantinasaurus*. The laterally projecting portion of the laterosphenoid forms the crista antotica, which divides the opening for CN V into two regions. Given that CN V is the trigeminal nerve, it is likely that these two foramina represent the passages for the three branches of the nerve (with the foramen anterior hosting CN V₁ and the posterior foramen hosting CN V₂₊₃); the fact that the two openings are present on both sides of the braincase, despite the less complete and poorer preservation of the right laterosphenoid, suggests that these foramina are genuine anatomical structures, not preservational or preparational artefacts. This would appear to link *Diamantinasaurus* with *Sarmientosaurus*; in the latter taxon, the presence of three discrete openings for CN V was regarded as autapomorphic (Martínez *et al.*, 2016). All other titanosaurs are characterized by a single ossified opening for CN V (Martínez *et al.*, 2016), and this appears to be the case in all eusauropods for which this can be assessed, with the exception of *Shunosaurus* Dong *et al.*, 1983, which also has two openings (Chatterjee & Zheng, 2002). We note that *Phuwiangosaurus* was described as having two openings for CN V (Suteethorn *et al.*, 2009) but could not corroborate this interpretation based on the published figures (in which the upper CN V opening appears to be a fossa, and in which the exit for CN VII was not identified). As in *Antarctosaurus*, *Bonatitan*, *Rapetosaurus* and *Saltasaurus*, the largest (and posteriormost) trigeminal nerve opening (18 mm anteroposteriorly × 13 mm dorsoventrally) in *Diamantinasaurus* is larger than that for the optic nerve, which is approximately circular, with a diameter of 10 mm (Huene, 1929; Powell, 1992, 2003; Curry Rogers & Forster, 2004; Martinelli & Forasiepi, 2004). The largest opening for CN V is interpreted to lie on the suture between the laterosphenoid and prootic, whereas the other is situated anterior to the crista antotica.

Orbitosphenoid: The orbitosphenoid meets its counterpart anteriorly and is fused to the frontal dorsally via an interdigitating suture. It is sutured

to the laterosphenoid posteriorly via a seemingly smooth surface, which is interpreted to have traced a line through several CN openings (see above) and to have contacted the basisphenoid ventrally. The openings for CN I (olfactory) would have passed between the sutured orbitosphenoids at the anterior extremity of the braincase. This region of the skull is incompletely preserved, although the opening for these nerves is large, as also observed in *Saltasaurus* (Powell, 1992). Posterioventral to the opening for CN I, on the anterolaterally facing surface of the braincase of *Diamantinasaurus*, is the opening for CN II (optic). It is fairly large (10 mm in diameter) and essentially circular. Immediately anterior to this, the lateral wall of the braincase is divided into two concave surfaces (which would have accommodated the eyes), separated by an essentially vertical ridge. Immediately posterior to the foramen for CN II, the foramen for CN III (oculomotor) is present. The latter is separated from the foramen for CN II by 5 mm of bone and is markedly smaller (6 mm in diameter). The foramen for CN IV (trochlear) is located immediately dorsal to CN III (separated by 10 mm) and posterodorsal to CN II (separated by 13 mm). As mentioned above, the orbitosphenoid forms the anterior border of CN III, CN IV and CN VI (the rest of which lies on the basisphenoid). The opening for CN VI (abducens) is located posterolateral to CN II and immediately ventral to the opening for CN III, as in *Antarctosaurus*, *Jainosaurus*, *Malawisaurus* and *Vahiny* (Powell, 2003; Gomani, 2005; Wilson *et al.*, 2009; Curry Rogers & Wilson, 2014). By contrast, in many other titanosaurs, including *Bonatitan*, *Rapetosaurus*, *Saltasaurus*, *Sarmientosaurus* and *Tapuiasaurus* (Powell, 1992, 2003; Curry Rogers & Forster, 2004; Martinelli & Forasiepi, 2004; Martínez *et al.*, 2016; Wilson *et al.*, 2016), the foramen for CN VI lies anteroventral to that for CN III.

Endocranium: The excellent preservation of the braincase of *Diamantinasaurus* facilitated a thorough description and interpretation of the endocranial cavity (Figs 8–11; Table 2). The endoneurocranial surface is well preserved, showing no post-mortem compressive distortion, except for some minor ruptures. However, the dorsal contour of the precerebellar domain of the natural endocast cannot be determined (Fig. 12); the right frontal is missing, and both parietals have been displaced. Most of the endoneurocranial cavity and the majority of the neural and vascular canals were filled with the same iron-rich sediment that also infiltrated some of the neurocranial bones of *Diamantinasaurus* (Fig. 13). This sediment enhanced the visibility of some structures, but expedited their segmentation only when it filled them exclusively (e.g. most of the neural and vascular canals, and the olfactory and optic

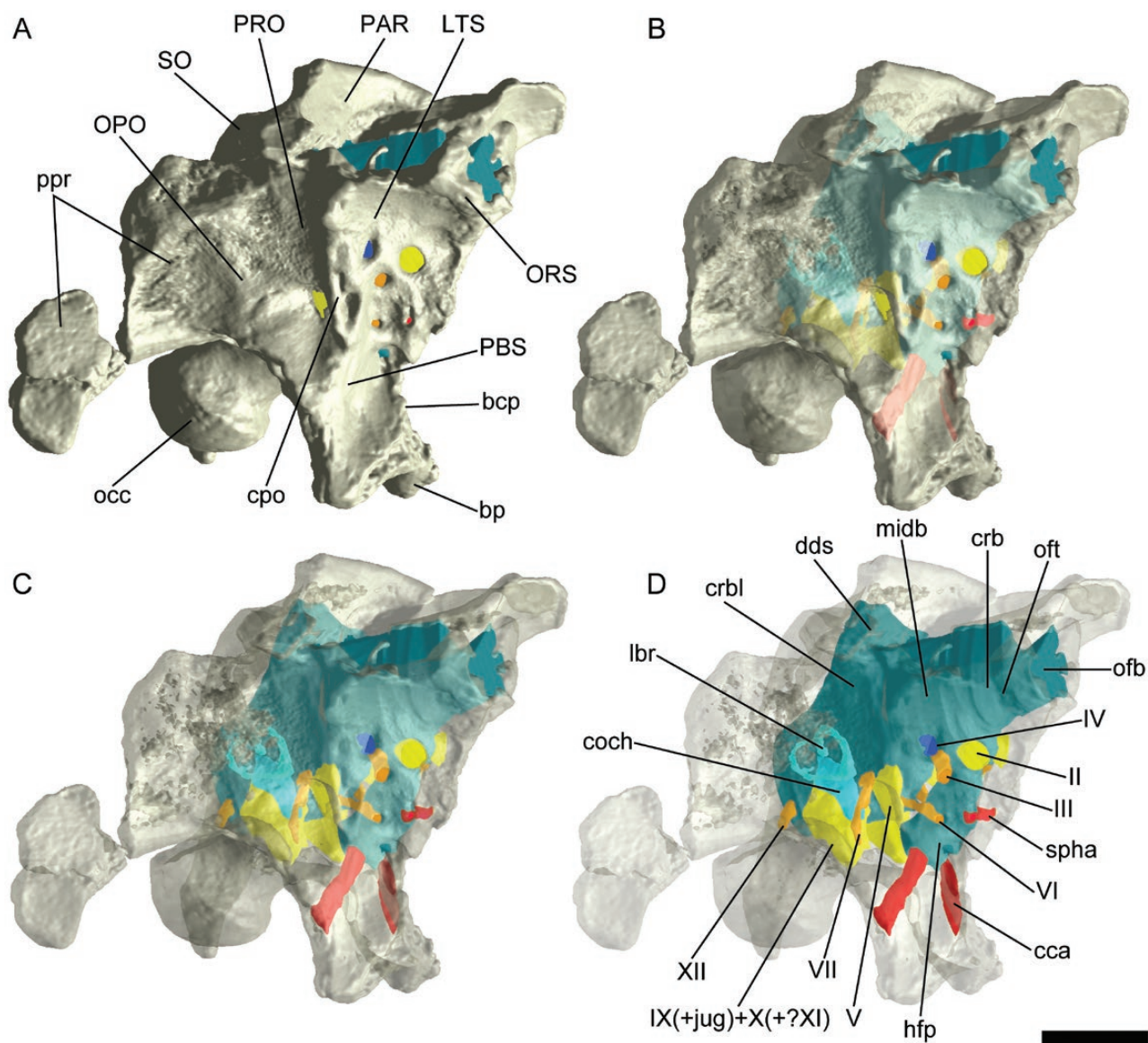


Figure 8. *Diamantinasaurus matildae* referred braincase (AODF 836). A–D, three-dimensional digital reconstruction of the endocranium and volume rendering of the braincase in anteroventral right lateral view, with the endocranium opaque and the surrounding neurocranial bones opaque to semitransparent. Scale bar: 40 mm.

tracts; Fig. 13A–C). On the contrary, this sediment also made the same procedure very difficult when it contaminated bone tissue surrounding the cavities and canals and obscured their original contours (Fig. 13D). Some problematic areas and objects were outlined by mirroring the better-preserved side (e.g. dorsal dural sinus; Fig. 13E), whereas others were approximated reasonably based on other partly visible objects (e.g. fissura metotica, vestibulum and cochlea). Some structures could not be reconstructed.

The surface rendered model of the endocranium of *Diamantinasaurus* terminates anteriorly at the

projection of the olfactory passage and posteriorly at the foramen magnum (Fig. 14). The maximum anteroposterior length of the endocranium is 118 mm. The hindbrain portion (the only part that can be measured) increases in dorsoventral height and transverse width from posterior to anterior. The overall maximum transverse width of the endocranium in *Diamantinasaurus* is presumed to have been across the cerebral hemispheres. As in most sauropods (Hopson, 1979), the endocranium of *Diamantinasaurus* is relatively short and deep and has a sigmoid shape in lateral view. The sigmoid pattern is given by two flexures: the pontine

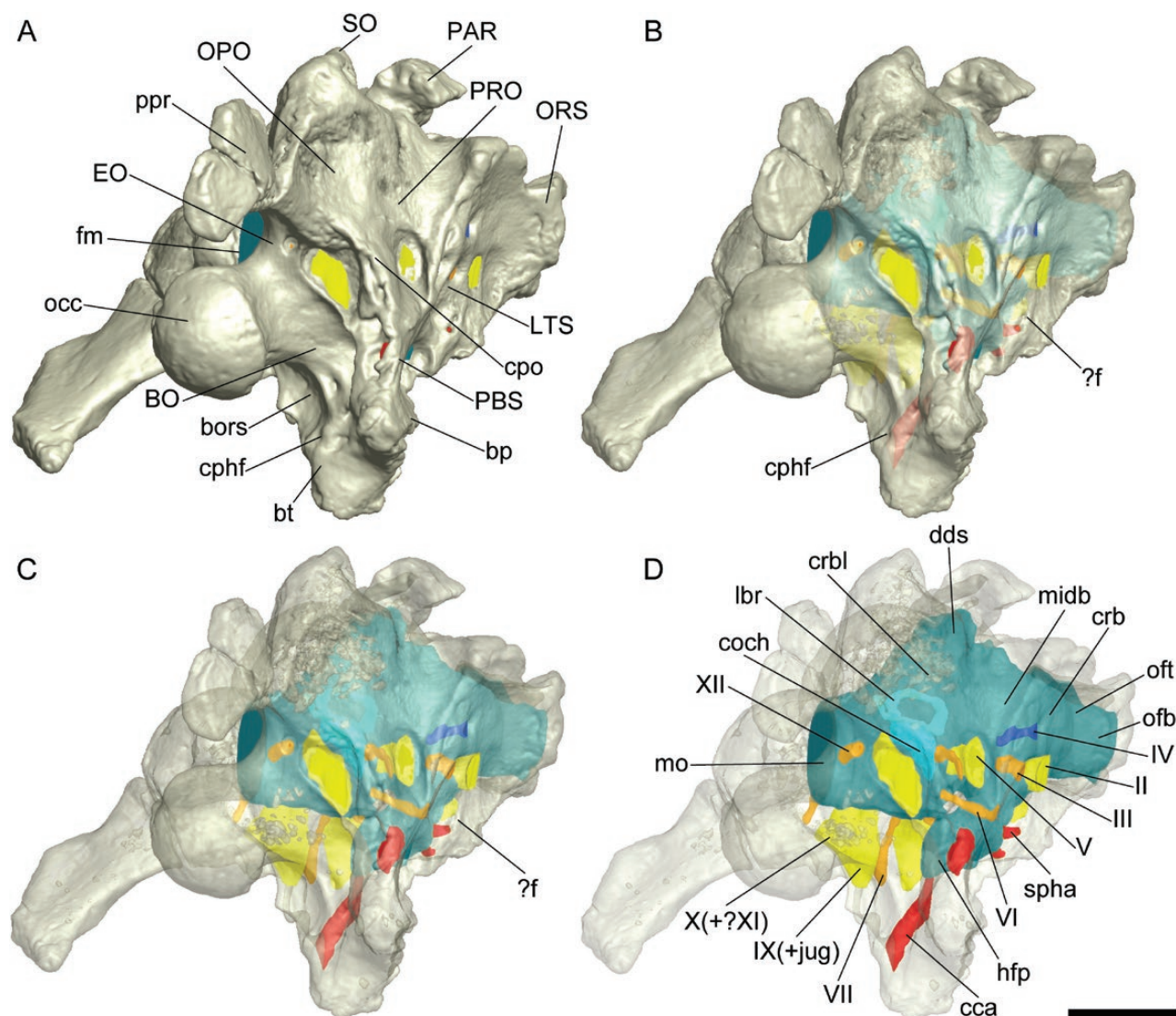


Figure 9. *Diamantinasaurus matildae* referred braincase (AODF 836). A–D, Three-dimensional digital reconstruction of the endocranium and volume rendering of the braincase in posteroventral right lateral view, with the endocranium opaque and the surrounding neurocranial bones opaque to semitransparent. Scale bar: 40 mm.

flexure (49°) is more prominent than the cerebral one (37°) in *Diamantinasaurus*. The sigmoid pattern and overall endocranium outline of *Diamantinasaurus* are similar to those seen in *Giraffatitan* (Janensch, 1935–1936; Knoll & Schwarz-Wings, 2009) and *Sarmientosaurus* (Martínez *et al.*, 2016).

The volume of the endoneurocranial cavity, including the hypophyseal extension, is $202\,000\text{ mm}^3$, and the volume of the canals transmitting the cranial nerves is $23\,000\text{ mm}^3$. Therefore, the total volume of the endocranium of *Diamantinasaurus* is $\sim 225\,000\text{ mm}^3$. This value is not definitive because of the missing dorsal portion mentioned above; nevertheless, the calculated total endocranium volume of *Diamantinasaurus* is much greater than that of *Apatosaurus* Marsh, 1877

[$125\,140\text{ mm}^3$ (Balanoff *et al.*, 2010)] or *Amargasaurus* Salgado & Bonaparte, 1991 [$150\,000\text{ mm}^3$ (Paulina Carabajal *et al.*, 2014)] and is comparable to estimates for the endocranium volume of *Giraffatitan* [$198\,000$ – $233\,000\text{ mm}^3$ (Knoll & Schwarz-Wings, 2009)].

On the forebrain endocranium, it was possible to recognize the olfactory tracts and bulbs, the cerebral hemispheres, the diencephalon, the optic tracts and the hypophyseal extension (Fig. 14F). The olfactory and cerebral domains are separated by a dorsally short constriction that is visible laterally. The olfactory endocranium rapidly expands anterior to the constriction and forms a bulbous structure. This structure shows a meandering surface anteriorly, where it displays a branch-like configuration that

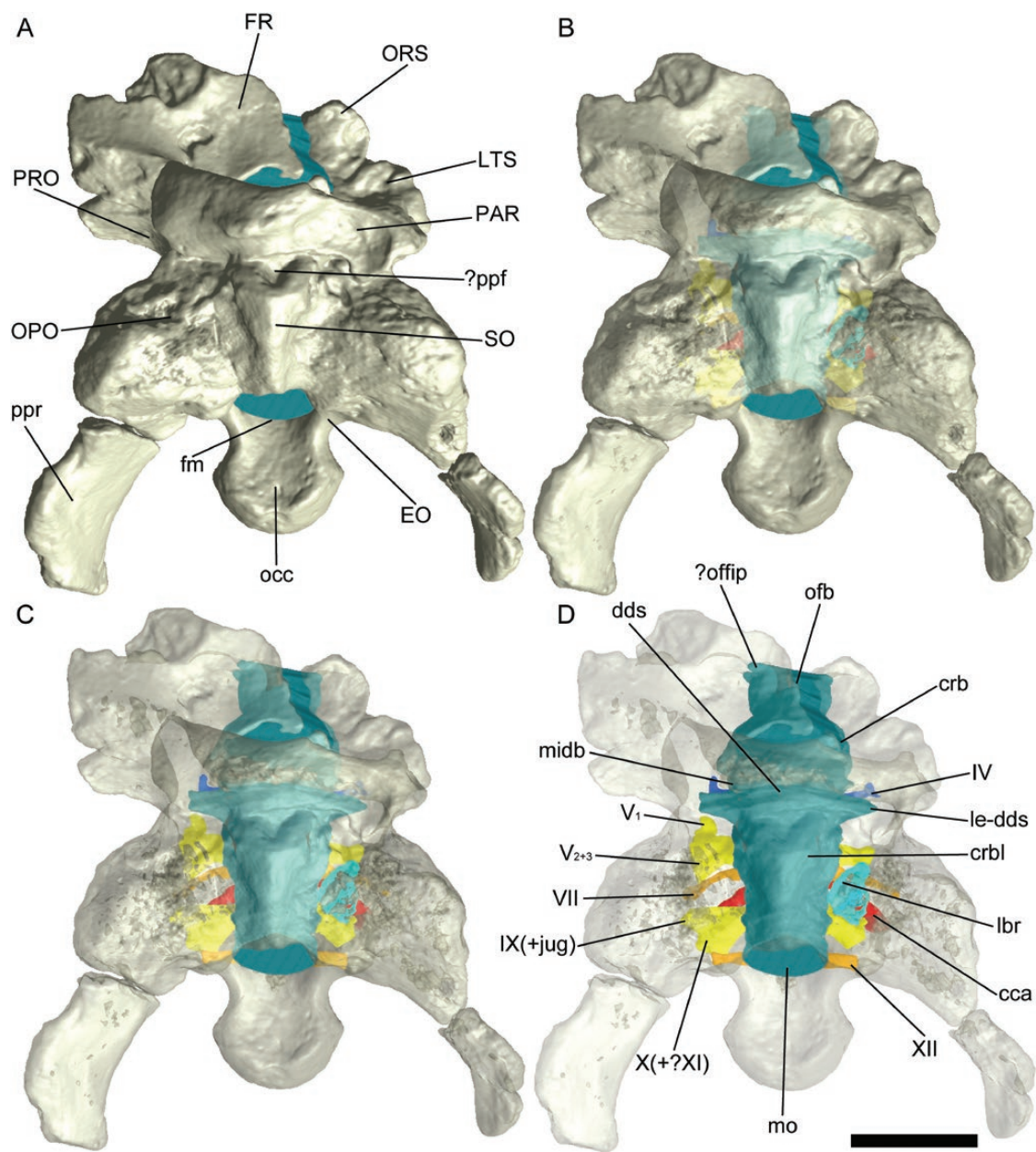


Figure 10. *Diamantinasaurus matildae* referred braincase (AODF 836). A–D, Three-dimensional digital reconstruction of the endocast and volume rendering of the braincase in dorsal view, with the endocast opaque and the surrounding neurocranial bones opaque to semitransparent. Scale bar: 50 mm.

probably corresponds to the projections of the olfactory filaments. If correct, the olfactory tracts are extremely short in *Diamantinasaurus*, and the bulbous structure as a whole should be designated the olfactory bulb (Fig. 14A–C). The path of these olfactory objects is reflected on the endoneurocranial surface of the orbitosphenoids and the left frontal, in part. The combined width of the olfactory bulbs is ~75% that of the cerebral hemispheres; this contrasts with the condition in *Apatosaurus*, in

which these widths are almost equal (Balanoff *et al.*, 2010). The cerebral endocast of *Diamantinasaurus* indicates that the hemispheres are expanded laterally. Posteriorly, the hemispheres are partly confluent and bounded by a shallow indentation from the post-cerebral endocast. The cerebral endocast is incomplete dorsally, in part because of the absence of the right frontal roof and in part because of erosion. Consequently, we cannot confirm the presence of a canal near the base of the olfactory

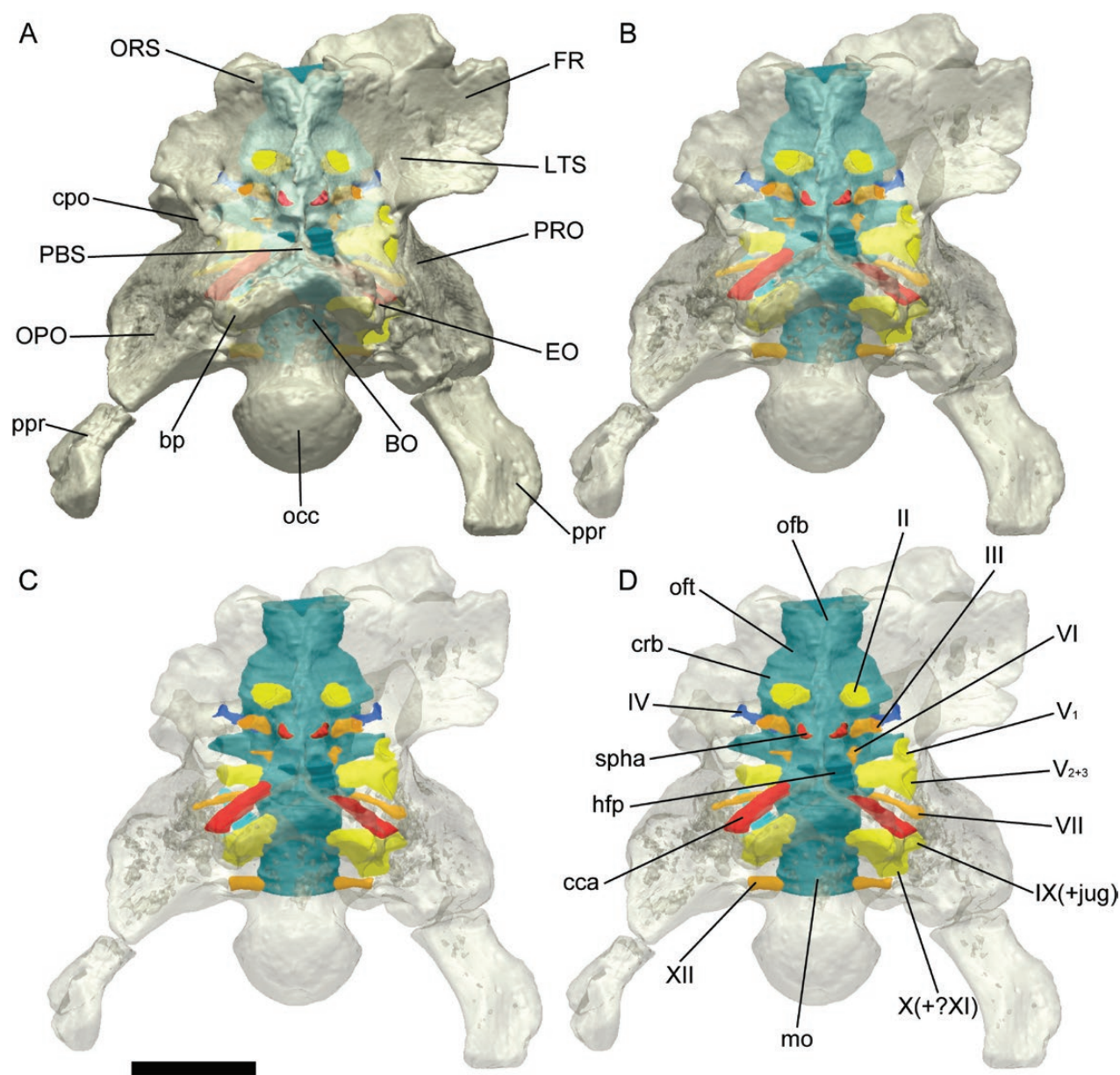


Figure 11. *Diamantinasaurus matildae* referred braincase (AODF 836). A–D, Three-dimensional digital reconstruction of the endocranium and volume rendering of the braincase in ventral view, with the endocranium opaque and the surrounding neurocranial bones semitransparent. Scale bar: 50 mm.

tracts in *Diamantinasaurus* that was interpreted in *Apatosaurus* to reflect the path of the supraorbital artery (Balanoff *et al.*, 2010).

The optic tract (CN II) exits the endoneurocranial cavity through a relatively large foramen in the orbitosphenoid. This foramen is circular and ~13 mm in diameter, and the canal itself is ~11 mm in length. The optic tract projects ventrolateral to the endocranium where the diencephalon would have been located in life. This contrasts with *Apatosaurus* (Balanoff *et al.*, 2010), in which the optic tract

projects laterally, and with *Diplodocus* Marsh, 1878 and *Camarasaurus*, in which these canals project anteroventrally (Witmer *et al.*, 2008).

From the same region, but further posteriorly, the hypophyseal endocranium descends ventrally and then posteroventrally (Figs 13F, 14A–D), contrasting with the anteroventral orientation observed in *Apatosaurus* (Balanoff *et al.*, 2010). This pendant structure is ≥ 46 mm long and expanded posteriorly. Based on comparisons of the mediolateral diameter of the infundibular stalk (26 mm) with the maximum

Table 2. Measurements of the endocast preserved within the referred braincase of *Diamantinasaurus matildae* (AODF 836)

Measurement (mm)	Position	Braincase
Dorsoventral height	Level with CN XII	48
	Level with CN X	50
	Level with CN VII	73
	Level with CN V	75
Transverse width	Level with CN XII	24
	Level with CN X	38
	Level with CN VII	43
	Level with CN V (ventral)	44
	Level with CN V (dorsal; across lateral extensions of dorsal dural sinus)	73

Abbreviation: CN, cranial nerve.

diameter at the level of the abducens (CN VI) canal (22 mm), and further to the distal maximum diameter at the level of the carotid canals (33 mm), we suggest that the infundibular stalk of *Diamantinasaurus* was well differentiated and separated from the pituitary body proper by a constriction (Fig. 14C). However, we could not recognize borders between the adenohipophyseal and neurohipophyseal compartments on the hypophyseal endocast. The size and robustness of the hypophyseal extension suggests that the pituitary gland was hypertrophied in adult *Diamantinasaurus*, as in other sauropods, including the non-neosauropod eusauropods *Shunosaurus* (Chatterjee & Zheng, 2002) and *Spinophorosaurus* Remes *et al.*, 2009 (Knoll *et al.*, 2012), diplodocoids (Janensch, 1935–1936; Sereno *et al.*, 2007; Witmer *et al.*, 2008; Balanoff *et al.*, 2010; Paulina Carabajal *et al.*, 2014), the early-branching macronarians *Camarasaurus* (Witmer *et al.*, 2008) and *Giraffatitan* (Janensch, 1935–1936; Knoll & Schwarz-Wings, 2009) and titanosaurs (Paulina Carabajal, 2012; Martínez *et al.*, 2016). The hypophyseal chamber appears to have been connected to the pharynx via a canal that is externally exposed by the craniopharyngeal foramen *sensu* Edinger (1942) (Fig. 10A, B). It is unlikely that this foramen transmitted the pituitary vein (see Knoll & Schwarz-Wings, 2009; Balanoff *et al.*, 2010), as interpreted by Tidwell & Carpenter (2003). The sella turcica, which housed the infundibular stalk and hypophyseal chambers, is penetrated by three pairs of canals that transmitted the abducens nerves (CN VI), the cranial carotid arteries (= internal carotid arteries) and their branches. The paired sphenopalatine arteries are situated at the mid-height of the pituitary.

The internal carotid arteries, which provide the major supply of blood for the brain and the vascularization

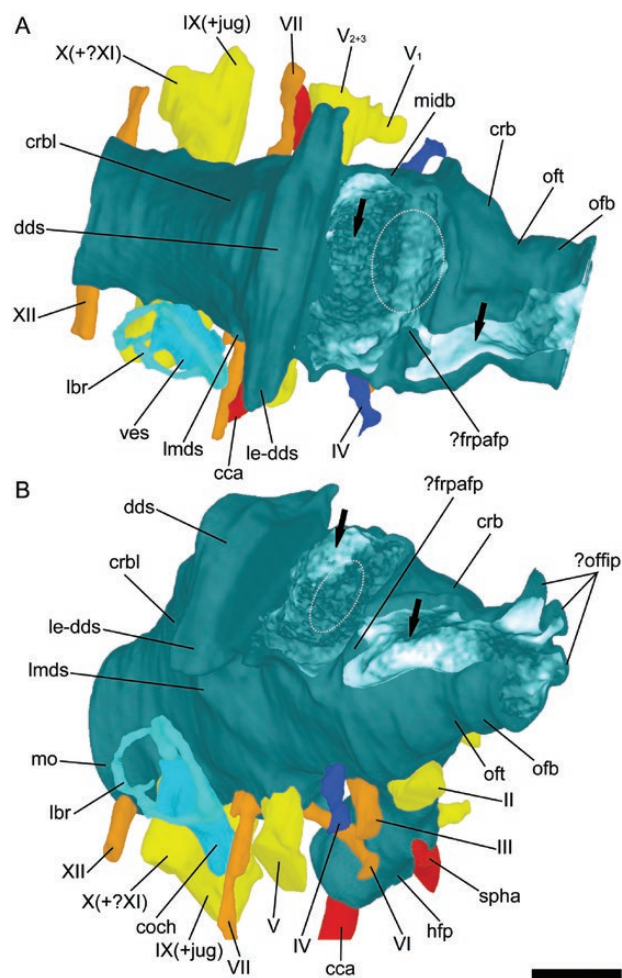


Figure 12. *Diamantinasaurus matildae* referred braincase (AODF 836). Three dimensional isosurface rendering of the endocast reconstructed from computed tomography scans in dorsal (A) and anterodorsal right lateral (B) views, showing incomplete anterodorsal portions of the endocast (arrows). Scale bar: 20 mm.

for the entire head (Burda, 1969; Baumel, 1993), enter the terminal part of the hypophyseal chamber via the lateral margins of the sella turcica. The canals they occupy penetrate the parabasisphenoid dorsal to the root of the basiptyergoid process (Fig. 10), are ~45 mm long and become narrower as they approach the hypophyseal chamber (arterial diameter 9.7 mm near the basiptyergoid process, 6.3 mm near the sella turcica). Once within the hypophyseal chamber, the carotid arteries usually form an intercarotic anastomosis before each bifurcates (Gillilan, 1967). The rostral division projects from the endoneurocranium towards the orbital cavity through its own foramen.

A pair of canals (maximum diameter 6 mm) extending from the anterior mid-portion of the hypophyseal endocast would have accommodated the

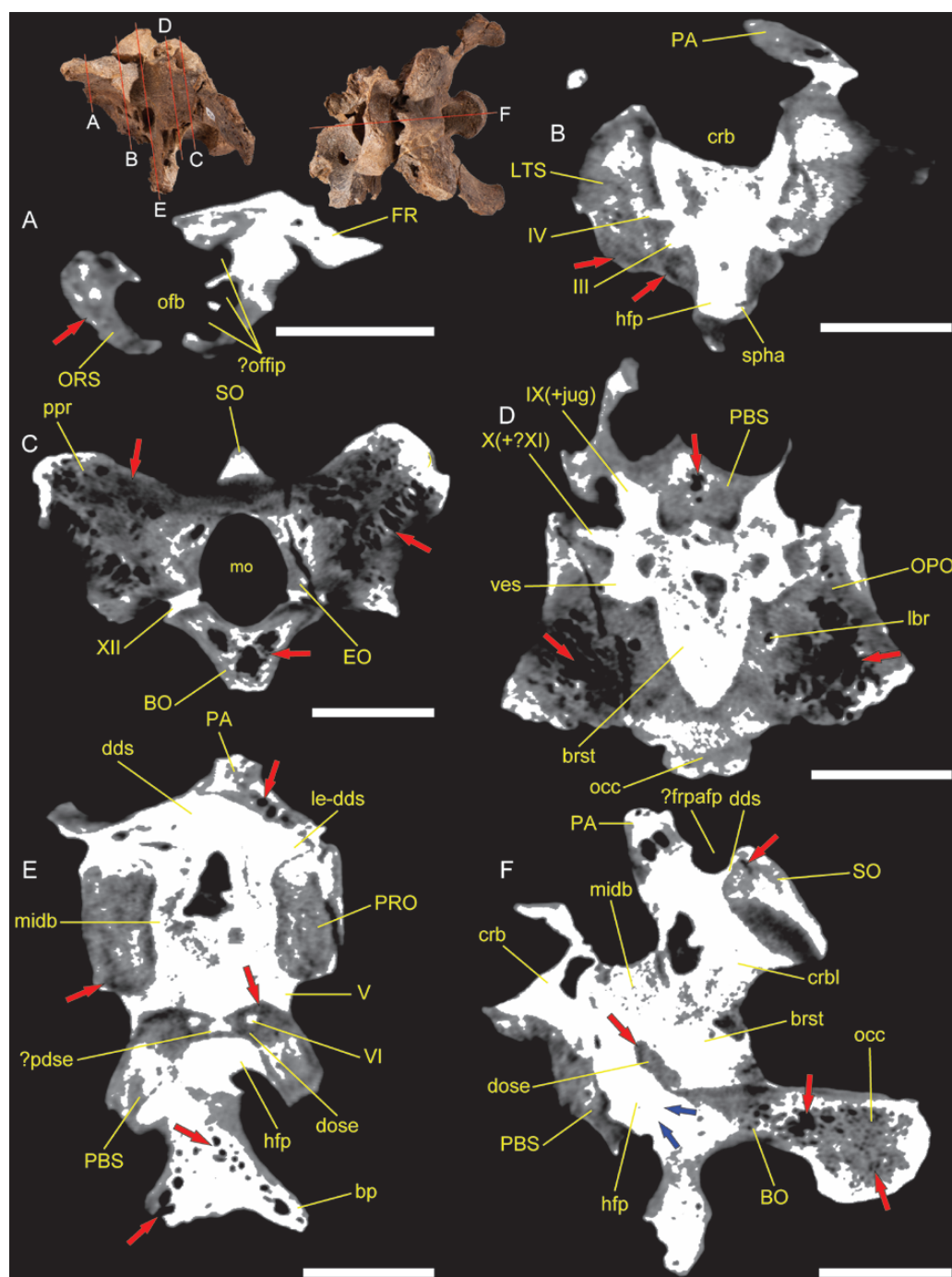


Figure 13. *Diamantinasaurus matildae* referred braincase (AODF 836). Two-dimensional computed tomography projections sectioned through the frontal in coronal (A–C, E), axial (D) and sagittal (F) planes. Note the increased pneumaticity (owing to the development of diverticula or sinuses) within the neurocranial bones (red arrows) and the caudal terminus of the hypophyseal fossa (blue arrows). Scale bars: 45 mm in A–F.

sphenopalatine arteries (Figs 8D, 9D, 11D, 12B, 13B, 14). These canals are located in the same position on the hypophyseal endocast of *Sarmientosaurus* (Martínez *et al.*, 2016) and CCMGE 628/12457 (Sues *et al.*, 2015). Another, much smaller opening (inner diameter

1.5 mm), which is located ~5 mm dorsal (on the left side) or anterodorsal (on the right side) to these canals (Figs 9B, C, 15), might have accommodated the internal ophthalmic artery; however, this foramen appears to be too small for this purpose.

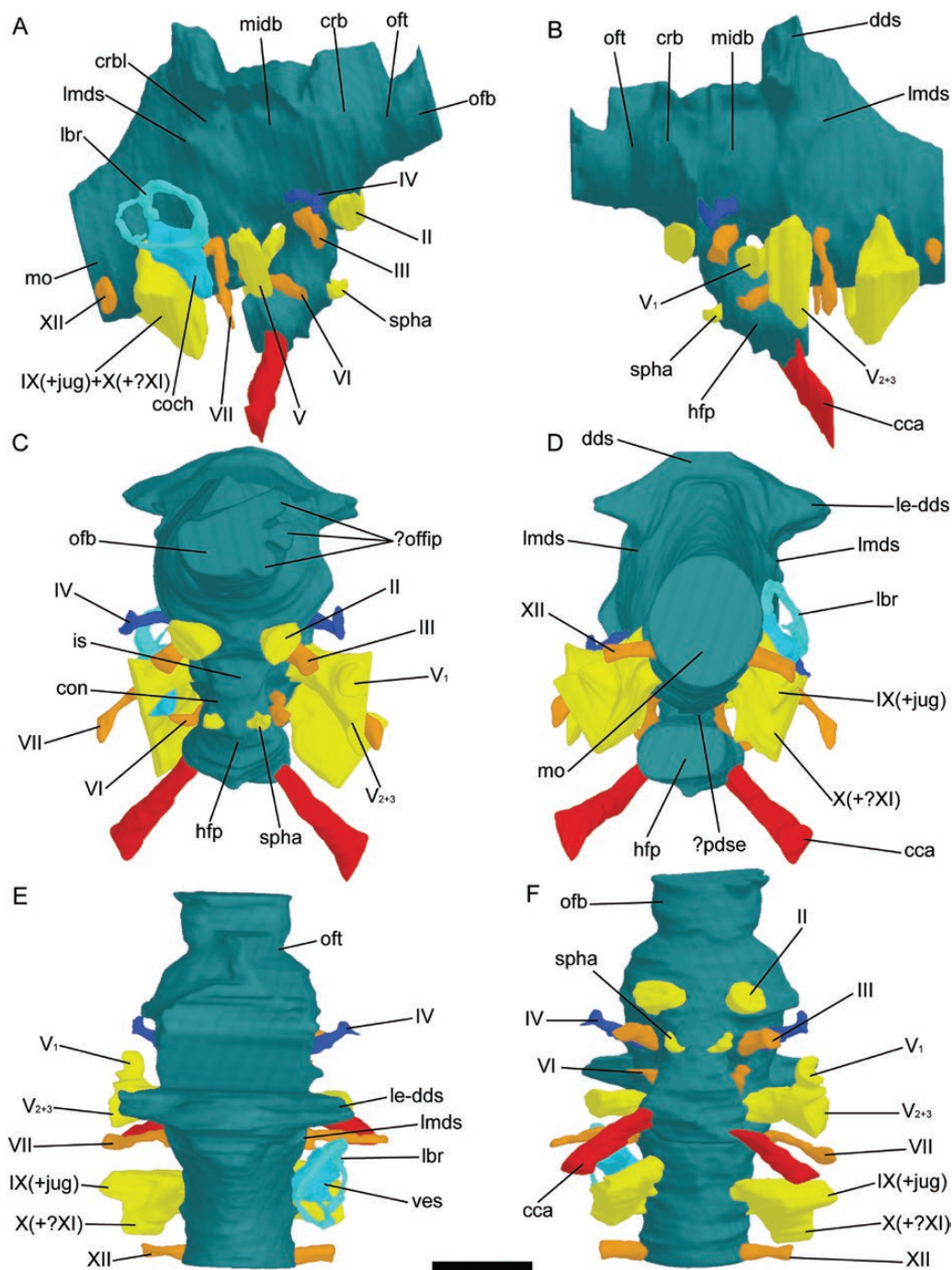


Figure 14. *Diamantinasaurus matildae* referred braincase (AODF 836). Three-dimensional isosurface rendering of the endocast reconstructed from computed tomography scans in right lateral (A), left lateral (B), anterior (C), posterior (D), dorsal (E) and ventral (F) views. Scale bar: 30 mm.

The posterior divisions of each internal carotid artery coalesce into a single basilar artery that projects along the ventral midline of the brainstem (Baumel, 1993). Based on *Spinophorosaurus*, Knoll *et al.* (2012) suggested that the basilar artery went through the

median canal that connects the pituitary space with the braincase cavity between the trigeminal and abducens nerves. This might also have been true for *Diamantinasaurus*, in which a Y-shaped sinus (termed herein as the pontine dural sinus extension) projects

anteriorly from the midline of the pontine flexure towards the dorsum sellae between the abducens canals (Figs 13E, 14D). Owing to poor preservation, we cannot confirm that this passage connected the hypophyseal and endoneurocranial cavities. However, the Y-shaped sinus might represent the site at which the posterior divisions of the internal carotid arteries merged into the basilar artery before the latter entered the endoneurocranial cavity in *Diamantinasaurus*. This structure neither morphologically nor topographically resembles the canal of unknown identity that extends through the dorsum sellae along the sagittal midline at a position dorsal to the abducens canals in *Apatosaurus* (Balanoff *et al.*, 2010).

The carotid canals in *Diamantinasaurus* converge at an angle of 75°, which is similar to the situation in *Amargasaurus* (Paulina Carabajal *et al.*, 2014), *Camarasaurus* (Witmer *et al.*, 2008) and *Diplodocus* (Witmer *et al.*, 2008), but greatly exceeds the angle of convergence (50°) seen in *Bonattitan* (Paulina Carabajal, 2012). The carotid canal enters the parabasisphenoid lateral to the root of the basiptyergoid process (*contra* Poropat *et al.* 2016). This is the plesiomorphic eusauropod condition (Paulina Carabajal, 2012; Paulina Carabajal *et al.*, 2014; Poropat *et al.*, 2016), which is also retained in the early-diverging titanosaurs *Malawisaurus* (Andrzejewski *et al.*, 2019) and *Sarmientosaurus* (Martínez *et al.*, 2016). By contrast, in most titanosaurs and in *Tambatitanis* (Saegusa & Ikeda, 2014) and, possibly, *Mongolosaurus* (Mannion, 2011), it opens medial to the basiptyergoid process (Paulina Carabajal, 2012); *Jainosaurus* (Chatterjee & Rudra, 1996), *Vahiny* (Curry Rogers & Wilson, 2014) and *Lirainosaurus* (Díez Díaz *et al.*, 2011) show reversals to the plesiomorphic state.

The midbrain endocast preserves putative optic lobes, in addition to oculomotor and trochlear nerves (Fig. 14A, B, E, F). The midbrain is relatively poorly outlined, as is typically the case in sauropods; indeed, even in *Nigersaurus* (Sereno *et al.*, 1999, which has been suggested to possess a small dural sinus, the midbrain is not discernible (Sereno *et al.*, 2007). In *Diamantinasaurus*, the midbrain domain is delineated by a shallow groove from the forebrain and the hindbrain domains. It shows a moderate degree of convexity that probably indicates the inferred placement of the optic tectum (Fig. 14A, B).

The oculomotor nerve (CN III) of *Diamantinasaurus* is situated on the ventrolateral surface of the midbrain, directly posterior to the optic tract. The canal is directed anterolaterally and ventrally and is ~14 mm long and 6 mm in diameter. The oculomotor canal is fully separated from the trigeminal fenestra laterally in *Diamantinasaurus*, as in most sauropods (Janensch, 1935–1936; Witmer *et al.*, 2008; Knoll

& Schwarz-Wings, 2009; Paulina Carabajal, 2012; Paulina Carabajal *et al.*, 2014).

The trochlear nerve (CN IV) originates from the midbrain, directly dorsal to the oculomotor nerve in *Diamantinasaurus*. The dimensions of the trochlear canal (length, 17 mm; diameter, 3.5 mm) suggest that the trochlear nerve was more slender than the oculomotor nerve. Although these proportions are typical for sauropods, the trochlear canal is substantially thinner than the oculomotor canal in some taxa [e.g. *Shunosaurus* (Chatterjee & Zheng, 2002)]. In other cases, the two canals have similar diameters [e.g. MGPIFD-GR 118 (Paulina Carabajal, 2012)], whereas in still others the trochlear canal is larger than the oculomotor one [e.g. *Giraffatitan* (Janensch, 1935–1936; Knoll & Schwarz-Wings, 2009)]. In the case of *Giraffatitan*, it has been suggested that the trochlear canal transmitted both the trochlear nerve and the anterior cerebral vein (Janensch, 1935–1936; Knoll & Schwarz-Wings, 2009). The dimensions of this foramen in *Diamantinasaurus* (Fig. 14) mean that it is possible that it accommodated both the trochlear nerve and a blood vessel, meaning that it would be equivalent to the epioptic fenestra *sensu* Janensch (1935–1936) or the orbitocerebral foramen *sensu* Witmer *et al.* (2008). A separate external opening for the orbitocerebral vein was not identified in *Diamantinasaurus*. Several other titanosaurs also lack this feature (Calvo & Kellner, 2006a; Paulina-Carabajal & Salgado, 2007; García *et al.*, 2008), although in many other sauropods a separate orbitocerebral vein opening is present [e.g. *Spinophorosaurus*, diplodocoids, *Camarasaurus* and some titanosaurs (Witmer *et al.*, 2008; Paulina Carabajal, 2012)].

In the hindbrain endocast of *Diamantinasaurus*, we recognize such structures as the expanded dorsal dural venous sinus, lateral middle dural sinus, pontine dural sinus extension (discussed above), putative cerebellar convexity, medulla oblongata, trigeminal and facial nerves, the complex cast of the metotic cavity, and the hypoglossal nerves (Fig. 14A, B, D–F). Although the hindbrain endocast is the most robust part of the *Diamantinasaurus* endoneurocranium, it is difficult to discern some neuroanatomical details because of hypertrophy of the interstices. The most evident is the dorsal protrusion of the endocast, which probably housed the cerebellum in part, but mostly the hypertrophied interstice and dural venous sinus (Hopson, 1979; Witmer *et al.*, 2008). The dural expansion is a prominent venous character of the endocast of many sauropods, although its development is variable, from being small to insignificant in *Shunosaurus* (Chatterjee & Zheng, 2002), *Nigersaurus* (Sereno *et al.*, 2007) and MPCM-HUE-8741 (Knoll *et al.*, 2013) to being considerably expanded in *Camarasaurus*

(Witmer *et al.*, 2008), *Giraffatitan*, *Dicraeosaurus* (Janensch, 1935–1936), MGPIFD-GR 18 (Paulina Carabajal, 2012) and *Diamantinasaurus*. The apex of the dorsal dural sinus of *Diamantinasaurus* forms a mushroom-shaped expansion, with two small wings (lateral extensions of the dorsal dural sinus; Figs 12, 14). This configuration is reminiscent of the condition seen in *Spinophorosaurus* (Knoll *et al.*, 2012) and *Camarasaurus* (Witmer *et al.*, 2008). It appears that the lateral extensions of the dorsal dural sinus did not communicate with the exterior on the right and left side of the braincase in *Diamantinasaurus*, but we cannot rule out the possibility that they did, because the high local concentration of iron in the adjacent bone region precludes assessment of this feature (Fig. 13E).

The posterior part of the dorsal dural sinus has a well-defined shape for most of its posterior surface area, despite the displacement of the parietals. A bilaterally symmetrical pair of slightly elevated ridges is situated at the posterior base of the dorsal dural sinus. The structure of *Diamantinasaurus* interpreted here as the lateral middle dural sinus might correspond to the dorsal head vein identified in *Giraffatitan* (Knoll & Schwarz-Wings, 2009) and *Camarasaurus* (Witmer *et al.*, 2008), the posterior middle cerebral vein preserved in *Camarasaurus* (Witmer *et al.*, 2008) and *Apatosaurus* (Balanoff *et al.*, 2010) or the dorsal–head/caudal–middle–cerebral vein system identified in *Spinophorosaurus* (Knoll *et al.*, 2012). Although the overall contours of the hindbrain indicate the presence of the cerebellum, it is difficult to discern such details as its size and shape. The flocculus cerebelli is not imprinted on the endoneurocranial surface of *Diamantinasaurus*, as is also the case in most sauropods for which this can be examined (Knoll *et al.*, 2019), with the exception of *Giraffatitan* (Janensch, 1935–1936; Knoll & Schwarz-Wings, 2009).

The trigeminal nerve (CN V) projects ventrolaterally from the brainstem endocast, dorsal to the pontine flexure. The size of the trigeminal canal (length, 17 mm; mid-diameter, 12–13 mm) suggests that it is the largest of the cranial nerves in *Diamantinasaurus*. On the left side of the *Diamantinasaurus* endocast (Figs 12A, 14B, C, E, F), there is evidence within the sidewall of the neurocranium for the division of this nerve into two rami (corroborating our observations of the external anatomy): the ophthalmic ramus (CN V₁) projects rostrally relative to the maxillomandibular ramus (CN V₂₊₃). This condition can also be observed in the early-branching sauropod *Shunosaurus* (Chatterjee & Zheng, 2002), wherein the Gasserian ganglion was probably positioned intracranially. By contrast, an extracranial placement appears to be more common among neosauropods [other than *Sarmientosaurus* (Martínez *et al.*, 2016)], including both diplodocoids (Holland, 1906; Berman & McIntosh,

1978; Witmer *et al.*, 2008; Balanoff *et al.*, 2010; Paulina Carabajal *et al.*, 2014) and macronarians, e.g. *Camarasaurus* (Witmer *et al.*, 2008), *Giraffatitan* (Janensch, 1935–1936; Knoll & Schwarz-Wings, 2009), *Antarctosaurus* and *Bonatitan* (Paulina Carabajal, 2012). An endoneurocranial position of the ganglion has been suggested for *Spinophorosaurus* (Knoll *et al.*, 2012).

The abducens nerve (CN VI) projects from the anteroventral surface of the brainstem endocast, lateral to the pontine dural sinus extension (Figs 12B, 13E, 14A–C, F, 15). The abducens canals (length, 22 mm; mid-diameter, 3.6 mm) traverse the dorsum sellae anteriorly and are also slightly directed ventrally and laterally. In *Diamantinasaurus*, the canals pass along the lateral margins of the hypophyseal chamber, and from there they exit the dorsum sellae directly, to enter the orbital region through individual foramina. Thus, *Diamantinasaurus* conforms to the derived condition that characterizes all members of Titanosauria, in which CN VI does not penetrate the pituitary fossa (Paulina Carabajal, 2012).

The facial nerve (CN VII) of *Diamantinasaurus* emerges from the brainstem endocast posterior to the trigeminal nerve and at a similar horizontal level (Fig. 14). The facial canal (length, 32 mm; diameter, 4 mm) projects ventrolaterally and turns in a slightly posterior direction immediately before reaching the external facial foramen (Fig. 15).

Some of the branches (vestibular and acoustic) of the vestibulocochlear nerve (CN VIII) can be followed down the endoneurocranial wall of the *Diamantinasaurus* braincase because they were filled with iron-rich sediment (Fig. 14D). Unfortunately, poor preservation precluded both their exact identification and a reasonable reconstruction of their relationship to the structures of the inner ear.

The metotic cavity of *Diamantinasaurus* is completely infilled with iron-rich matrix. Consequently, although the overall shape of the metotic cavity can be discerned roughly, it is not possible to determine the projections of the various vascular, neural and sensory structures that usually pass through this region in modern reptiles (Goodrich, 1930; Bellairs & Kamal, 1981). The metotic endocast, which is ~16 mm long and 12 mm wide, probably includes a partial cast of the jugular vein, the glossopharyngeal nerve (CN IX), the vagus nerve (CN X), the accessory nerve (CN XI), the space corresponding to the tympanic cavity and the space that housed the extracapsular part of the perilymphatic duct (Fig. 13D). Internally, the metotic endocast of *Diamantinasaurus* shows three separate structures; from anterior to posterior, these correspond to the root of the glossopharyngeal nerve (and, probably, the jugular passage), the larger root of the vagus nerve (and, plausibly, the accessory

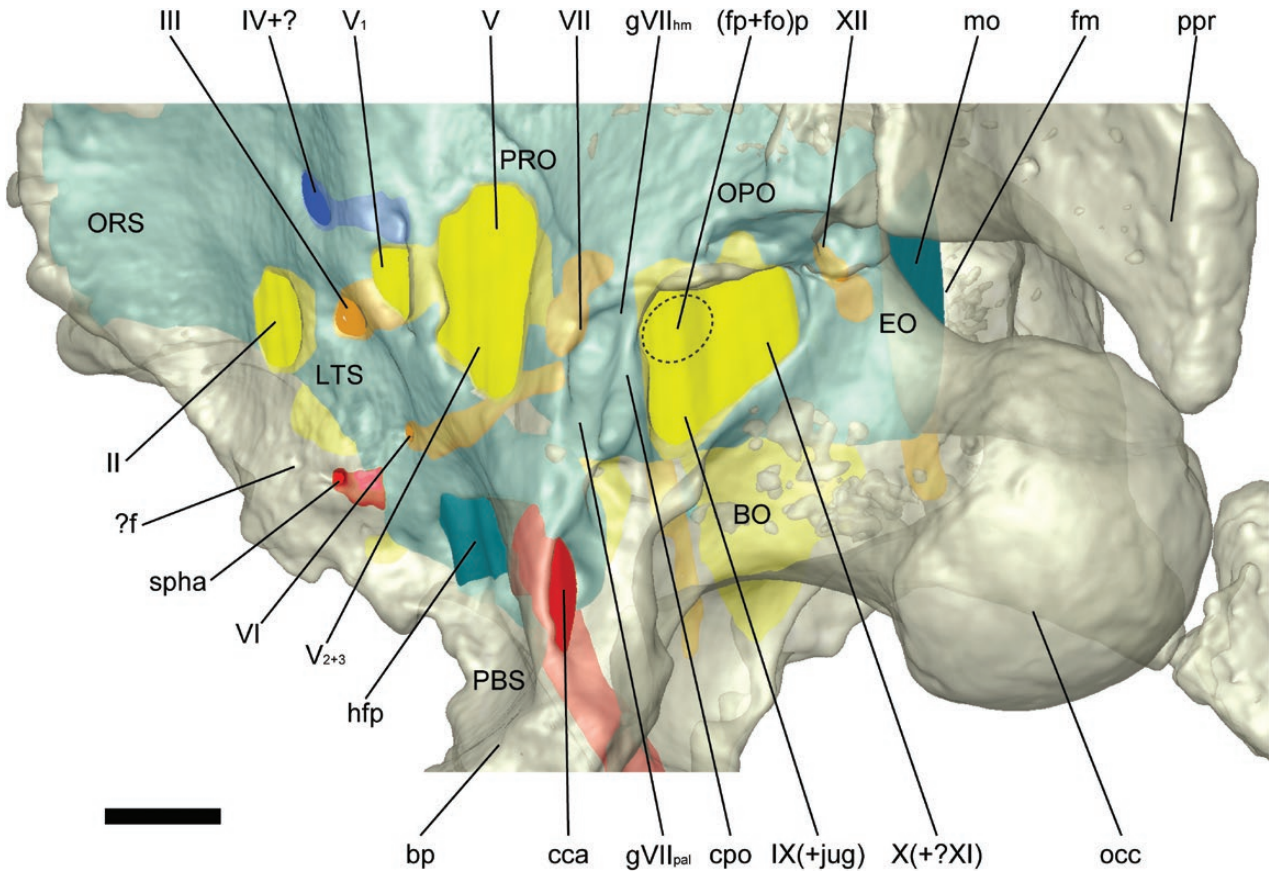


Figure 15. *Diamantinasaurus matildae* referred braincase (AODF 836). Three-dimensional digital reconstruction of the endocast (opaque) and volume rendering of braincase (semitransparent) in left lateral view. Scale bar: 15 mm.

nerve) and the vestibular segment of the inner ear. Externally, the metotic endocast is exposed through a single large window. The crista interfenestralis and other bony septa, if present, are not visible because of matrix infilling. Thus, our interpretation of the metotic endocast of *Diamantinasaurus* is speculative (Fig. 15). We cautiously suggest that the glossopharyngeal nerve and the jugal vein occupied the anteroventral portion of the endocast, whereas the anterodorsal portion presumably hosted the foramen ovale and foramen perilymphaticum. The posterodorsal portion of the metotic endocast was occupied by the vago-accessory nerve complex and was probably separated from the structures listed above by a bony strut.

In *Diamantinasaurus*, a single, ventrolaterally oriented canal (length, 15 mm; diameter, 5.5 mm) transmitted the hypoglossal nerve(s) (CN XII) from the brainstem endocast at the edge of the foramen magnum, as in most titanosaurs (Paulina Carabajal, 2012). It is, therefore, reasonable to assume that a part of the medulla oblongata projected slightly beyond the braincase.

Endosseous labyrinth: The cast of the endosseous labyrinth of the inner ear of *Diamantinasaurus* is more clearly discernible on the right side of the specimen (Fig. 16); consequently, only the right vestibule and cochlea were reconstructed. Their configuration and shape should be considered as approximate.

The crus commune is slightly curved posteromedially. The anterior semicircular canal is elevated more dorsally than the posterior semicircular canal, albeit much less so than in *Diplodocus* (Witmer *et al.*, 2008), *Giraffatitan* (Knoll & Schwarz-Wings, 2009) or *Spinophorosaurus* (Knoll *et al.*, 2012). The relative proportions of the anterior and posterior semicircular canals in *Diamantinasaurus* are similar to those in *Sarmientosaurus* (Martínez *et al.*, 2016); notably, in derived titanosaurs, anterior and posterior semicircular canals are subequal in size (Paulina Carabajal, 2012). Although the anterior semicircular canal appears to be more robust than the other two canals in *Diamantinasaurus*, this is likely to be an artefact of preservation. The ampullar region of the anterior semicircular canal is expanded, recalling the

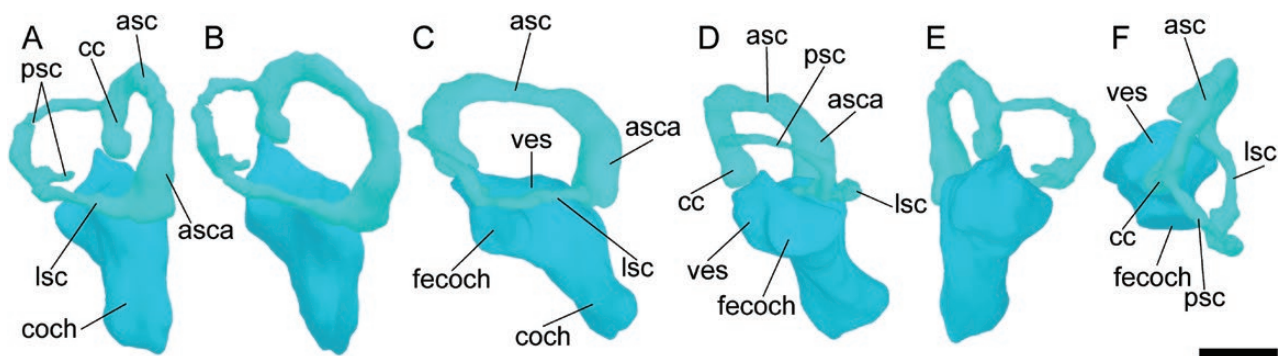


Figure 16. *Diamantinasaurus matildae* referred braincase (AODF 836). Three-dimensional isosurface rendering of the endosseous labyrinth reconstructed from computed tomography scans of the in anterior (A), anterolateral (B), lateral (C), posterior (D), medial (E) and dorsal (F) views. Scale bar: 10 mm.

condition in *Sarmientosaurus* and *Jainosaurus* (Knoll *et al.*, 2012; Martínez *et al.*, 2016), but distinguishing *Diamantinasaurus* from CCMGE 628/12457 (Sues *et al.*, 2015), wherein the ampullae are indistinct. The lateral and posterior semicircular canals are smaller, but more arcuate along their lengths, than the anterior semicircular canal. Neither the anterior nor the posterior semicircular canal extends ventral to the plane delimited by the lateral semicircular canal. The anterior semicircular canal is oriented at an angle of 41° relative to the sagittal plane of the endocast. The angle between the anterior and lateral semicircular canals is ~100° in *Diamantinasaurus*, similar to the condition in *Giraffatitan* (Knoll & Schwarz-Wings, 2009). Although this angle is greater in some titanosaurs [e.g. 110° in MPCM-HUE-1667 (Knoll *et al.*, 2015)], it is lower in others [e.g. 85° in MPCM-HUE-8741 (Knoll *et al.*, 2013)]. The angle between the anterior and posterior semicircular canals is also ~100° in *Diamantinasaurus*, which is similar to the condition in *Antarctosaurus* (Paulina Carabajal, 2012), but greater than that seen in CCMGE 628/12457 and *Malawisaurus* [both 90° (Sues *et al.*, 2015; Andrzejewski *et al.*, 2019)], *Giraffatitan* [80° (Knoll *et al.*, 2013)], an indeterminate titanosaur (FAM 03.064) from the latest Cretaceous of France [70° (Knoll *et al.*, 2019)] and *Sarmientosaurus* [63° (Martínez *et al.*, 2016)]. In *Diamantinasaurus*, the angle between the lateral and posterior semicircular canals is almost 130° and is unusually wide, wider even than the corresponding angle of *Spinophorosaurus* [100° (Knoll *et al.*, 2012)]. The cochlear region might have been as long as the anterior semicircular canal and appears to have hosted the cochlear fenestra.

Surangular: The right surangular (Fig. 17) is incomplete anteriorly, posteriorly and ventrally. Viewed laterally or medially, its dorsal margin is shallowly concave. Anteriorly, the surangular is broadly convex, and it is here that the articulation

point with the dentary can be observed. The dorsal half of the lateral surface is concave, whereas the ventral half is convex. The articular surface for the angular appears not to be preserved. The posterior surangular foramen, which faces posterolaterally, is positioned towards the posterior end of the preserved portion of the surangular, as in *Camarasaurus*, *Giraffatitan*, *Sarmientosaurus*, *Nemegtosaurus*, *Rapetosaurus* and *Tapuiasaurus* (Janensch, 1935–1936; Madsen *et al.*, 1995; Curry Rogers & Forster, 2004; Wilson, 2005; Martínez *et al.*, 2016; Wilson *et al.*, 2016).

The dorsal margin of the medial surface hosts a pronounced double arch. The anterior arch is incomplete, as is the dentary articulation point, whereas the posterior arch fades out posteriorly. Ventral to the double arch, the medial surface of the surangular is concave. The posterior section of this concavity is shallow, whereas the fragmentary anterior portion (the adductor fossa) appears to have been deeper and, possibly, preserves the posterior margin of the anterior surangular foramen; if so, it seems likely that this foramen was enlarged in *Diamantinasaurus*, as in *Nemegtosaurus*, *Rapetosaurus* and *Tapuiasaurus* (Curry Rogers & Forster, 2004; Wilson, 2005; Wilson *et al.*, 2016). A small bone fragment, preserved on the ventral surface immediately below the junction of the two arches, might be part of the surangular, but this cannot be demonstrated unequivocally.

Postcranial axial skeleton

The terminology used herein for the vertebral laminae follows Wilson (1999) and Wilson (2012) and that for the vertebral fossae follows Wilson *et al.* (2011). All preserved presacral vertebrae show camellate internal texture, following the definition of Wedel (2003). All postaxial cervical centra are opisthocoelous, as is typical for Sauropoda (Gauthier, 1986; Upchurch, 1995, 1998). In addition, all of the preserved dorsal

centra are opisthocoelous, as in most macronarians (Salgado *et al.*, 1997; Wilson & Sereno, 1998), with no change in the degree of opisthocoely throughout the dorsal series. Measurements for all postcranial axial elements can be found in Table 3.

Atlas-axis complex: Sauropod atlas-axis complexes, like skulls, are relatively rare. Among titanosauriforms, both the atlas and the axis are known in the indeterminate 'Potter Creek' brachiosaurid from the Late Jurassic of the USA (Jensen, 1987; D'Emic & Carrano, 2020), *Abydosaurus* Chure *et al.*, 2010, *Erketu* Ksepka & Norell, 2006, *Futalognkosaurus* Calvo *et al.*, 2007 (Calvo *et al.*, 2007b), *Giraffatitan* (Janensch, 1950), *Mongolosaurus* (Gilmore, 1933; Mannion, 2011), *Neuquensaurus* (Huene, 1929; Powell, 2003) and *Tapuiasaurus* (Zaher *et al.*, 2011). The atlases of *Quetecsaurus* González Riga & Ortíz David, 2014, *Rapetosaurus* (Curry Rogers, 2009), *Tambatitanis*

(Saegusa & Ikeda, 2014) and an indeterminate titanosaur from Brazil (Martinelli *et al.*, 2015) have also been described, as have the axes of *Alamosaurus* Gilmore, 1922 (Lehman & Coulson, 2002), *Bonitasaura* (Gallina & Apesteguía, 2015), *Euhelopus* (Wiman, 1929; Wilson & Upchurch, 2009), *Phuwiangosaurus* (Suteethorn *et al.*, 2009), *Pitekunsaurus* (Filippi & Garrido, 2008), *Saltasaurus* (Powell, 1992, 2003), *Sarmientosaurus* (Martínez *et al.*, 2016), *Yunmenglong* Lü *et al.*, 2013 and indeterminate titanosaurs from India [196/CRP/GSI/05 (Wilson & Mohabey, 2006)] and Brazil [Peirópolis 'Series A': MCT 1487-R (Powell, 1987, 2003)].

Atlas: The atlas of *Diamantinasaurus* (Fig. 18) is represented by only a weathered intercentrum. In anterior view, the atlantal intercentrum is semicircular, with the dorsal surface concave to accommodate the spinal cord (Fig. 18A). The anterior surface is concave

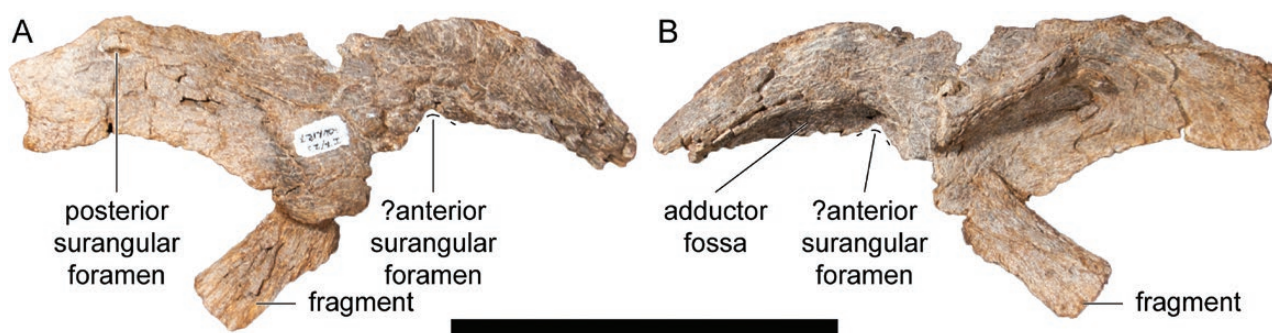


Figure 17. *Diamantinasaurus matildae* referred right surangular (AODF 836) in lateral (A) and medial (B) views. Scale bar: 100 mm.

Table 3. Measurements of postcranial axial skeletal elements of *Diamantinasaurus matildae* (AODF 836)

Measurement (mm)	Cervical vertebrae					Dorsal vertebrae		
	Atlas	Axis	III	VI	Neural arch	VII	VIII	
Total length	40	140	196	272	400	–	278	
Total height	44	211	179	165	170	–	450	
Centrum length	–	113	171	243	–	255	243	
Anterior articular face	Height	74	66	61	–	120	130	
	Width	86	68	72	95	–	159	161
Posterior articular face	Height	44	84	60	86	–	144	172
	Width	75	71	> 39	96	–	171	183
Anterior neural canal	Height	–	34	33	32	–	37	–
	Width	–	35	42	40	–	40	–
Posterior neural canal	Height	–	37	34	32	–	45	–
	Width	–	28	33	37	50	49	–

Definitions: height, dorsoventral; length, anteroposterior; width, transverse.



Figure 18. *Diamantinasaurus matildae* referred atlas neurocentrum (AODF 836) in anterior (A), ventral (B), left lateral (C), posterior (D), ventral (E) and right lateral (F) views. Scale bar: 100 mm.

for reception of the occipital condyle. The posterior surface is mostly convex, except dorsomedially, where it is concave to accommodate the odontoid process of the axis (Fig. 18D). In lateral view (Fig. 18C, F), the intercentrum is sub-rectangular, with dorsal and ventral margins of approximately the same length. By contrast, the anterior end is dorsoventrally taller than the posterior one, because this surface flares to surround the anterior articular concavity [also apparent in dorsal (Fig. 18E) and ventral (Fig. 18B) views]. The ventral part of the posterior articular surface lacks the ventrolateral projections seen in *Erketu* (Ksepka & Norell, 2006), *Mongolosaurus* (Gilmore, 1933; Mannion, 2011), *Quetecsaurus* (González Riga & Ortíz David, 2014) and *Tambatitanis* (Saegusa & Ikeda, 2014).

Axis: The axis (Fig. 19) is essentially complete (albeit worn), with the centrum and neural arch solidly sutured. The average elongation index (aEI *sensu* Chure *et al.*, 2010) of the axis is 1.46 in *Diamantinasaurus*, which is autapomorphically short among early-branching titanosaurs. Proportionally, it is most similar to the axes of the saltasaurids *Alamosaurus* [~1.52 (Lehman & Coulson, 2002)], *Neuquensaurus* (1.92; MLP CS 1311; P.D.M., pers. obs., 2013) and *Saltasaurus* (1.41; PVL 4017-1; P.D.M., pers. obs., 2013). The axis of *Pitekunsaurus* is more elongate (2.50; MAU-Pv-AG-446/3; P.D.M., pers. obs., 2014), whereas those of both *Bonitasaura* (Gallina & Apesteguía, 2015) and the lognkosaurian *Futalognkosaurus* (MUCPv-323; S.F.P. pers. obs., 2018) have aEI values closer to 3.0.

The dorsal surface of the anterior articular facet of the axial centrum of *Diamantinasaurus* is slightly

concave to accommodate the spinal cord (Fig. 19A). The odontoid process, which is fused to the anterior surface of the centrum, is hemi-conical and broadest posterodorsally. From its anterior apex, it slopes sharply in a posteroventral direction (Fig. 19B, F). The remainder of the anterior articular facet is shallowly concave. Although much of the cotylar rim is missing, it is clear that the posterior articular facet was deeply concave (Fig. 19C). The dorsal margin of the posterior cotyle is slightly concave to accommodate the spinal cord (Fig. 19C). The ventral surface of the centrum is flared anteriorly (where it meets the parapophyses) and narrows further posteriorly (Fig. 19E); were the posterior cotyle complete, there would, presumably, also have been a similar degree of posterior flaring. Although the ventral surface is convex both anteroposteriorly and transversely, it lacks a midline keel. As such, *Diamantinasaurus* retains the plesiomorphic eusauropod condition, which also characterizes *Alamosaurus* (Lehman & Coulson, 2002), *Neuquensaurus* and *Saltasaurus* (Powell, 2003) among titanosaurs and which distinguishes it from the axes of *Bonitasaura* (Gallina & Apesteguía, 2015) and *Futalognkosaurus* (Calvo *et al.*, 2007b). However, it should be noted that the axial keel of *Futalognkosaurus* is made more prominent by the presence of pneumatic foramina on the ventral surface of each parapophyseal stalk, and a similar foramen can be seen on the left parapophysis of the axis of *Diamantinasaurus* (Fig. 19E). Thus, although no axial keel appears to be present in *Diamantinasaurus*, it is possible that the ventral surface would have been more strongly convex when the parapophyses were complete. Each lateral surface of the axial centrum is invaded by a

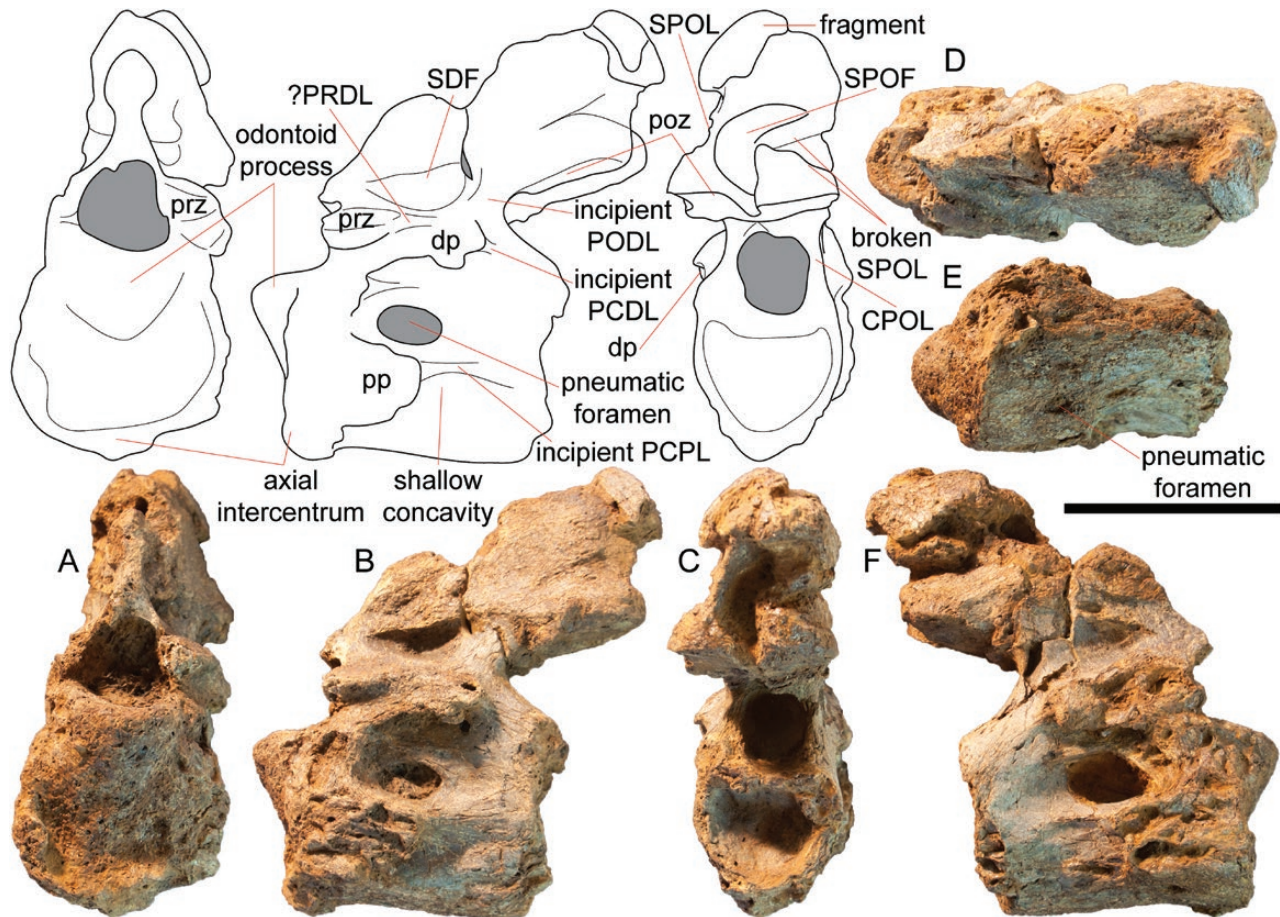


Figure 19. *Diamantinasaurus matildae* referred axis (AODF 836) in anterior (A), left lateral (B), posterior (C), dorsal (D), ventral (E) and right lateral (F) views. Scale bar: 100 mm.

small pneumatic foramen (27 mm anteroposteriorly), set within a shallow pneumatic fossa (50 mm anteroposteriorly). The base of the parapophysis is positioned anteroventral to the pneumatic fossa and situated entirely on the centrum. Both parapophyses are incomplete. Posterior to the parapophysis and ventral to the pneumatic fossa, a second shallow concavity can be observed. The subtle ridge between the pneumatic fossa and this concavity might be a rudimentary PCPL. Dorsal to the parapophysis and anterior to the pneumatic fossa, a raised section of bone (against which the atlas would have articulated) connects the parapophysis to the prezygapophysis and the diapophysis. The prezygapophyseal facets are small and shallowly concave, although the degree to which they are worn prevents their anterior extent from being determined. Each prezygapophysis lies lateral to the neural canal, and a rudimentary PRDL connects it posteriorly with the base of the diapophysis. Both diapophyses are incomplete; nevertheless, it is clear that their bases sit entirely on the neural arch. A subtle PCDL extends from the posterior margin of

the diapophysis along the centrum, and an incipient PODL is developed between the diapophysis and the postzygapophysis. The neural spine is strongly inclined posterodorsally. A small, anteroposteriorly elongate fossa is present on each side of the neural spine, posterodorsal to the base of each prezygapophysis. Posteriorly, this fossa is bordered by the incipient PODL. The postzygapophyseal articular surfaces are flat and face ventrally. Only 10 mm separates the postzygapophyses on the midline, and a deep SPOF is present between their dorsal margins, the SPOLs (the right one of which is broken; Fig. 19C) and the posteroventral surface of the neural spine. The neural spine itself is transversely expanded posteriorly, such that it is triangular in dorsal view (Fig. 19D). Near the anterior margin of the neural spine, a small (20 mm), posterodorsally inclined depression is present on the lateral surface. This gives the impression that the anterior margin of the neural spine possessed a structure similar to a PRSL, although this is uncertain. A small fragment of bone remains attached to the posterodorsal-most point of the neural spine.

Cervical vertebra III: Cervical vertebra III is reasonably well preserved (Fig. 20), but has suffered some post-mortem distortion and weathering. The centrum is better preserved on the left side (Fig. 20B), whereas the neural arch is more complete on the right side (Fig. 20F). Broken sections of the centrum reveal the camellate texture of the internal bone, which comprises coels ≤ 20 mm in length that are separated by bone < 1 mm thick. Although neither the anterior condyle nor the posterior cotyle is completely preserved, it is clear that the centrum was strongly opisthocoelous. Both the anterior condyle (Fig. 20A) and posterior cotyle (Fig. 20C) are convex on their lateral and ventral margins but slightly concave dorsally, in line with the neural canal openings. Posterior to the parapophyses, the ventral surface is transversely narrow and forms a keel (Fig. 20E). A ventral keel is absent from the postaxial cervical centra of most macronarians (Upchurch, 1998; Mannion et al., 2013), although its presence characterizes a small number of early-branching somphospondylans (e.g. *Erketu*), in addition to several titanosaurs, including members of Lognkosauria, *Overosaurus*, *Rapetosaurus* (Coria et al., 2013) and *Savannasaurus* (Poropat et al., 2016, 2020a; González Riga et al., 2018). The parapophysis is located

at the anteroventral corner of the centrum, immediately posterior to the anterior condyle (Fig. 20B), and a short, stout ACPL is present. As preserved, the parapophysis extends approximately half the length of the centrum. Dorsal to the parapophysis lies the lateral pneumatic foramen, which sits within a fossa and is split by an anterodorsally oriented lamina. The presence of a well-developed lateral excavation contrasts with the cervical centra of most somphospondylans, which are often characterized by a shallow fossa or lack an excavation altogether (Upchurch, 1998; Wilson, 2002; Curry Rogers, 2005). However, the lateral surfaces of the cervical centra of a small number of titanosaurs are also excavated, including *Savannasaurus* (Poropat et al., 2016) and *Sarmientosaurus* (Martínez et al., 2016). Posterior to the pneumatic foramen, the lateral face of the centrum is shallowly concave dorsoventrally. The PCPL forms the ventral margin of the pneumatic fossa. The right prezygapophysis appears to have suffered some distortion (Fig. 20A). Based on the preserved orientation of the postzygapophyses of the axis, the prezygapophyses of cervical vertebra III should be effectively horizontal; thus, the right prezygapophysis faces more strongly medially and anteroventrally than it would have in life. The

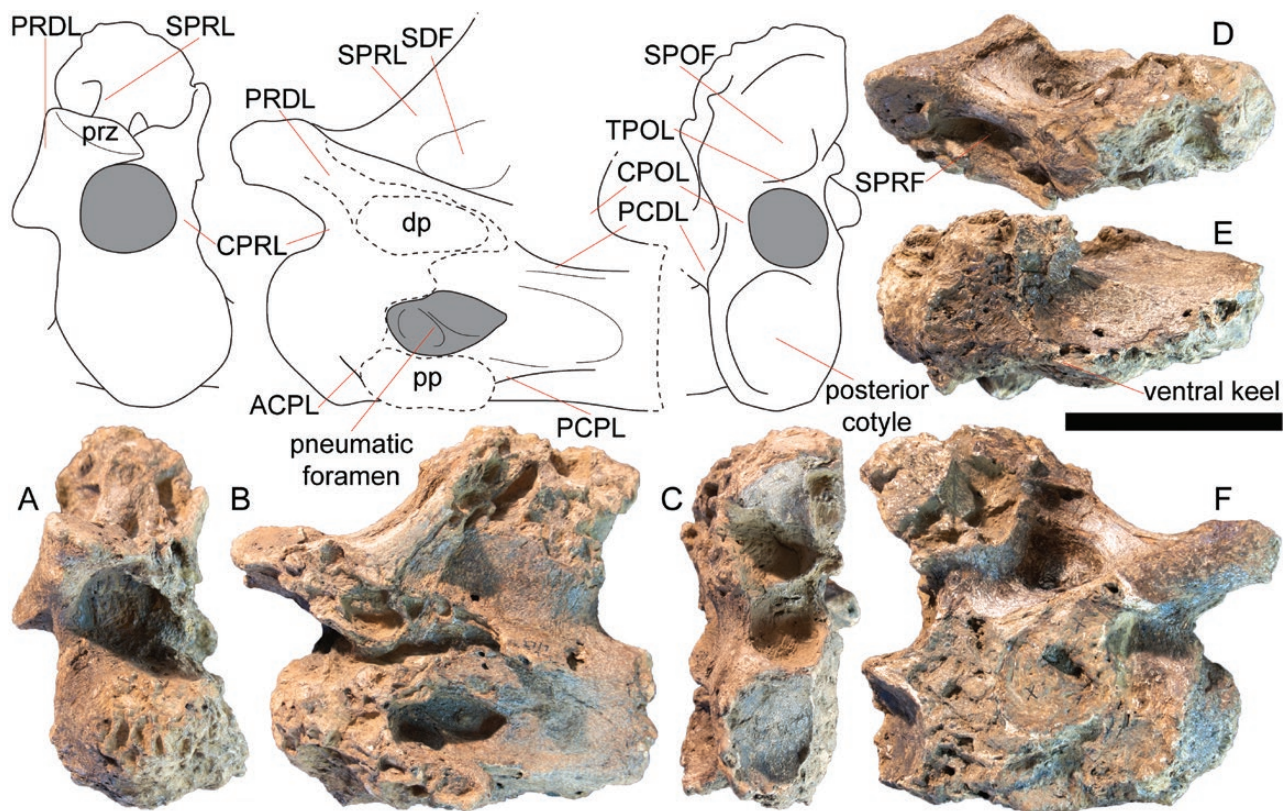


Figure 20. *Diamantinasaurus matildae* referred cervical vertebra III (AODF 836) in anterior (A), left lateral (B), posterior (C), dorsal (D), ventral (E) and right lateral (F) views. Scale bar: 100 mm.

prezygapophyses project beyond the anterior margin of the condyle, contrasting with those of the anterior cervical vertebrae of *Rapetosaurus* and saltasaurines (Curry Rogers, 2005, 2009; Poropat *et al.*, 2016). Each lateral margin of the anterior neural canal opening is formed by a stout CPRL; no CPRF appears to have been present. A prong-like pre-epiphysis projects from the anterior surface of the CPRL, a short distance ventral to the prezygapophyseal articular surface. A well-developed PRDL is preserved on the right side (Fig. 20F). Neither diapophysis is preserved, although the base of the left one is observable (Fig. 20B). The diapophysis appears to have been similar in size to the parapophysis, was positioned at approximately the level of the neurocentral suture and was firmly connected to the posterodorsal margin of the centrum via a PCDL; whether or not an ACDL was present cannot be determined. It is unlikely that an SPDL or PODL was present in cervical vertebra III, based on the preserved portion. Both postzygapophyses have been lost, although their bases are still observable. A stout CPOL connects each postzygapophysis to the centrum, and a TPOL is present between them (Fig. 20C). These laminae form the lateral and dorsal margins of the posterior neural canal, respectively; no CPOF was present. Although the neural spine is incompletely preserved, it seems unlikely that it was bifurcated at its apex. A prominent SPRL is present on each side, and between the paired SPRLs lies a well-developed PRSF (Fig. 20D); no PRSL was present within this fossa. Immediately posterior to each SPRF, a SDF is present, with the right SDF far deeper than the left one. Given the presence of an SPOF on the posterior surface of the neural spine, it is likely that the lateral margins of this fossa were formed by the paired SPOLs; however, neither SPOL is preserved. The ventral margin of the SPOF is formed by the TPOL. There is no POSL within the SPOF.

Cervical vertebra VI: This cervical vertebra (Fig. 21) is tentatively interpreted as the sixth in the sequence based on its length relative to that of the other preserved vertebrae (including two fragmentary centra not described herein, which, based on their anteroposterior lengths, are cervical vertebrae IV and V). Cervical vertebra VI is nearly complete, missing only the postzygapophyses, the apex of the neural spine and the cervical ribs. The centrum is strongly opisthocoeleous, with the anterior condyle projecting 40 mm beyond the anterior margin of the centrum (Fig. 21B, E). The rim of the posterior cotyle is incomplete, and the cotyle itself is partly infilled with matrix (and fragments of the left side of the cotylar rim), precluding accurate measurement of its depth (Fig. 21D). The approximate aEI of this

vertebra is 2.7; among macronarians, similar values (< 3.0) are seen only in early-branching forms (e.g. *Camarasaurus*, *Europasaurus* Sander *et al.*, 2006) and late-branching lithostrotian titanosaurs, such as *Alamosaurus* and *Saltasaurus* (Mannion *et al.*, 2013). The ventral surface of the centrum is concave both anteroposteriorly and transversely (Fig. 21F), with the latter caused, in part, by the slight anteroventral projection of the parapophyses (Fig. 21A, D). Each parapophysis is situated immediately posterior to the anterior condyle and is connected to the centrum via a prominent ACPL and PCPL (Fig. 21B, E). The dorsal surface of the left parapophysis bears two small concavities that are either absent or obscured by matrix on the right parapophysis, but these are not equivalent to the more extensive excavations that characterize the parapophyses of most non-somphospondylan neosauropods (Upchurch, 1998). The more medial of these is separated from the lateral pneumatic foramen by a thin plate of bone. The lateral pneumatic foramen (40 mm long anteroposteriorly) is fairly shallow and set within a pneumatic fossa (81 mm long anteroposteriorly). Although a fracture separates the neural arch from the centrum, it seems likely that the neurocentral suture was fused and that this merely represents post-mortem damage. The widely spaced prezygapophyses are connected by a TPRL (Fig. 21A), the anterior margin of which is deeply concave in dorsal view (Fig. 21C). Each prezygapophysis projects 35 mm beyond the apex of the anterior condyle and is supported ventrally by a CPRL. The TPRL forms the dorsal margin of the anterior neural canal opening, whereas each CPRL is separated from direct contact with the anterior neural canal opening by a shallow CPRF. A horizontal PRDL connects the prezygapophysis with the diapophysis, which is situated dorsal to the parapophysis. The ventral surface of the diapophysis is flat; ventral to this, the lateral wall of the neural arch hosts a shallow CDF, which is separated from the lateral pneumatic fossa below by a horizontal ridge. The diapophysis is connected to the centrum via a horizontal PCDL and, although incomplete, it is clear that a PODL was also present, projecting posterodorsally from the diapophysis towards where the postzygapophysis was situated. The PCDL, PODL and CPOL border a shallow POCDF. Each postzygapophysis was supported ventrally by a CPOL, and this forms the lateral margin of the posterior neural canal opening; no CPOF was present. Only the base of the neural spine is preserved, but portions of several laminae are evident. Each prezygapophysis was connected to the neural spine via an SPRL, and an SPRF lies between the SPRLs; no PRSL is present. The absence of SPDLs means that the SDF is bordered by the SPRL, PRDL

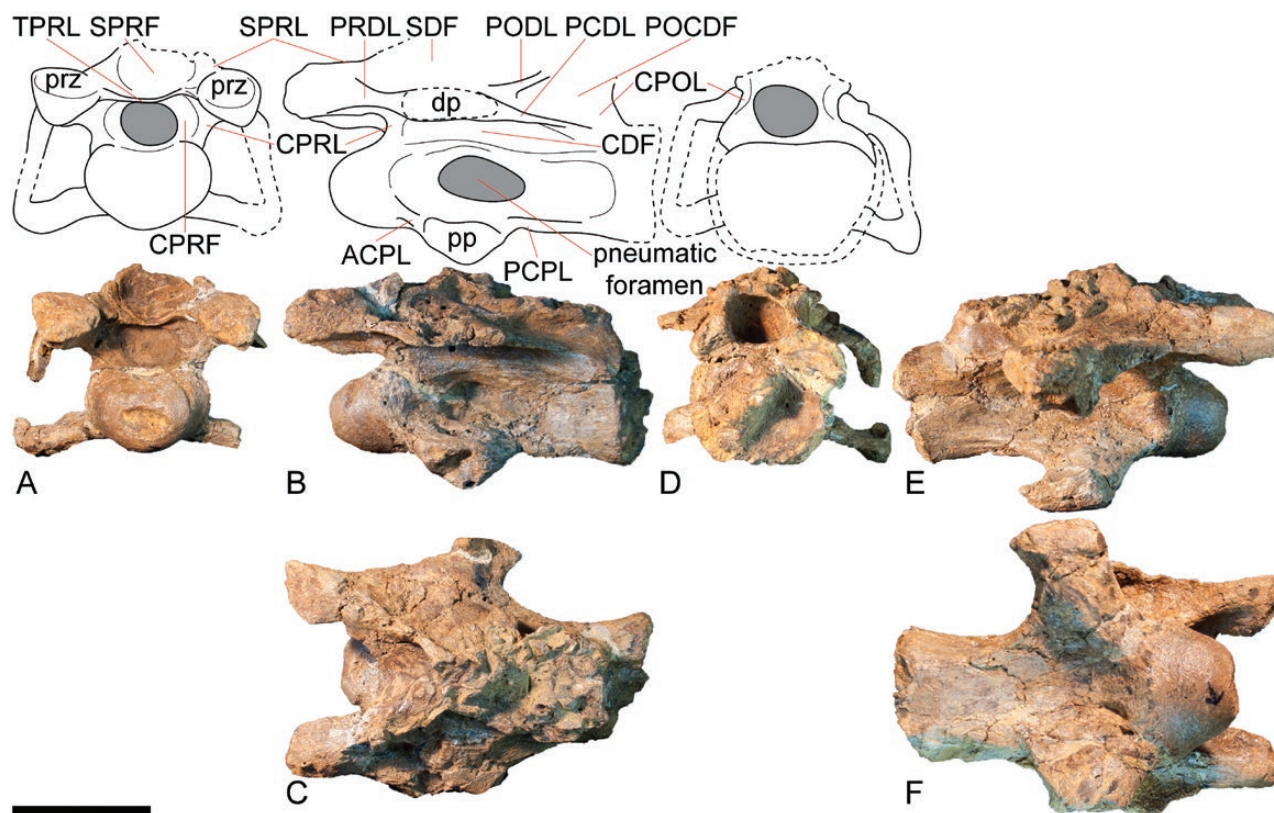


Figure 21. *Diamantinasaurus matildae* referred cervical vertebra VI (AODF 836) in anterior (A), left lateral (B), dorsal (C), posterior (D), right lateral (E) and ventral (F) views. Scale bar: 100 mm.

and PODL; the posterodorsal margin of this fossa is not preserved, but is presumed to have been the SPOL.

Posterior cervical neural arch: This large, incomplete neural arch preserves partial prezygapophyses, diapophyses and postzygapophyses, the laminae associated with these apophyses, and the base of the neural spine. The prezygapophyses are widely separated and joined by a V-shaped TPRL (Fig. 22A), which is incomplete anteriorly. Each prezygapophysis is supported ventrally by an anterolaterally projecting CPRL, but a pre-epiphysis is evidently absent (if present, it was small). The CPRL, TPRL and the dorsolateral margin of the neural canal border a CPRF; the paired CPRFs are separated on the midline by a thickened vertical strut that runs between the dorsal margin of the neural canal and the ventral margin of the TPRL. A prominent PRDL links the prezygapophysis to the diapophysis (Fig. 22B, E). The lateral margin of the more complete right PRDL is straight in dorsal view (Fig. 22D). The diapophysis, which is incompletely preserved on both sides, is situated at approximately the midlength of the neural arch. Posteriorly, the diapophysis is connected to the postzygapophysis via a PODL. The lateral margin of the more complete left

PODL is concave in dorsal view (Fig. 22D). Posterior to the CPRL and ventral to the diapophysis, a series of three fossae is present; however, the middle one of these appears to represent the weathered remnants of a stout ACDL, which was occupied internally by a single large pneumatic coel. The anterior fossa is the PRCDF, bordered anteriorly by the CPRL, dorsally by the PRDL and posteriorly by the very thin anterior border of the ACDL. The posterior border of the ACDL forms the anterior margin of the POCDF, which is bordered dorsally by the PODL and posteromedially by the CPOL. Neither postzygapophysis is complete, and the presence or absence of a TPOL cannot be ascertained, but epiphyses are absent. The neural spine is incomplete but was evidently not bifurcated. Each prezygapophysis is connected to the neural spine via a well-developed SPRL, and between the paired SPRLs and the TPRL a deep SPRF is present; there is no PRSL. The SPRL, PRDL, diapophysis, PODL and SPOL define a broad and deeply concave SDF; SPDLs are absent. The right SDF is divided by a ridge; thus, the more dorsal portion of this fossa is SDF1 and the more ventral SDF2 (Wilson *et al.*, 2011). A comparable ridge also appears to be present within the left SDF, although this region is damaged. Each

postzygapophysis is connected to the neural spine via a well-developed SPOL, and the paired SPOLs define a deep and broad SPOF (Fig. 22C); there is no POSL.

Cervical rib: The best-preserved cervical rib (Fig. 23) is from the right side and appears to have been from an anterior cervical vertebra. This cervical rib is 316 mm long and preserves the incomplete bases of both the tubercular and capitular heads and a virtually complete distal projection. The broken surface of the tubercular head reveals an internal hollow (Fig. 23A), and the broken capitular head reveals a similar, albeit shallower hollow. A subtle concavity is present on the fragmentary anterior surface of the cervical rib, ventral to the base of the tubercular head; similar concavities were observed on the cervical ribs of the type specimen of *Diamantinasaurus* (Poropat *et al.*, 2015b). The distal projection of the cervical rib is broadly dominated by four ridges that shift in position proximodistally. The first ridge ('dorsal') extends from the posterior margin of the tuberculum along the dorsal surface of the proximal one-fifth of the distal projection (Fig. 23A, B). The second ridge ('dorsolateral') originates on the lateral surface of the tuberculum (Fig. 23D) but

migrates diagonally (in dorsal view; Fig. 23A) such that it runs along the midline of the dorsal margin at midlength. The third ridge ('ventrolateral') extends along the ventrolateral margin of the proximal one-third of the distal projection but migrates such that it is situated at the midheight of the lateral margin by midlength. The fourth and final ridge ('ventromedial') is subtle, extending along the ventromedial margin of the mid-section of the distal projection. Despite the presence of dorsolateral and dorsal ridges, the dorsal surface of the distal projection lacks a prominent trough; this aligns AODF 836 with *D. matildae*, in which the absence of such a trough has been regarded as potentially autapomorphic (Poropat *et al.*, 2015b).

Dorsal vertebrae: AODF 836 preserves four dorsal vertebrae. Two are represented solely by partial centra, whereas the other two preserve nearly complete centra, firmly sutured to incomplete neural arches (Figs 24, 25). The two more complete exemplars form the basis for the description below; based on comparisons with the dorsal vertebrae of *Savannasaurus* (Poropat *et al.*, 2020a), they are herein interpreted as dorsal vertebrae VII and VIII (neither of which is represented in the

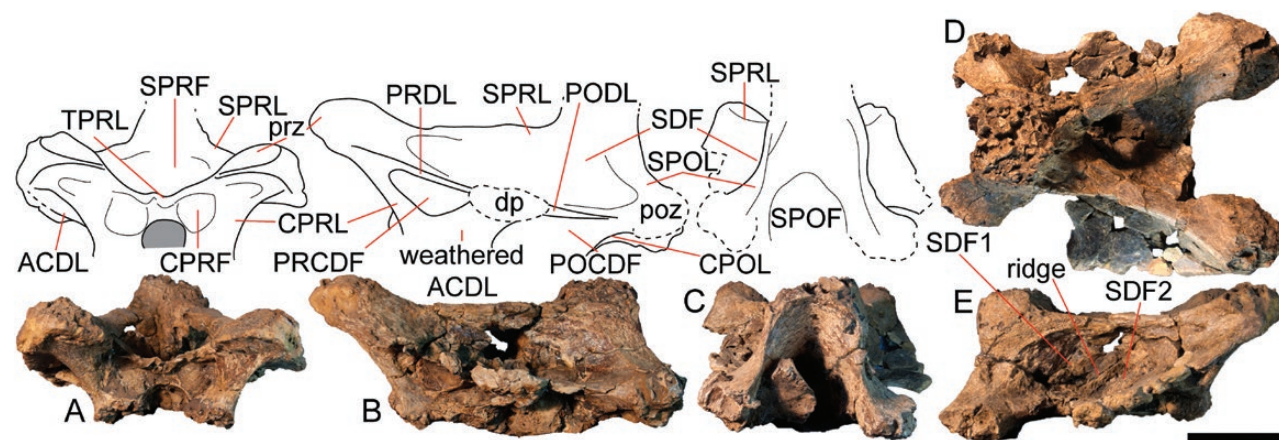


Figure 22. *Diamantinasaurus matildae* referred middle cervical vertebral neural arch (AODF 836) in anterior (A), left lateral (B), posterior (C), dorsal (D) and right lateral (E) views. Scale bar: 100 mm.

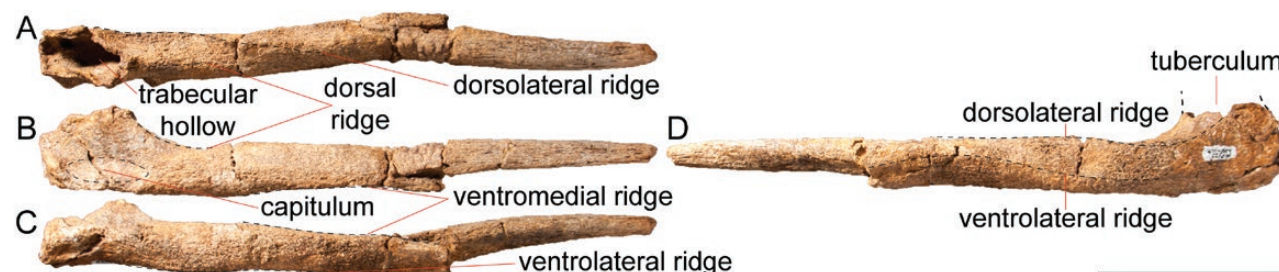


Figure 23. *Diamantinasaurus matildae* referred left cervical rib (AODF 836) in dorsal (A), lateral (B), ventral (C) and medial (D) views. Scale bar: 100 mm.

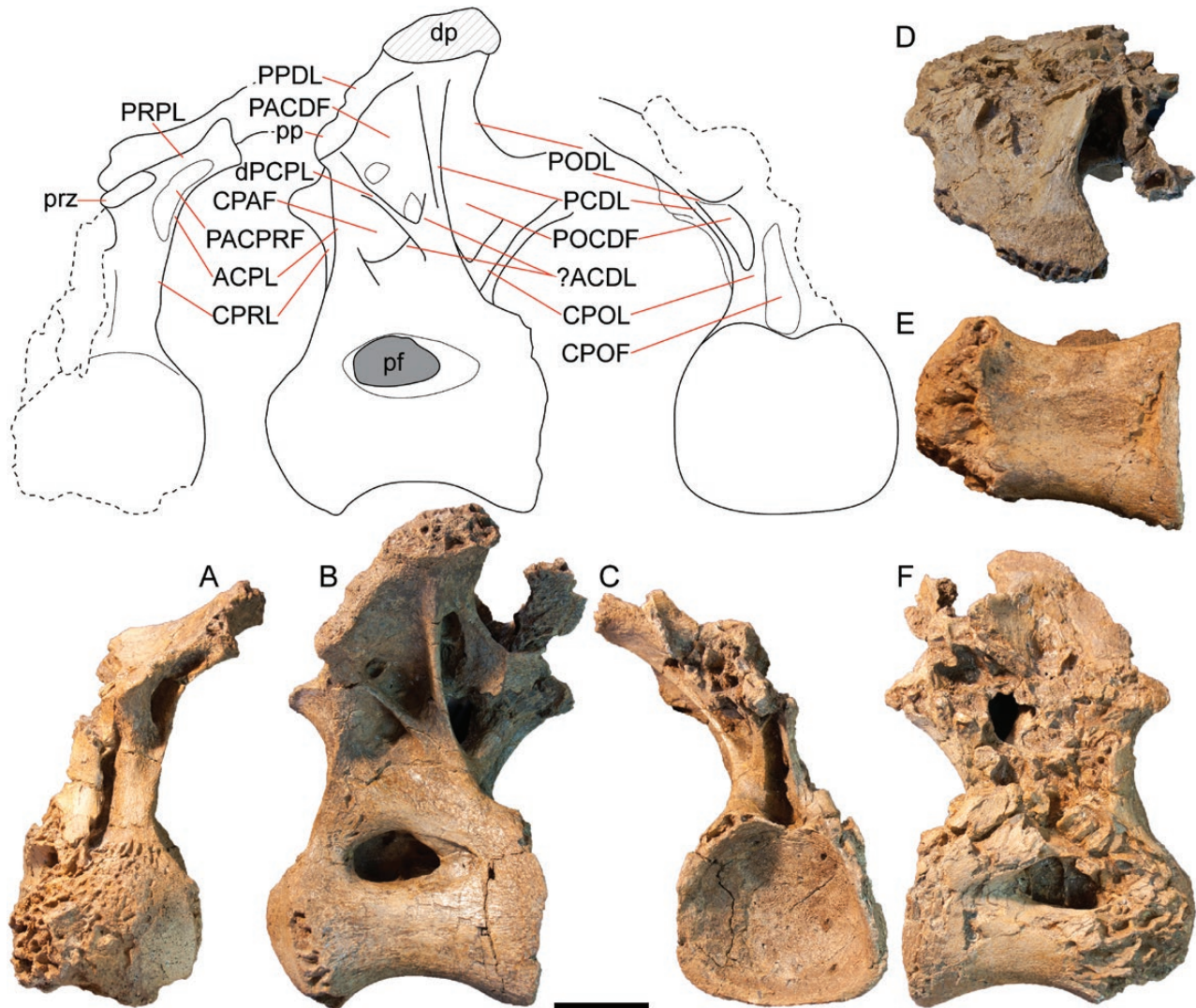


Figure 25. *Diamantinasaurus matildae* referred middle dorsal vertebra B (AODF 836) in anterior (A), left lateral (B), posterior (C), dorsal (D), ventral (E) and right lateral (F) views. Scale bar: 100 mm.

set. It is likely that the CPRF was bounded dorsally by a TPRL, although this lamina cannot be observed clearly in either dorsal vertebra VII (wherein it is incomplete) or VIII (which has suffered distortion in this region). Neither parapophysis is preserved in dorsal vertebra VII, whereas in dorsal vertebra VIII the left parapophyseal process is present, but the articular facet has been lost. Each parapophysis was supported ventrally by an ACPL that is much thinner than the CPRL, with which it shares a ventral base. In dorsal vertebra VIII, the ACPL and CPRL, together with the PRPL, define a deeply invaginated PACPRF that is more clearly visible anteriorly than laterally. As in both the paratype of *Diamantinasaurus* (Poropat *et al.*, 2015b) and *Savannasaurus* (Poropat *et al.*, 2020a), each parapophysis in the dorsal vertebrae of AODF 836 is

supported posteroventrally by a pair of PCPLs. These are a dPCPL, which projected from the same point on the centrum as the PCDL (or, as on the right side of dorsal vertebra VII, was essentially confluent with it: Fig. 24F), and a poorly-defined vPCPL that was more or less confluent with the ACPL. The ACPL, vPCPL and dPCPL form the borders of a moderately deep CPAF; the ACDL, which appears to be firmly coalesced with the PCDL, also contributes to this fossa. The dPCPL, the stout PPDL and the ACDL+PCDL enclose a PACDF. The diapophysis is ventrally supported by the PCDL, which is coalesced with the ACDL such that it appears to be anteroposteriorly expanded at its ventral end. A PODL is clearly evident in both dorsal vertebrae VII and VIII, meaning that the POCDF and POSDF were fully divided, as in dorsal vertebrae

VII–X of *Savannasaurus* (Poropat *et al.*, 2020a). In dorsal vertebra VIII, the POCDF hosts numerous deep foramina that appear to be a result of pre-fossilisation weathering; these reveal the camellate internal texture of the neural arch. The postzygapophyseal articular facets face ventrolaterally and are broader mediolaterally than they are long anteroposteriorly. The postzygapophysis is supported ventrally by a robust CPOL, which forms the posterior margin of the POCDF in each dorsal vertebra and, together with the dorsal margin of the centrum, defines a deep CPOF (Figs 24E, 25C). The postzygapophyses do not meet on the midline, and no TPOL is present between them; this feature is shared with both *Savannasaurus* and the paratype of *Diamantinasaurus* (Poropat *et al.*, 2015b, 2020a). Although dorsal vertebrae VII and VIII both preserve incomplete neural spines, it is clear that each was inclined posterodorsally–anteroventrally. Whether or not the neural spine was bifurcated is unclear, but it seems unlikely based on the preserved portions. Likewise, the presence or absence of lateral aliform processes could not be determined on any of the preserved vertebrae. Dorsal vertebra VIII preserves a pair of SPRLs [as in dorsal vertebra VII of *Savannasaurus* (Poropat *et al.*, 2020a); Fig. 25D], between which lies an SPRF; no PRSL is present. An undivided SPDL is present on dorsal vertebra VII (Fig. 24A, F). The SPDL, PODL and (presumably) the SPOL emarginate a deep POSDF. The SPOLs are prominent on dorsal vertebra VII and form the lateral margins of the SPOF. The lack of a TPOL means that the SPOF and CPOF are confluent (Figs 24E, 25C), as in both *Savannasaurus* and the paratype of *Diamantinasaurus* (Poropat *et al.*, 2015b, 2020a). The SPOF is bisected by a prominent POSL, which extends ventrally almost as far as the dorsal margin of the posterior neural canal opening, as in both *Savannasaurus* and the paratype of *Diamantinasaurus* (Poropat *et al.* 2015b, 2016, 2020a).

Sacrum: An incomplete sacrum comprises the ventral surfaces of two co-ossified centra (Fig. 26A). The transversely narrower of these is 165 mm long, and the broader centrum is 116 mm long. This sacrum closely resembles the fragmentary paratype sacrum of *Diamantinasaurus*. The centra are transversely convex along the midline (forming a subtle ridge), the ventrolateral margins of the centra flare inward, and the ventral ridge flares slightly at the preserved intercentral sutures (Poropat *et al.*, 2015b).

Appendicular skeleton

Right scapula: AODF 836 includes a fragmentary, poorly preserved right scapula (Fig. 27), which shows two features present in the holotype of *D. matildae*

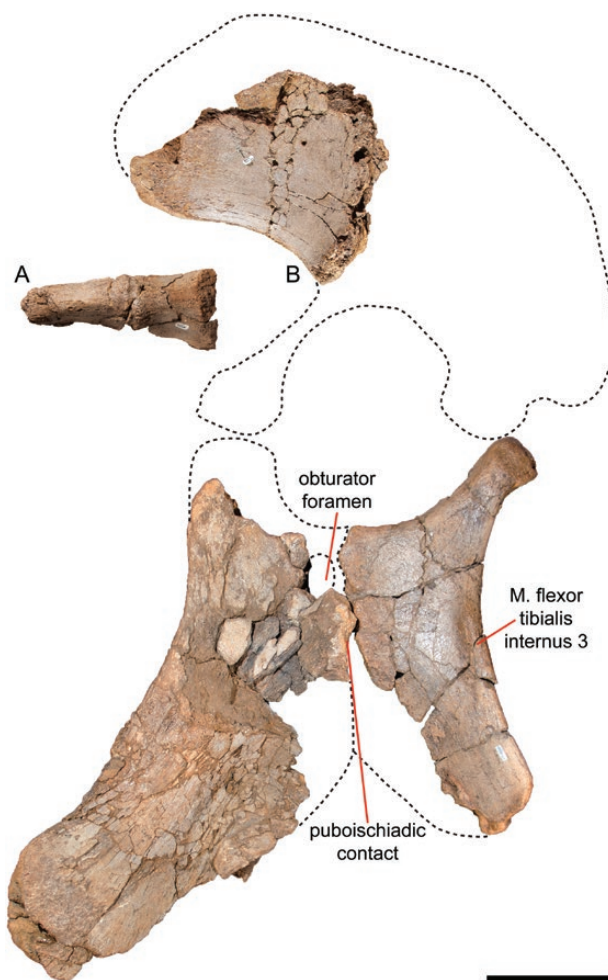


Figure 26. *Diamantinasaurus matildae* referred sacral and pelvic elements (AODF 836). A, sacral vertebrae in ventral view. B, left iliac acetabular process, pubis and ischium in lateral view. Scale bar: 200 mm.

(Poropat *et al.*, 2015b): (1) a laterally bevelled glenoid fossa; and (2) a flattened ridge on the ventral surface, separated from the glenoid region by a smooth, anteroposteriorly concave area (Poropat *et al.*, 2016). The AODF 836 scapula is otherwise largely uninformative, although the restoration of it presented herein differs from that provided by Poropat *et al.* (2016) because the posteroventral corner of the acromion plate was subsequently identified on the specimen.

Left and right ilia: The preacetabular lobes of both the left and right ilia are preserved (Fig. 26B; Table 4). These are essentially identical to the preacetabular lobe of the left ilium of the holotype of *D. matildae* (Poropat *et al.*, 2015b). The ventral surface is thin near the base, but thicker towards the anteroventral tip; and the anteroventral tip is not the anteriormost portion of the preacetabular lobe.

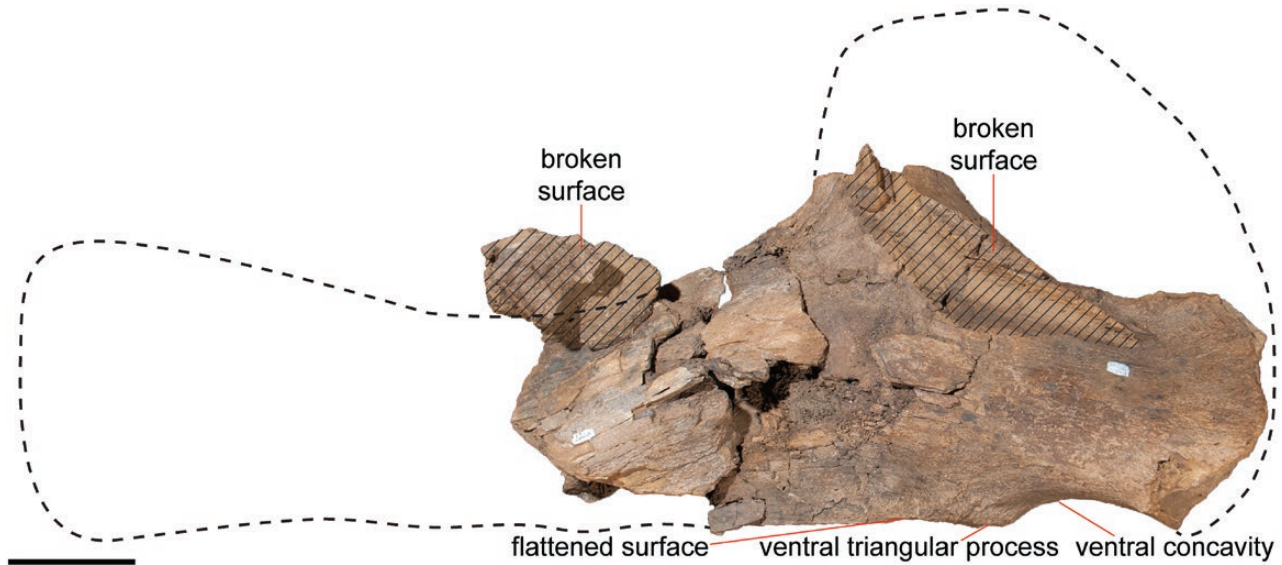


Figure 27. *Diamantinasaurus matildae* referred right scapula (AODF 836) in lateral view. Scale bar: 100 mm.

Table 4. Measurements of ilia of *Diamantinasaurus matildae* (AODF 836)

Measurement (mm)	Left	Right
Maximum anteroposterior length of preserved element	375	340

Left and right pubes: The left and right pubes of AODF 836 (Fig. 26B; Table 5) are virtually identical to those of the holotype specimen of *D. matildae* (Hocknull *et al.*, 2009; Poropat *et al.*, 2015b). The position of the obturator foramen, the overall relative proportions of the pubis and the curvature and thickness of the element all correspond well to the holotype of *D. matildae*, but do not match the pubes of *Savannasaurus*; the pelvic elements of *Savannasaurus*, although undistorted, are significantly thinner than those of *D. matildae* (Poropat *et al.*, 2015b) or AODF 836. The left pubis of AODF 836 is more complete than the right, although the acetabular margins and iliac peduncles of both are not preserved. Both pubes preserve the ventral margins of the obturator foramen, although this feature is more completely preserved in the left pubis. On neither are the ‘grooves’ and ‘ridges’ reported in the holotype specimen present (Poropat *et al.*, 2015b); reassessment of these structure shows that they are almost certainly taphonomic in origin and not autapomorphic for *D. matildae*. The discrepancies in size between the left and right pubes of AODF 836 can be explained by the fact that these elements were fused along the midline: a small portion of the mid-shaft of the right pubis remains firmly attached to the left one.

Left and right ischia: The complete left ischium (Fig. 26B; Table 5), which is far better preserved than the incomplete right one, is virtually identical to the holotype ischium of *D. matildae* (Poropat *et al.*, 2015b). The proximal end is well developed, with a defined iliac articular process and a relatively reduced plate-like shaft. The ischia would have been fused along the midline, as in all titanosaurs (Upchurch, 1998; Wilson, 2002). The proximodistal length of the ischium is ~75% that of the preserved portion of the pubis, comparable with this value (69%) in the holotype of *D. matildae* (Poropat *et al.*, 2015b). The proximalmost point of the iliac articular process can be divided broadly into three surfaces. The largest of these slopes laterally and faces posterodorsally and would, presumably, have been the site of attachment for a muscle or tendon. The iliac articular surface itself is smaller, sub-triangular, and slopes ventromedially. Between and posterior to these surfaces is a notch, which represents the smallest of the three faces of the iliac process. The acetabular margin (280 mm) is broadly concave, faces dorsolaterally on the iliac process, and rotates to face mainly dorsally as it curves anteroventrally towards the pubic articulation. Below the acetabular margin, the lateral surface of the ischium is smooth and convex, whereas the medial surface is concave. The lateral surface of the ischial plate faces posterolaterally at the proximal end, curving to face posteroventrally at the distal end. A raised lateral ridge is present on the posterior margin at approximately the halfway point of the ischium, which would have been the attachment point for muscle flexor tibialis internus 3. The reduction or absence of this feature was identified

a Bremer support value of three in our equal weights parsimony analysis (Fig. 28). A posteriori pruning of *Sarmientosaurus* from the MPTs resolves AODF 836 as the sister taxon of *Diamantinasaurus*, supporting its referral. The contemporaneous Australian somphospondylan *Wintonotitan* Hocknull *et al.*, 2009 is recovered outside of Titanosauria in both analyses. Unlike previous iterations of this matrix, the extended implied weights topology is highly congruent with that of the equal weights parsimony analysis (Supporting Information, Figs S3, S4). Most previous versions using some form of implied weighting, including those that have applied a *k*-value of nine (Mannion *et al.*, 2019a), have recovered nearly all somphospondylans within Titanosauria, including a diverse ‘Andesauroidea’. Here, the taxa included within Titanosauria are identical between the two analyses, with the interrelationships largely congruent (following exploration via the Pruned Trees tool in TNT), and no ‘Andesauroidea’ is recovered.

DISCUSSION

DIAMANTINASAURIA – AN EARLY-BRANCHING CLADE OF GONDWANAN TITANOSAURS

Detailed comparison of AODF 836 with the holotype specimens of *Diamantinasaurus* and *Savannasaurus*, in tandem with comprehensive osteological descriptions (Poropat *et al.*, 2015b, 2016, 2020a; this study), has highlighted numerous morphological features that unite them to the exclusion of all other titanosaurs (except perhaps *Sarmientosaurus*; see section ‘*Sarmientosaurus* as a diamantinasaurian’). That these taxa form a clade has been supported in several phylogenetic analyses, including those presented herein. Consequently, we propose the name Diamantinasauria for the most inclusive clade that includes *D. matildae* but not *Saltasaurus loricatus*. Based on the two individuals of *Diamantinasaurus* (AODF 603 and AODF 836) and the type specimen of *Savannasaurus* (AODF 660), the following morphological features unite these members of Diamantinasauria.

Cervical centra with prominent lateral pneumatic foramina

This feature can be assessed only for AODF 836 (axis and cervical vertebrae III and V) and *Savannasaurus* (posterior cervical vertebra), but it is observed consistently. Given that well-developed pneumatic foramina tend not to be present on the cervical vertebral centra of derived titanosaurs, at least not in the anterior–middle section of the neck, this is most likely to be a plesiomorphic titanosaurian character that is retained in Diamantinasauria.

Interpostzygapophyseal laminae (TPOs) absent in dorsal vertebrae

All preserved dorsal vertebrae of *Savannasaurus* and both specimens of *Diamantinasaurus* consistently lack TPOs; their absence unites the spinopostzygapophyseal fossa (SPOF) and centropostzygapophyseal fossa (CPOF) as a single fossa (the SPOF+CPOF). Although this feature is irregularly observed along the dorsal series in some other sauropods (see above, and discussion by Poropat *et al.*, 2020a), the lack of TPOs is consistent in the dorsal vertebrae of diamantinasaurians.

Hyposphene–hypantrum articulations absent throughout dorsal vertebral series

As with the preceding character, the consistent absence of hyposphene–hypantrum articulations in the dorsal vertebrae of *Savannasaurus* and both *Diamantinasaurus* specimens is notable. The potential phylogenetic implications of this character are complex, but were discussed at length elsewhere (Poropat *et al.*, 2020a); in short, based on the phylogenetic distribution of this character state, the loss of these structures in diamantinasaurians was possibly independent from that in advanced titanosaurs.

Amphicoelous anterior caudal centra

Among diamantinasaurians, this character can be assessed only in *Savannasaurus*. Absence of strongly procoelous anterior caudal centra is almost certainly plesiomorphic for Titanosauria, given the condition in *Andesaurus* (Mannion & Calvo, 2011) and taxa immediately outside the titanosaur radiation. It is not currently clear whether the amphicoelous condition in *Savannasaurus* represents a reversal to the non-titanosaurian condition or whether the mildly procoelous anterior centra of *Andesaurus* represent an independent acquisition from that of later-branching titanosaurs. The latter generally have strongly procoelous caudal centra (Salgado *et al.*, 1997), although the opisthocelous condition in *Opisthocoeleicaudia* Borsuk-Białynicka, 1977 potentially suggests a more complex history of the evolution of caudal vertebral morphology.

D-Shaped sternal plate

Among diamantinasaurians, the sternal plate has been described only for *Savannasaurus* (Poropat *et al.*, 2016, 2020a). However, at least one incomplete (and undescribed) sternal plate is preserved in the type specimen of *Diamantinasaurus*, and it is also D-shaped, rather than reniform (S.F.P., pers. obs.,

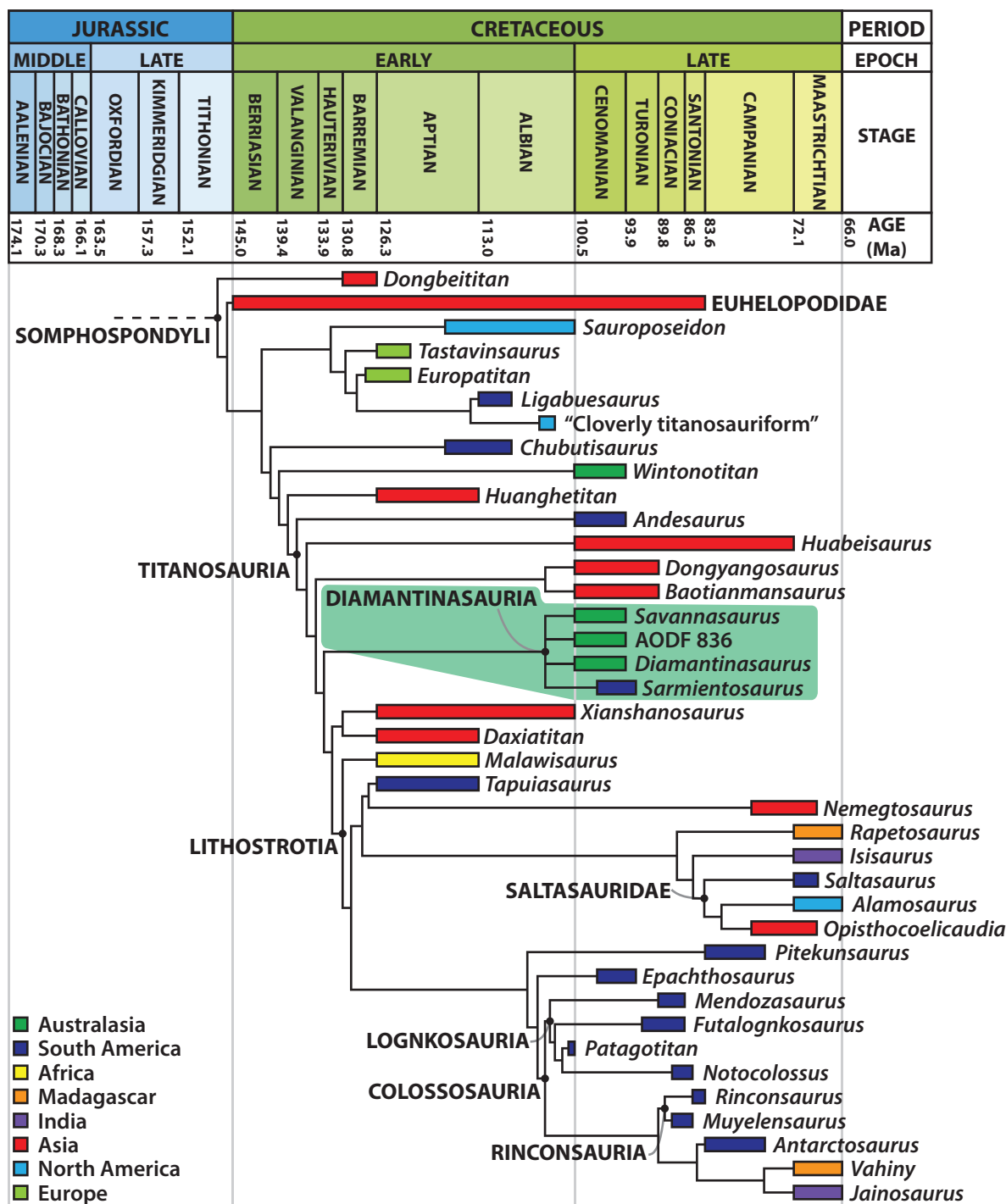


Figure 28. Time-calibrated agreement subtree showing the relationships within Somphospondyli based on the results of the extended implied weights phylogenetic analysis. Euhelopodidae has been collapsed into a single lineage, and *Sarmientosaurus* has been restored to the position it occupied before pruning. Note that the overall topology is consistent with that produced by the equal weights analysis.

2019). Thus, the sternal plate of diamantinasaurians differs in shape from those of most titanosauriforms, including later-branching titanosaurs.

Presence of manual phalanges

Manual phalanges were recovered with the type specimens of both *Diamantinasaurus* and

Savannasaurus (Hocknull *et al.*, 2009; Poropat *et al.*, 2015b, 2016, 2020a). The presence of manual phalanges is probably plesiomorphic for Titanosauria (González Riga *et al.*, 2019), given their retention in diamantinasaurians. As such, this character state is probably a symplesiomorphy, supporting an early-branching titanosaurian position for Diamantinasauria, rather than a synapomorphy of the clade. However, our understanding of the evolution of this feature in titanosaurs is extremely limited, with *Epachthosaurus* Powell, 1990 being the earliest-diverging titanosaur known to have lost its manual phalanges entirely (Martínez *et al.*, 2004; Poropat *et al.*, 2015a).

SARMIENTOSAURUS AS A DIAMANTINASAURIAN

All phylogenetic analyses conducted in this study returned *Sarmientosaurus* in a polytomy with *Savannasaurus* and the two specimens of *Diamantinasaurus*. Thus, based on our results and our definition of Diamantinasauria, *Sarmientosaurus* is a member of this newly erected clade. If correct, this would provide fresh support for previously hypothesized interchange between titanosaurians in Australia and South America during the mid-Cretaceous (Poropat *et al.*, 2016; see below).

Sarmientosaurus is represented by a virtually complete skull and a series of fragmentary anterior–middle cervical vertebrae. Consequently, the type and only known specimen of this taxon does not overlap anatomically with the type specimens of either *Diamantinasaurus* or *Savannasaurus*. However, it can be compared with the referred specimen of *Diamantinasaurus* (AODF 836) described herein. As outlined above, numerous features are shared between *Sarmientosaurus* and AODF 836: (1) the quadrate fossa faces posterolaterally; (2) the parietal occipital process is slightly taller than the foramen magnum; (3) the occipital fossa is restricted to the medial half of the parietal; (4) the basal tubera are narrowly divergent (~40°); (5) the laterosphenoid hosts more than one opening for the trigeminal nerve (CN V; two in *Diamantinasaurus*, three in *Sarmientosaurus*); (6) the anterior semicircular canal is much larger than its posterior counterpart; and (7) the cervical centra possess prominent lateral pneumatic foramina [also seen in the sole preserved posterior cervical vertebra of *Savannasaurus* (Poropat *et al.*, 2020a)]. Some of these features are more widespread within Titanosauria (e.g. a posterolaterally facing quadrate fossa), whereas others appear to be plesiomorphic for that clade (e.g. prominent lateral pneumatic foramina in cervical centra). By contrast, at least one of these features (the presence of more than one opening on each side for CN V) has otherwise only ever been observed in

Sarmientosaurus among neosauropods (Martínez *et al.*, 2016).

Despite the similarities between *Sarmientosaurus* and *Diamantinasaurus* listed above, there are also differences. For example, the braincase of *Sarmientosaurus* possesses two exits for CN XII, whereas *Diamantinasaurus* has only one; thus, the latter displays the morphology once considered ‘typical’ for Titanosauria (Paulina Carabajal, 2012), albeit one that has since been shown to have a much more complex distribution within that clade (Knoll *et al.*, 2019). More notable, however, are the apparent similarities and differences between the cervical vertebrae. The axis of AODF 836 is short anteroposteriorly relative to its dorsoventral height, seemingly contrasting with the incomplete axis of *Sarmientosaurus*, which, as described, is long and low, with substantially longer postzygapophyses than observed in other sauropod axes (Martínez *et al.*, 2016). The axis of *Sarmientosaurus* was also described as lacking lateral pneumatic fossae (Martínez *et al.*, 2016), which, if true, would constitute a clear difference between *Sarmientosaurus* and *Diamantinasaurus*. However, the incompleteness of the axis in *Sarmientosaurus* might mean that these structures were simply not preserved, rather than genuinely absent. The axial neural spine of *Sarmientosaurus* is substantially shorter than that of *Diamantinasaurus*, although again this might be because it is incomplete.

The two most complete cervical vertebrae in *Sarmientosaurus* were interpreted as the sixth and seventh by Martínez *et al.* (2016). Each is reasonably well preserved and (in detail, at least) similar to the middle cervical vertebrae of *Diamantinasaurus*. A lateral pneumatic excavation, dorsally bounded by a horizontal lamina, is present on each side of the centrum of cervical six in both *Sarmientosaurus* (Martínez *et al.*, 2016) and *Diamantinasaurus* (Fig. 21). Martínez *et al.* (2016) regarded the presence of ‘centroprezygapophyseal pillars’, i.e. posteriorly unsupported CPRLs, as an autapomorphy of *Sarmientosaurus*. However, as discussed by those authors, this might be an artefact of preservation. In the middle cervical neural arch of *Diamantinasaurus* (Fig. 22), the formation of a PRCDF immediately posterior to the CPRL means that the bone in this region is extremely thin. It is not implausible that a similarly delicate sheet of bone was lost in the middle cervical vertebrae of *Sarmientosaurus* (Martínez *et al.*, 2016). Finally, in the middle cervical vertebrae of both *Sarmientosaurus* and *Diamantinasaurus*, the apex of the neural spine is situated well posterior to the midlength of the centrum. Despite these similarities, there is one obvious difference between the middle cervical vertebrae of *Diamantinasaurus* and *Sarmientosaurus*: their degree of elongation. In cervical

six of *Sarmientosaurus*, the average elongation index is 4.71, whereas in cervical six of *Diamantinasaurus* it is 2.67. If the serial positions of all cervical vertebrae concerned are approximately correct, this represents a substantial incongruence. Simply put, it would imply that *Sarmientosaurus* had a far longer neck, relative to body size, than *Diamantinasaurus*.

Assuming that *Sarmientosaurus* is a diamantinasaurian, it would be reasonable to expect some degree of morphological divergence from Australian relatives, given its spatial (and minor temporal) separation from them. However, it is also possible that these anatomical differences indicate a more distant relationship between *Sarmientosaurus* and diamantinasaurians than the results of the phylogenetic analyses presented herein suggest. Under this scenario, many of their seemingly shared features would be more widespread amongst early-diverging titanosaurs (or somphospondylans slightly outside of Titanosauria), but the incompleteness of early titanosaur fossils, coupled with the absence of these features in better-preserved early-diverging somphospondylans and later-branching titanosaurs, results in their false recovery as diamantinasaurian synapomorphies. Consequently, we tentatively support *Sarmientosaurus* as a diamantinasaurian, pending the discovery of more complete postcranial material of this genus, in addition to increased sampling of early titanosaurs in general.

PALAEOBIOGEOGRAPHICAL IMPLICATIONS OF DIAMANTINASAURIA

The origins and biogeographical history of mid-Cretaceous Australian dinosaur faunas have proved to be controversial (e.g. [Agnolin *et al.*, 2010](#); [Barrett *et al.*, 2011](#); [Benson *et al.*, 2012](#); [Novas *et al.*, 2013](#)). This topic was reviewed by [Poropat *et al.* \(2015b\)](#). Here, we focus our discussion on developments during the past 5 years. Although potentially an oversimplification, it is convenient to divide explanations of the origin of Australian Cretaceous dinosaur faunas into two broad categories. The first set of hypotheses argues for the existence of largely cosmopolitan dinosaur clades during the Jurassic, with regional differences developing in the Cretaceous as a result of extinction ([Barrett *et al.*, 2011](#); [Benson *et al.*, 2012](#); [Fitzgerald *et al.*, 2012](#); [Rich *et al.*, 2014](#)). Curiously, under this scenario it seemed that Australian faunas were more similar to those from Laurasia, especially East Asia, than they were to those from other parts of Gondwana (e.g. [Benson *et al.*, 2012](#)). One potential explanation for apparent similarities between mid-Cretaceous Australian and East Asian faunas, despite separation of these areas by thousands of kilometres of ocean, is that these regions had more mesic climates, whereas

other Pangaeian fragments were more arid ([Benson *et al.*, 2012](#)). For example, if tyrannosauroids preferred higher-latitude, cooler, more humid environments, whereas abelisauroids preferred hotter and drier climates, this could explain observations such as the presence of the latter clade in South America, Africa, and so on, and their absence in Australia, in the mid-Cretaceous ([Benson *et al.*, 2012](#)). The second set of hypotheses focus on closer biotic similarities between Australia and other parts of Gondwana, especially South America ([Molnar, 1992](#); [Upchurch *et al.*, 2002](#); [Smith *et al.*, 2008](#); [Agnolin *et al.*, 2010](#); [Herne *et al.*, 2010](#); [Novas *et al.*, 2013](#); [Poropat *et al.*, 2015b, 2016](#); [Bell *et al.*, 2016](#)). These explanations invoke trans-Antarctic dispersal in the mid-Cretaceous (often mediated by latitudinal shifts in climate) and vicariance.

The first point to note is that, despite occasionally strident debate in the literature, these two broad categories of hypotheses are not mutually exclusive. It is possible for a major clade, such as Titanosauria, to be cosmopolitan, while simultaneously containing less-inclusive clades with more restricted Gondwanan or trans-Antarctic distributions. Likewise, there is nothing in biogeographical theory to suggest that regional extinction and vicariance can never work together to create differences between biotas. The goal of palaeobiogeographers working on this issue is thus not to overturn one of these broad hypothesis sets, but to disentangle their combined role in producing Australian dinosaur faunas.

Recent Australian discoveries, although still often fragmentary, have tended to strengthen the case for strong biotic affinities between Australia and South America during the mid-Cretaceous. For example, [Brougham *et al.* \(2020\)](#) described a cervical vertebra from the Grimman Creek Formation, near Lightning Ridge, which they identified as the first evidence for the presence of the theropod clade Noasauridae in Australia. Noasauridae is currently known only from Gondwanan landmasses ([Poropat *et al.*, 2020b](#)), and the Grimman Creek cervical vertebra shares derived features that (at present) are seen elsewhere only in *Noasaurus* Bonaparte & Powell, 1980 from the Maastrichtian of Argentina ([Brougham *et al.*, 2020](#)). However, caution is required at this stage, because other noasaurids are so incomplete that it is difficult to evaluate the true phylogenetic significance of these potential synapomorphies. This illustrates a common problem: many of the Australian dinosaur specimens that lie at the heart of the current controversy are incomplete and thus have uncertain affinities [e.g. compare [Agnolin *et al.* \(2010\)](#) and [Novas *et al.* \(2013\)](#) with [Benson *et al.* \(2012\)](#) and [Rich *et al.* \(2014\)](#)]. For example, [Barrett *et al.* \(2011\)](#) proposed that an isolated cervical vertebra belonged to an Australian spinosaurid (see also [Benson *et al.*, 2012](#)), whereas

Novas *et al.* (2013) reassessed each of the relevant characters and concluded that it could not be identified beyond indeterminate Averostrina or Tetanurae. More recently, Poropat *et al.* (2019) described new Australian megaraptorid remains, allowing them to demonstrate that the putative spinosaurid cervical was more plausibly identified as a megaraptorid.

Until relatively recent times, the mid-Cretaceous Australian dinosaur fossil record largely lacked well-preserved specimens that could be incorporated into phylogenetic data sets and thus inform this biogeographical debate. Clearly, phylogenetic topologies themselves are subject to debate and change and therefore do not offer a panacea, but they can yield more secure grounds for testing biogeographical hypotheses than do isolated specimens that can be compared only on the basis of a handful of character states. Substantial progress has been made over the past 5–10 years, with a number of more complete dinosaur specimens being reported from Australia and added to phylogenetic data sets (e.g. Poropat *et al.*, 2015b, 2016; Bell *et al.*, 2016, 2019; Herne *et al.*, 2018). These studies have typically demonstrated that although mid-Cretaceous Australian dinosaurs are indeed usually members of large clades with virtually global distributions, they also tend to have their closest relatives among Gondwanan taxa, notably often those from South America. In particular, Herne *et al.* (2019) found evidence in support of a Gondwanan clade of elasmarian ornithomorphs that included a cluster of small-bodied taxa from the Cretaceous of Australia and South America. This clade potentially also encompasses taxa from Antarctica (Rozadilla *et al.*, 2016; Herne *et al.*, 2019). However, caution is again warranted because this elasmarian clade had only weak support, and the larger-bodied Australian iguanodontian *Muttaborrasaurus* Bartholomai & Molnar, 1981 did not display close affinities with exclusively Gondwanan taxa (Herne *et al.*, 2019). Bell *et al.* (2019) described a new early-branching iguanodontian, *Fostoria dhimbangunmal* Bell *et al.*, 2019, from the Cenomanian Griman Creek Formation. Their phylogenetic analysis placed *Fostoria* Bell *et al.*, 2019 as the sister taxon to a Gondwanan clade that included *Muttaborrasaurus* in addition to *Anabisetia* Coria & Calvo, 2002 from the Turonian of Argentina and *Talenkauen* Novas *et al.*, 2004 from the Campanian–Maastrichtian of Argentina (Rozadilla *et al.*, 2019). Once more, the phylogenetic topology, although suggestive, was regarded as weakly supported by Bell *et al.* (2019), and these authors considered it premature to infer any biogeographical implications at that time. As an example of the labile nature of ornithomorph relationships, a recent analysis recovered *Muttaborrasaurus* and *Fostoria* as the earliest-diverging members of Rhabdodontomorpha, otherwise known only from Europe, whereas only South American and Antarctic species (including *Anabisetia*

and *Talenkauen*) were recovered within Elasmaria (Dieudonné *et al.*, 2020).

Australovenator wintonensis Hocknull *et al.*, 2009 is the most completely preserved non-avian theropod currently known from Australia (White *et al.*, 2012, 2013, 2015). It is generally accepted that this taxon is a megaraptoran (Novas *et al.*, 2013; Bell *et al.*, 2016; Poropat *et al.*, 2019), although its exact position within this group is debated (Lamanna *et al.*, 2020). Older phylogenetic studies placed *Australovenator* Hocknull *et al.*, 2009 as the sister taxon of *Fukuiraptor* (Azuma & Currie, 2000) from Japan (Benson *et al.*, 2010). However, more recently there has been support for a monophyletic Gondwanan Megaraptoridae that includes *Megaraptor* Novas, 1998 from Argentina and *Australovenator*, with *Fukuiraptor* as sister taxon to this clade (Novas *et al.*, 2013; Bell *et al.*, 2016; Porfiri *et al.*, 2018). Bell *et al.* (2016) applied quantitative biogeographical methods (Statistical Dispersal-Vicariance Analysis [S-DIVA] and Bayesian Binary Markov [BBM]) to their phylogenies and found that Megaraptora originated in Laurasia and then dispersed into Gondwana, where it gave rise to Megaraptoridae. Australian and South American megaraptorids are each other's closest relatives and imply at least one trans-Antarctic dispersal event between ~102 and 92 Mya. By contrast, recent work on tyrannosauroids found that the mid-Cretaceous South American *Santanaraptor* Kellner, 1999 was not the closest relative of Australian forms such as *Timimus hermani* Rich & Vickers-Rich, 1994, a result that is more consistent with an early Pangaeian radiation of this clade in the Jurassic, followed by regional extinction (Delcourt & Grillo, 2018). However, given that only one tyrannosauroid specimen from South America and two from Australia are currently known [assuming that megaraptorans are not tyrannosauroids (Novas *et al.*, 2016; Porfiri *et al.*, 2018)], sampling failure could easily have obscured trans-Antarctic relationships.

In this context, the phylogenetic results of the present work contribute further support to the hypothesis that, at least at finer taxonomic levels, Cretaceous dinosaurian faunas of Australia often display affinities with those of South America. In preliminary phylogenetic analyses, *Diamantinasaurus* clustered with latest Cretaceous Asian taxa, such as *Opisthocoelicaudia* (Hocknull *et al.*, 2009), and apparently added evidence in favour of cosmopolitanism or closer biotic affinities between Australia and Laurasia than with other Gondwanan areas (e.g. Barrett *et al.*, 2011). This position shifted slightly as a result of the discovery of more material of *Diamantinasaurus*, the addition of *Savannasaurus* and updated phylogenetic work (Poropat *et al.*, 2015b, 2016; Mannion *et al.*, 2017). In the study by Mannion *et al.* (2017), in particular, Australian titanosaurs

formed a monophyletic group that was the sister taxon of a larger clade containing some Laurasian taxa and a large number of Gondwanan taxa. Moreover, Poropat *et al.* (2016) applied the quantitative biogeographical method BIOGEOBEARS, a maximum likelihood approach that estimates ancestral areas (Matzke, 2013, 2014). These analyses suggested that a large clade of somphospondylans had become widespread across much of Pangaea during the Jurassic and earliest Cretaceous, with subsequent faunas differentiating as a result of both regional extinction and dispersal. Poropat *et al.* (2016) combined data on fossil record sampling, climatic shifts and biogeographical history to infer dispersal from South America to Australia in the late Albian or later. This event coincided with global warming that resulted in a southward shift of more temperate conditions, potentially increasing the feasibility of the dispersal of sauropods across Antarctica.

The Australian Cretaceous sauropod record comprises footprints demonstrating that sauropods lived in north-west Australia during the Valanginian–Barremian (Thulborn *et al.*, 1994; Thulborn, 2012; Salisbury *et al.*, 2017) and body fossils that evince the presence of somphospondylan titanosauriforms (including non-titanosaurian somphospondylans and early-branching titanosaurs) in north-east Australia (Queensland and New South Wales) throughout the late Albian–Cenomanian (Longman, 1933; Coombs & Molnar, 1981; Molnar, 2001, 2010, 2011a, b; Molnar & Salisbury, 2005; Hocknull *et al.*, 2009; Poropat *et al.*, 2015a, b, 2016, 2017, 2020a). Sauropods are unknown in the Cretaceous of south-central and south-east Australia, despite abundant evidence of ornithomimid, ankylosaurian and theropod dinosaurs in Barremian–to Albian-aged deposits in this region (Rich & Rich, 1989; Rich & Vickers-Rich, 1999; Barrett *et al.*, 2010a, b; Benson *et al.*, 2012; Herne *et al.*, 2018, 2019; Poropat *et al.*, 2018, 2019, 2020b). Consequently, sauropods are presumed to have been genuinely absent in this region at this time. This implies that the Albian–Cenomanian sauropods of north-east Australia descended either from lineages that persisted in northern Australia from the Barremian until the Albian [specifically, in areas not submerged by the Eromanga Sea (Cook *et al.*, 2013)] or from sauropods that entered Australia during or after the Albian. By that time, the only other continents to which Australia was connected were Zealandia to the east (Mortimer *et al.*, 2017) and Antarctica (via Tasmania) to the south-east (Seton *et al.*, 2012). The fact that the Cenomanian-aged *Diamantinasaurus* (represented by AODF 603 and AODF 836) and *Savannasaurus* (AODF 660) from Australia form a clade with the Cenomanian–to Turonian-aged *Sarmientosaurus musacchioi* from South America implies interchange of early-branching

titanosaurians across Antarctica slightly before or during the Cenomanian stage (Poropat *et al.*, 2016). As with the phylogenies of ornithomimids and theropods discussed above, our current topology offers only relatively weak support (Bremer support = 3) for a sister-taxon relationship between a South American form (*Sarmientosaurus*) and Australian titanosaurs (*Diamantinasaurus* and *Savannasaurus*), reflecting the incompleteness of the postcranial skeleton of the former taxon, in particular. Nevertheless, our currently best-supported topology (Fig. 28) represents a further example of the shift towards discovery of close biotic affinities among the mid-Cretaceous dinosaurs of South America and Australia, and it directly supports the inferred presence of ancestors of the Australian titanosaurs in South America predicted by the BIOGEOBEARS results of Poropat *et al.* (2016).

In summary, the dichotomy between cosmopolitanism plus regional extinction and close biotic affinities with South America, as explanations of the origins of mid-Cretaceous Australian dinosaurian faunas, is a false one. Current evidence does suggest that, at higher taxonomic levels, Australian dinosaurs are often members of widespread clades. However, at lower levels (i.e. typically, relationships between small clusters of genera or species) a picture of close affinity with Gondwanan taxa, especially those in South America, is beginning to emerge. This matches the general pattern noted by Upchurch *et al.* (2002), who proposed that statistically significant continent-scale vicariance signals seem to manifest themselves at the generic level among dinosaurs. Although caution is required because of the perennial issues of sampling failure and phylogenetic instability in biogeographical reconstructions (e.g. Mannion *et al.*, 2019b; Kubo, 2020), recent analyses have started to find evidence for South America–Australia sister-taxon relationships among ornithomimids, megaraptorids and titanosaurs. This runs counter to the claims of a lack of such evidence in earlier studies that supported cosmopolitanism plus regional extinction (e.g. Barrett *et al.*, 2011; Benson *et al.*, 2012; Fitzgerald *et al.*, 2012). The more recent phylogenetic results also tend to undermine the hypothesis that Australian and South American dinosaurian faunas differentiated in the Cretaceous as a result of developing more mesic and more arid climatic regimens, respectively (e.g. Benson *et al.*, 2012). The interpretation proposed here is consistent with the recent biogeographical analyses of Kubo (2020), who used a phylogenetic network approach and a dinosaurian supertree to demonstrate that Cretaceous Australian dinosaur faunas have their closest links to South America, within a larger Gondwanan set of biotic affinities. It will be important to test these ideas further via discoveries of more complete specimens of key taxa, such as *Sarmientosaurus*, combined with the

ongoing process of adding and revising phylogenetic characters.

THE TIMING AND SELECTIVITY OF TRANS-ANTARCTIC SAUROPOD DISPERSALS

In neither Australian nor southern South American (Patagonian) Cenomanian faunas were diamantinasaurians the only sauropods present. In addition to *Sarmientosaurus*, the lower Bajo Barreal Formation of southern Argentina has yielded the rebbachisaurid diplodocoid *Katapultosaurus goicocheai* Ibiricu *et al.*, 2013 (Ibiricu *et al.*, 2012, 2013, 2015) and the early-branching titanosaur *Epachthosaurus sciuttoi* Powell, 1990 (Martínez *et al.*, 2004; Ibiricu *et al.*, 2020). Although no teeth are presently known for *Katapultosaurus* Ibiricu *et al.*, 2013, phylogenetic bracketing implies that it, like all diplodocoids, had narrow-crowned teeth (Whitlock, 2011a). In support of this hypothesis, a narrow-crowned sauropod tooth from the lower Bajo Barreal Formation (UNPSJB-PV 847), originally assigned to Titanosauridae (Powell *et al.*, 1989), has recently been reinterpreted as being from a rebbachisaurid (Alvarez *et al.*, 2019). Thus, sauropods with both narrow- and (relatively) broad-crowned (i.e. *Sarmientosaurus*) teeth coexisted in the earliest Late Cretaceous of Patagonia. Lack of anatomical overlap between *Epachthosaurus* (which preserves most of the postcranial skeleton, except for the neck) and *Sarmientosaurus* (known only from the skull and anterior–middle cervical vertebrae) currently precludes comparison of these two taxa. However, as pointed out by Martínez *et al.* (2016), rare sauropod cranial elements from the lower Bajo Barreal Formation [e.g. the maxilla UNPSJB-PV 583 (Sciutto & Martínez, 1994)] support the notion that at least one other titanosaurian taxon, with slightly narrower-crowned teeth than *Sarmientosaurus*, lived alongside it.

In contrast to the lower Bajo Barreal Formation of Patagonia, the Winton Formation (and, indeed, the Australian fossil record as a whole; Frauenfelder *et al.*, 2020) preserves no evidence of rebbachisaurid sauropods, nor of any sauropods with narrow-crowned teeth. Although future discoveries might change this, based on current evidence the only non-diamantinasaurian sauropod known from the Winton Formation is the non-titanosaurian somphospondylan *Wintonotitan watti* (Hocknull *et al.*, 2009; Poropat *et al.*, 2015a). Rigorous assessment of niche partitioning between *Wintonotitan* and diamantinasaurians is precluded by the incompleteness of the former and by the fact that no sauropod teeth or dentulous elements have yet been reported from the Winton Formation.

Whether or not we should expect to find sauropods with narrow-crowned teeth in the Winton Formation

(specifically, diplodocoids) remains an open question. Before the Jurassic–Cretaceous transition, flagellicaudatan diplodocoids (dicraeosaurids and diplodocids) would have been able to enter Australia from the west, because Madagascar and India formed a contiguous land area between eastern Africa, Antarctica and south-west Australia (Seton *et al.*, 2012). Given that dicraeosaurids and diplodocids were both thriving in eastern Africa (Janensch, 1914, 1929, 1935–1936, 1961; Remes, 2006, 2009; Schwarz-Wings & Böhm, 2014) and Patagonia (Rauhut *et al.*, 2005, 2015; Salgado *et al.*, 2015b) during the latest Jurassic and persisted into the earliest Cretaceous of southern Africa (McPhee *et al.*, 2016) and Patagonia (Gallina *et al.*, 2014, 2019; Paulina Carabajal *et al.*, 2018; Coria *et al.*, 2019; Windholz *et al.*, 2020), they would have had ample opportunity to enter Australia at this time. However, by the end of the Barremian, both diplodocids and dicraeosaurids appear to have gone extinct worldwide; the dicraeosaurids of the La Amarga Formation are the geologically youngest flagellicaudatans known (Salgado & Bonaparte, 1991; Salgado & Calvo, 1992; Apesteguía, 2007; Gallina, 2016; Windholz *et al.*, 2021). Thus, even if flagellicaudatans occupied Australia, they might not have persisted until the mid-Cretaceous. For rebbachisaurids, the scenario was somewhat different. The oldest putative rebbachisaurids date to the latest Jurassic of North America (Carpenter, 2018) and the earliest Cretaceous of Europe (Taylor, 2018), implying a northern origin for the clade. Although rebbachisaurids appear not to have persisted into the Cretaceous in North America, they occupied Europe until at least the early Aptian (Dalla Vecchia, 1999; Pereda Suberbiola *et al.*, 2003; Mannion, 2009; Mannion *et al.*, 2011; Torcida Fernández-Baldor *et al.*, 2011). Rebbachisaurids make their earliest appearances in Afro-Arabia in the late Hauterivian–early Barremian (*Histriasaurus* Dalla Vecchia, 1998 from present-day Croatia; Dalla Vecchia, 2005) and South America in the Barremian (*Zapalasaurus* Salgado *et al.*, 2006), by which time Africa and Indo-Madagascar had detached from Antarctica and each other (Seton *et al.*, 2012). Based on the distribution of their earliest occurrences, rebbachisaurids are likely to have dispersed into Africa from Europe (via the ‘Apulian route’), then from north-west Africa into north-east South America before or during the Barremian (Lindoso *et al.*, 2019; Pereira *et al.*, 2020). During the mid-Cretaceous, rebbachisaurids proliferated in northern Africa (Serenó *et al.*, 1999, 2007; Fanti *et al.*, 2013, 2014, 2015; Mannion & Barrett, 2013; Wilson & Allain, 2015), north-east South America (Carvalho *et al.*, 2003; Medeiros & Schultz, 2004; Castro *et al.*, 2007; Lindoso *et al.*, 2019; Pereira *et al.*, 2020) and Patagonia (Calvo & Salgado, 1995; Bonaparte, 1996; Calvo, 1999; Salgado *et al.*, 2004, 2006, 2012; Gallina & Apesteguía,

2005; Apesteguía, 2007; Carballido *et al.*, 2010, 2012; Haluza *et al.*, 2012; Paulina Carabajal *et al.*, 2016; Canudo *et al.*, 2018). Some of the geologically youngest rebbachisaurids in South America (Ibiricu *et al.*, 2013, 2015) are the highest-latitude (palaeolatitude of ~52°S) representatives of the clade (Ibiricu *et al.*, 2012), but their remains have never been recovered from southern Patagonia. By contrast, titanosaurs are known from the southern extent of Patagonia in the latest Cretaceous (e.g. Lacovara *et al.*, 2014; Novas *et al.*, 2019). Taken at face value, we might therefore infer that rebbachisaurids never ventured into high palaeolatitudes (approaching 60°), as is also supported by their absence from southern Africa (Mannion & Barrett, 2013). Thus, following this line of reasoning, rebbachisaurids never dispersed as far south as Antarctica and therefore would not have been able to expand into Australia. However, no dinosaur fossils are currently known from southern Patagonia during the mid-Cretaceous, including titanosaurs, and the African record is also extremely patchy (e.g. Benson *et al.*, 2013; Mannion & Barrett, 2013). As such, we cannot be sure that rebbachisaurids were genuinely absent from these high-latitude ranges at this time, with our earliest high-latitude sampling window (Campanian) occurring long after the demise of the group.

If diamantinasaurians could traverse Antarctica to occupy both South America and Australia during the mid-Cretaceous, why could (or did) rebbachisaurids not? Perhaps the barrier to their dispersal was palaeoenvironmental. During the Albian–Cenomanian, the palaeofloras of the Gondwanan continents (by that time restricted to South America, Antarctica, Australia and Zealandia) were under sufficiently strong palaeolatitudinal control that several distinct floristic provinces have been recognized (Herngreen *et al.*, 1996; Cantrill & Poole, 2012; Mays, 2014). Lower-latitude Gondwanan floral provinces were characterized by abundant ferns and angiosperms, whereas the highest-latitude (i.e. southernmost) regions were dominated by conifers (Mays, 2014). A recent comparison of several Gondwanan mid-Cretaceous palynofloras demonstrated that those of the Mata Amarilla Formation in Patagonia are more similar to penecontemporaneous palynofloras of New Zealand and Antarctica than those of the coeval, and geographically more proximal, Cañadón Seco (an equivalent of the lower Bajo Barreal Formation) and Huincul formations from further north in Argentina (Santamarina *et al.*, 2020). Instead, the latter palynofloras were aligned with those of the Eromanga Basin: the Winton Formation and the underlying Mackunda Formation, Allaru Mudstone and Toolebuc Formation (Santamarina *et al.*, 2020). Both the lower Bajo Barreal and Huincul formations preserve

rebbachisaurids, whereas the Winton Formation does not. Rising temperatures during the late Albian reduced the latitudinal thermal gradient (Huber *et al.*, 2018) and facilitated the dispersal of angiosperms into the polar regions (Korasidis *et al.*, 2016; Korasidis & Wagstaff, 2020), along with diamantinasaurian titanosaurs. However, the same warming and floral change does not appear to have facilitated the spread of rebbachisaurids; indeed, it might even have been detrimental for this group (see ‘*Diamantinasaurian palaeoecology*’ section below).

The Australian sauropod record also lacks evidence for titanosaurs with procoelous caudal centra. The geologically oldest titanosaur from South America with strongly procoelous caudal centra is the late Albian *Patagotitan mayorum* Carballido *et al.*, 2017. By the Cenomanian–Turonian, titanosaurs with strongly procoelous caudal centra were widespread in Patagonia [e.g. *Epachthosaurus sciuttoi* (Martínez *et al.*, 2004), *Drusilasaura deseadensis* (Navarrete *et al.*, 2011), and *Quetecsaurus rusconii* (González Riga & Ortíz David, 2014)]. Despite their absence in the Cenomanian-aged Winton Formation (and in the Australian record generally), procoelous caudal vertebrae pertaining to titanosaurs have been identified in Campanian- to Maastrichtian-aged deposits in both New Zealand (Molnar & Wiffen, 2007) and Antarctica (Cerdeña *et al.*, 2012). These titanosaurs were almost certainly South American emigrants; if so, their arrival in New Zealand presumably pre-dated the Santonian (~85 Mya) onset of seafloor spreading in the Tasman Sea (Bache *et al.*, 2014). Before 95 Mya, the same palaeoenvironmental barrier that excluded rebbachisaurids from polar latitudes during the mid-Cretaceous might likewise have impeded the southward dispersal of titanosaurs with procoelous caudal centra, thereby precluding their entry into Australia. However, when that same barrier was lifted between 95 and 85 Mya, derived titanosaurs evidently dispersed, whereas rebbachisaurids were already in terminal decline and soon went extinct.

DIAMANTINASAURIAN PALAEOECOLOGY

The endocranial morphology of *Diamantinasaurus* is similar to that of *Sarmientosaurus*. Thus, some of the ecological interpretations inferred for the latter taxon by Martínez *et al.* (2016), particularly related to feeding height, might be transferable to *Diamantinasaurus* or to diamantinasaurians generally. However, the two specimens of *Diamantinasaurus* and the sole specimen of *Savannasaurus* preserve elements unknown in *Sarmientosaurus*, thereby facilitating a more complete assessment of the feeding envelope of diamantinasaurians.

Martínez *et al.* (2016) interpreted *Sarmientosaurus* to have been a low-level browser, based on the downward tilt of the snout relative to the neck when the skull was oriented in its 'alert posture' (determined from the orientation of the semicircular canals relative to the skull overall), and the extensive pneumatization of the cervical vertebrae. Although this interpretation is plausible, both the snout shape and the distribution and morphology of the teeth of *Sarmientosaurus* are more closely aligned with those of sauropods that are thought to have been higher-level browsers, such as brachiosaurids (Upchurch & Barrett, 2000). The neck of *Diamantinasaurus*, based on the vertebrae available, does not appear to have been particularly elongate, potentially supporting a low- to mid-level browsing niche for this taxon. However, the cervical ribs of *Savannasaurus* are elongate (Poropat *et al.*, 2020a), a feature more commonly seen in higher-browsing sauropods (Upchurch & Barrett, 2000). Furthermore, based on the preserved portions of the limbs of the *Diamantinasaurus* type specimen (Poropat *et al.*, 2015b), there would have been little discrepancy between the forelimb, which was ~2.4 m tall (humerus, 1068 mm; ulna, 700 mm; longest metacarpal, 412 mm; plus ~10% cartilage at each joint), and the hindlimb, which was ≥ 2.35 m tall without the pes (femur, 1345 mm; tibia, 795 mm; plus ~10% cartilage at each joint). Forelimb length to hindlimb length ratios of close to 1.0 (rather than close to 0.7) are again characteristic of sauropods often interpreted as medium- or high-level browsers (Upchurch & Barrett, 2000).

Rebbachisaurids appear to have been the low-level feeders *par excellence* among sauropods. The highly derived rebbachisaurid, *Nigersaurus* Sereno *et al.*, 1999, from the Aptian–Albian Elrhaz Formation of Niger has been identified as a highly specialized low-level feeder (Sereno & Wilson, 2005) that potentially subsisted mainly on horsetails and ferns (Sereno *et al.*, 2007), based on its anteriorly flattened and expanded Π -shaped jaws, its 'battery' of extremely narrow-crowned teeth and the presence of labial wear facets on those teeth (implying abrasion against a flat substrate, i.e. the ground). The few cranial remains known for other rebbachisaurid taxa [notably, *Lavocatisaurus agriensis* Canudo *et al.*, 2018, *Limaysaurus tessonei* (Calvo & Salgado, 1995) (Paulina Carabajal & Calvo, 2015) and an indeterminate rebbachisaurid from the Candeleros Formation of Argentina, MMCh-PV 71 (Paulina Carabajal *et al.*, 2016)] appear to be broadly similar to those of *Nigersaurus*, implying that the entire clade was specialized for low-level browsing. Such behaviour might have been suited only to savannah-type biomes (Whitlock, 2011a); thus, if such habitats were small in extent, non-contiguous or absent at high latitudes during the mid-Cretaceous (as suggested by

the heightened diversity and abundance of conifers in palaeofloras; see above), the palaeoenvironmental barrier that prevented the dispersal of rebbachisaurids into Australia via Antarctica might have been the conifer-dominated high-latitude floral province.

Assuming, for the sake of argument, that *Sarmientosaurus* and other diamantinasaurians were low-level browsers, they appear to have been nowhere near as specialized for that way of life as rebbachisaurids or, indeed, some later-branching titanosaurs [e.g. *Antarctosaurus wichmannianus* (Huene, 1929; Powell, 2003), *Baalsaurus mansillai* (Calvo & González Riga, 2019), *Bonitasaura salgadoi* Apesteguía, 2004 (Gallina & Apesteguía, 2011), and *Brasilotitan nemophagus* Machado *et al.*, 2013]. Given that the jaws of *Sarmientosaurus* are not anteriorly flattened, that the teeth are not entirely (or even mostly) restricted to the front of the mouth and that the downward inclination of the head in 'alert posture' was less extreme than in rebbachisaurids (Sereno *et al.*, 2007), the case for *Sarmientosaurus* as a specialist low-level browser appears far less robust than that for dicraeosaurids, diplodocids and rebbachisaurids (Whitlock, 2011a). The microwear patterns observed on the teeth of *Sarmientosaurus*, comprising grooves that are mostly parallel but that sometimes intersect, in addition to rarer pits of varying size and distributional density (Martínez *et al.*, 2016), also argue against predominantly low-level feeding in this taxon, and instead are more in line with mid-height (1–10 m) browsing (Whitlock, 2011a).

If diamantinasaurians were mid-level feeders, they presumably would not have been in direct competition with rebbachisaurids for food. Moreover, as generalist mid-level feeders rather than specialist low-level feeders, they might have been better able to adapt to new environments and food sources than rebbachisaurids. Verification of these tentative hypotheses will have to await the discovery of more complete diamantinasaurian material; however, they could hold the key to why these titanosaurs, but not rebbachisaurids, reached Australia.

CONCLUSION

The complete description of the referred specimen of *D. matildae* (AODF 836) presented herein, coupled with an expanded phylogenetic analysis, highlights the similarities between it and the type specimen, while concomitantly revealing that *Diamantinasaurus* forms a clade with the sympatric species *Savannasaurus elliottorum* and with the contemporaneous South American titanosaur *Sarmientosaurus musacchioi*. This clade, herein named Diamantinasauria, is presently known only from the Cenomanian–earliest Turonian, but crucially spans both southern South

- transition from Mesozoic subduction to continental breakup in the Zealandia sector of eastern Gondwana. *Gondwana Research* **26**: 1060–1078.
- Balanoff AM, Bever GS, Ikejiri T. 2010.** The braincase of *Apatosaurus* (Dinosauria: Sauropoda) based on computed tomography of a new specimen with comments on variation and evolution in sauropod neuroanatomy. *American Museum Novitates* **3677**: 1–29.
- Barrett PM, Benson RBJ, Rich TH, Vickers-Rich P. 2011.** First spinosaurid dinosaur from Australia and the cosmopolitanism of Cretaceous dinosaur faunas. *Biology Letters* **7**: 933–936.
- Barrett PM, Kear BP, Benson RBJ. 2010a.** Opalized archosaur remains from the Bulldog Shale (Aptian: Lower Cretaceous) of South Australia. *Alcheringa* **34**: 293–301.
- Barrett PM, Rich TH, Vickers-Rich P, Tumanova TyA, Inglis M, Pickering D, Kool L, Kear BP. 2010b.** Ankylosaurian dinosaur remains from the Lower Cretaceous of southeastern Australia. *Alcheringa* **34**: 205–217.
- Baumel JJ. 1993.** Systema cardiovasculare. In: Baumel JJ, King AS, Breazile JE, Evans HE, Van den Berge JC, eds. *Handbook of avian anatomy: nomina anatomica avium*, 2nd edn. Cambridge: Nuttall Ornithological Society, 407–475.
- Bell PR, Brougham T, Herne MC, Frauenfelder T, Smith ET. 2019.** *Fostoria dhimbangunmal* gen. et sp. nov., a new iguanodontian (Dinosauria, Ornithopoda) from the mid-Cretaceous of Lightning Ridge, New South Wales, Australia. *Journal of Vertebrate Paleontology* **39**: e1564757.
- Bell PR, Cau A, Fanti F, Smith E. 2016.** A large-clawed theropod (Dinosauria: Tetanurae) from the Lower Cretaceous of Australia and the Gondwanan origin of megaraptorid theropods. *Gondwana Research* **36**: 473–487.
- Bellairs AdA, Kamal AM. 1981.** The chondrocranium and the development of the skull in Recent reptiles. In: Gans C, Parsons TS, eds. *Biology of the Reptilia, Vol. 11. Morphology F*. London: Academic Press, 1–263.
- Benson RBJ, Carrano MT, Brusatte SL. 2010.** A new clade of archaic large-bodied predatory dinosaurs (Theropoda: Allosaurioidea) that survived to the latest Mesozoic. *Naturwissenschaften* **97**: 71–78.
- Benson RBJ, Mannion PD, Butler RJ, Upchurch P, Goswami A, Evans S. 2013.** Cretaceous tetrapod fossil record sampling and faunal turnover: implications for biogeography and the rise of modern clades. *Palaeogeography, Palaeoclimatology, Palaeoecology* **372**: 88–107.
- Benson RBJ, Rich TH, Vickers-Rich P, Hall M. 2012.** Theropod fauna from southern Australia indicates high polar diversity and climate-driven dinosaur provinciality. *PLoS One* **7**: e37122.
- Berman DS, Jain SL. 1982.** The braincase of a small sauropod dinosaur (Reptilia: Saurischia) from the Upper Cretaceous Lameta Group, central India, with review of Lameta Group localities. *Annals of the Carnegie Museum* **51**: 405–422.
- Berman DS, McIntosh JS. 1978.** Skull and relationships of the Upper Jurassic sauropod *Apatosaurus* (Reptilia, Saurischia). *Bulletin of the Carnegie Museum of Natural History* **8**: 1–35.
- Bonaparte JF. 1996.** Cretaceous tetrapods of Argentina. In: Arratia G, ed. *Contributions of southern South America to vertebrate paleontology: Müncher Geowissenschaftliche Abhandlung Reihe A: Geologie und Paläontologie, Band 30*. Munich: Dr. Friedrich Pfeil, 73–130.
- Bonaparte JF, Powell JE. 1980.** A continental assemblage of tetrapods from the Upper Cretaceous beds of El Brete, northwestern Argentina (Sauropoda-Coelurosauria-Carnosauria-Aves). *Mémoires de la Société Géologique de France (Nouvelle Série)* **139**: 19–28.
- Borsuk-Białynicka M. 1977.** A new camarasaurid sauropod *Opisthocoeleicaudia skarzynskii* gen. n., sp. n. from the Upper Cretaceous of Mongolia. *Palaeontologia Polonica* **37**: 5–64.
- Brougham T, Smith ET, Bell PR. 2020.** Noasaurids are a component of the Australian ‘mid’-Cretaceous theropod fauna. *Scientific Reports* **10**: 1428.
- Bryan SE, Cook AG, Allen CM, Siegel C, Purdy DJ, Greentree JS, Uysal IT. 2012.** Early–mid Cretaceous tectonic evolution of eastern Gondwana: from silicic LIP magmatism to continental rupture. *Episodes* **35**: 142–152.
- Burda DJ. 1969.** Developmental aspect of intracranial arterial supply in the alligator brain. *Journal of Comparative Neurology* **135**: 369–380.
- Calvo JO. 1999.** Dinosaurs and other vertebrates of the Lake Ezequiel Ramos Mexia Area, Neuquén - Patagonia, Argentina. In: Tomida Y, Rich TH, Vickers-Rich P, eds. *Proceedings of the Second Gondwanan Dinosaur Symposium. National Science Museum Monograph 15*. Tokyo: National Science Museum, 13–45.
- Calvo JO, Coria RA, Salgado L. 1997.** Uno de los más completos titanosáuridos (Dinosauria-Sauropoda) registrados en el mundo. [One of the most complete titanosaurids (Dinosauria-Sauropoda) reported in the world.] *Ameghiniana* **34**: 534.
- Calvo JO, González Riga B. 2019.** *Baalsaurus mansillai* gen. et sp. nov. a new titanosaurian sauropod (Late Cretaceous) from Neuquén, Patagonia, Argentina. *Anais da Academia Brasileira de Ciências* **91**: e20180661.
- Calvo JO, González Riga BJ, Porfiri JD. 2007a.** A new titanosaur sauropod from the Late Cretaceous of Neuquén, Patagonia, Argentina. *Arquivos do Museu Nacional, Rio de Janeiro* **65**: 485–504.
- Calvo JO, Kellner AW. 2006a.** Description of a sauropod dinosaur braincase (Titanosauridae) from the Late Cretaceous Rio Colorado Subgroup, Patagonia. *Anais da Academia Brasileira de Ciências* **78**: 175–182.
- Calvo JO, Kellner AWA. 2006b.** New titanosaurid braincase from the Rio Colorado Formation (Late Cretaceous), Neuquén, Patagonia, Argentina. In: *IV Simpósio Brasileiro de Paleontologia de Vertebrados*, Rio Claro, São Paulo, Brazil: Universidade Estadual Paulista (UNESP) 9–10.
- Calvo JO, Porfiri JD, González Riga BJ, Kellner AWA. 2007b.** Anatomy of *Futalognkosaurus dukei* Calvo, Porfiri, González Riga & Kellner, 2007 (Dinosauria, Titanosauridae) from the Neuquén Group (Late Cretaceous), Patagonia, Argentina. *Arquivos do Museu Nacional, Rio de Janeiro* **65**: 511–526.

- Calvo JO, Salgado L. 1995.** *Rebbachisaurus tessonei* sp. nov. a new Sauropoda from the Albian–Cenomanian of Argentina: new evidence on the origin of the Diplodocidae. *Gaia* **11**: 13–33.
- Cantrill DJ, Poole I. 2012.** *The vegetation of Antarctica through geological time*. New York: Cambridge University Press.
- Canudo JI, Carballido JL, Garrido A, Salgado L. 2018.** A new rebbachisaurid sauropod from the Aptian–Albian, Lower Cretaceous Rayoso Formation, Neuquén, Argentina. *Acta Palaeontologica Polonica* **63**: 679–691.
- Carballido JL, Garrido AC, Canudo JI, Salgado L. 2010.** Redescription of *Rayososaurus agrioensis* Bonaparte (Sauropoda, Diplodocoidea), a rebbachisaurid from the early Late Cretaceous of Neuquén. *Géobios* **43**: 493–502.
- Carballido JL, Pol D, Otero A, Cerda IA, Salgado L, Garrido AC, Ramezzani J, Cúneo NR, Krause MJ. 2017.** A new giant titanosaur sheds light on body mass evolution among sauropod dinosaurs. *Proceedings of the Royal Society B: Biological Sciences* **284**: 20171219.
- Carballido JL, Salgado L, Pol D, Canudo JI, Garrido A. 2012.** A new basal rebbachisaurid (Sauropoda, Diplodocoidea) from the Early Cretaceous of the Neuquén Basin; evolution and biogeography of the group. *Historical Biology* **24**: 631–654.
- Carpenter K. 2018.** *Maraapunisaurus fragillimus*, n.g. (formerly *Amphicoelias fragillimus*), a basal rebbachisaurid from the Morrison Formation (Upper Jurassic) of Colorado. *Geology of the Intermountain West* **5**: 227–244.
- Carpenter K, Tidwell V. 1998.** Preliminary description of a *Brachiosaurus* skull from Felch Quarry 1, Garden Park, Colorado. *Modern Geology* **23**: 69–84.
- Carvalho IdS, Avilla LdS, Salgado L. 2003.** *Amazonsaurus maranhensis* gen. et sp. nov. (Sauropoda, Diplodocoidea) from the Lower Cretaceous (Aptian–Albian) of Brazil. *Cretaceous Research* **24**: 697–713.
- Castro DF, Bertini RJ, Santucci RM, Medeiros MA. 2007.** Sauropods of the Itapecuru Group (Lower/Middle Albian), São Luís-Grajaú Basin, Maranhão State, Brazil. *Revista Brasileira de Paleontologia* **10**: 195–200.
- Cerda IA, Paulina Carabajal A, Salgado L, Coria RA, Reguero MA, Tambussi CP, Moly JJ. 2012.** The first record of a sauropod dinosaur from Antarctica. *Naturwissenschaften* **99**: 83–87.
- Chatterjee S, Rudra DK. 1996.** KT events in India: impact, rifting, volcanism and dinosaur extinction. *Memoirs of the Queensland Museum* **39**: 489–532.
- Chatterjee S, Zheng Z. 2002.** Cranial anatomy of *Shunosaurus*, a basal sauropod dinosaur from the Middle Jurassic of China. *Zoological Journal of the Linnean Society* **136**: 145–169.
- Chiappe LM, Salgado L, Coria RA. 2001.** Embryonic skulls of titanosaur sauropod dinosaurs. *Science* **293**: 2444–2446.
- Chure D, Britt BB, Whitlock JA, Wilson JA. 2010.** First complete sauropod dinosaur skull from the Cretaceous of the Americas and the evolution of sauropod dentition. *Naturwissenschaften* **97**: 379–391.
- Clarke AH. 2005.** On the vestibular labyrinth of *Brachiosaurus brancai*. *Journal of Vestibular Research* **15**: 65–71.
- Cook AG, Bryan SE, Draper JJ. 2013.** Post-orogenic Mesozoic basins and magmatism. In: Jell PA, ed. *Geology of Queensland*. Brisbane: Geological Survey of Queensland, 515–575.
- Coombs WP Jr, Molnar RE. 1981.** Sauropoda (Reptilia, Saurischia) from the Cretaceous of Queensland. *Memoirs of the Queensland Museum* **20**: 351–373.
- Coria RA, Calvo JO. 2002.** A new iguanodontian ornithopod from Neuquen Basin, Patagonia, Argentina. *Journal of Vertebrate Paleontology* **22**: 503–509.
- Coria RA, Filippi LS, Chiappe LM, García R, Arcucci AB. 2013.** *Overosaurus paradasorum* gen. et sp. nov., a new sauropod dinosaur (Titanosauria: Lithostrotia) from the Late Cretaceous of Neuquén, Patagonia, Argentina. *Zootaxa* **3683**: 357–376.
- Coria RA, Salgado L. 1999.** Nuevos aportes a la anatomía craneana de los saurópodos titanosáuridos. *Ameghiniana* **36**: 98.
- Coria RA, Salgado L. 2005.** Last Patagonian non-avian theropods. In: Carpenter K, ed. *The carnivorous dinosaurs*. Bloomington and Indianapolis: Indiana University Press, 153–160.
- Coria RA, Windholz GJ, Ortega F, Currie PJ. 2019.** A new dicraeosaurid sauropod from the Lower Cretaceous (Mulichinco Formation, Valanginian, Neuquén Basin) of Argentina. *Cretaceous Research* **93**: 33–48.
- Curry Rogers K. 2009.** The postcranial osteology of *Rapetosaurus krausei* (Sauropoda: Titanosauria) from the Late Cretaceous of Madagascar. *Journal of Vertebrate Paleontology* **29**: 1046–1086.
- Curry Rogers K, Forster CA. 2001.** The last of the dinosaur titans: a new sauropod from Madagascar. *Nature* **412**: 530–534.
- Curry Rogers K, Forster CA. 2004.** The skull of *Rapetosaurus krausei* (Sauropoda: Titanosauria) from the Late Cretaceous of Madagascar. *Journal of Vertebrate Paleontology* **24**: 121–144.
- Curry Rogers K, Wilson JA. 2014.** *Vahiny depereti*, gen. et sp. nov., a new titanosaur (Dinosauria, Sauropoda) from the Upper Cretaceous Maevarano Formation, Madagascar. *Journal of Vertebrate Paleontology* **34**: 606–617.
- Curry Rogers KA. 2005.** Titanosauria: a phylogenetic overview. In: Curry Rogers KA, Wilson JA, eds. *The sauropods: evolution and paleobiology*. Berkeley: University of California Press, 50–103.
- D’Emic MD, Carrano MT. 2020.** Redescription of brachiosaurid sauropod dinosaur material from the Upper Jurassic Morrison Formation, Colorado, USA. *The Anatomical Record* **303**: 732–758.
- Dalla Vecchia FM. 1999.** Atlas of the sauropod bones from the upper Hauterivian–lower Barremian of Bale/Valle (SW Istria, Croatia). *Natura Nascosta* **18**: 6–41.
- Dalla Vecchia FM. 2005.** Between Gondwana and Laurasia: Cretaceous sauropods in an intraoceanic carbonate platform. In: Tidwell V, Carpenter K, eds. *Thunder-lizards: the sauropodomorph dinosaurs*. Bloomington and Indianapolis: Indiana University Press, 395–429.
- Delcourt R, Grillo ON. 2018.** Tyrannosauroids from the Southern Hemisphere: implications for biogeography,

- evolution, and taxonomy. *Palaeogeography, Palaeoclimatology, Palaeoecology* **511**: 379–387.
- Dieudonné P-E, Cruzado-Caballero P, Godefroit P, Tortosa T. 2020.** A new phylogeny of cerapodan dinosaurs. *Historical Biology*. Available at: <https://doi.org/10.1080/08912963.2020.1793979>.
- Díez Díaz V, García G, Knoll F, Pereda Suberbiola X, Valentin X. 2012.** New cranial remains of titanosaurian sauropod dinosaurs from the Late Cretaceous of Fox-Amphoux-Métisson (Var, SE France). *Proceedings of the Geologists' Association* **123**: 626–637.
- Díez Díaz V, García G, Pereda Suberbiola X, Jentgen-Ceschino B, Stein K, Godefroit P, Valentin X. 2018.** The titanosaurian dinosaur *Atsinganosaurus velauciensis* (Sauropoda) from the Upper Cretaceous of southern France: new material, phylogenetic affinities, and palaeobiogeographical implications. *Cretaceous Research* **91**: 429–456.
- Díez Díaz V, Pereda Suberbiola X, Sanz JL. 2011.** Braincase anatomy of the titanosaurian sauropod *Lirainosaurus astibiae* from the Late Cretaceous of the Iberian Peninsula. *Acta Palaeontologica Polonica* **56**: 521–533.
- Edinger T. 1942.** The pituitary body in giant animals fossil and living: a survey and a suggestion. *Quarterly Review of Biology* **17**: 31–45.
- Fanti F, Cau A, Cantelli L, Hassine M, Auditore M. 2015.** New information on *Tataouinea hannibalis* from the Early Cretaceous of Tunisia and implications for the tempo and mode of rebbachisaurid sauropod evolution. *PLoS One* **10**: e0123475.
- Fanti F, Cau A, Hassine M. 2014.** Evidence of titanosauriforms and rebbachisaurids (Dinosauria: Sauropoda) from the Early Cretaceous of Tunisia. *Journal of African Earth Sciences* **90**: 1–8.
- Fanti F, Cau A, Hassine M, Contessi M. 2013.** A new sauropod dinosaur from the Early Cretaceous of Tunisia with extreme avian-like pneumatization. *Nature Communications* **4**: 2080.
- Filippi LS, García RA, Garrido AC. 2011.** A new titanosaur sauropod dinosaur from the Upper Cretaceous of North Patagonia, Argentina. *Acta Palaeontologica Polonica* **56**: 505–520.
- Filippi LS, Garrido AC. 2008.** *Pitekunsaurus macayai* gen. et sp. nov., nuevo titanosaurio (Saurischia, Sauropoda) del Cretácico Superior de la Cuenca Neuquina, Argentina. *Ameghiniana* **45**: 575–590.
- Filippi LS, Salgado L, Garrido AC. 2019.** A new giant basal titanosaur sauropod in the Upper Cretaceous (Coniacian) of the Neuquén Basin, Argentina. *Cretaceous Research* **100**: 61–81.
- Fitzgerald EMG, Carrano MT, Holland T, Wagstaff BE, Pickering D, Rich TH, Vickers-Rich P. 2012.** First ceratosaurian dinosaur from Australia. *Naturwissenschaften* **99**: 397–405.
- Gallina PA. 2016.** Reappraisal of the Early Cretaceous sauropod dinosaur *Amargatitanis macni* (Apesteguía, 2007), from northwestern Patagonia, Argentina. *Cretaceous Research* **64**: 79–87.
- Gallina PA, Apesteguía S. 2005.** *Cathartesaura anaerobica* gen. et sp. nov., a new rebbachisaurid (Dinosauria, Sauropoda) from the Huincul Formation (Upper Cretaceous), Río Negro, Argentina. *Revista del Museo Argentino de Ciencias Naturales* **7**: 153–166.
- Gallina PA, Apesteguía S. 2011.** Cranial anatomy and phylogenetic position of the titanosaurian sauropod *Bonitasaura salgadoi*. *Acta Palaeontologica Polonica* **56**: 45–60.
- Gallina PA, Apesteguía S. 2015.** Postcranial anatomy of *Bonitasaura salgadoi* (Sauropoda, Titanosauria) from the Late Cretaceous of Patagonia. *Journal of Vertebrate Paleontology* **35**: e924957.
- Gallina PA, Apesteguía S, Canale JI, Haluza A. 2019.** A new long-spined dinosaur from Patagonia sheds light on sauropod defense system. *Scientific Reports* **9**: 1392.
- Gallina PA, Apesteguía S, Haluza A, Canale JI. 2014.** A diplodocid sauropod survivor from the Early Cretaceous of South America. *PLoS One* **9**: e97128.
- García RA. 2007a.** Consideraciones sobre la fenestra preantorbital en embriones de dinosaurios saurópodos del Cretácico de Patagonia. *Ameghiniana* **44**: 467–471.
- García RA. 2007b.** An “egg-tooth”-like structure in titanosaurian sauropod embryos. *Journal of Vertebrate Paleontology* **27**: 247–252.
- García RA, Cerda IA. 2010.** Dentition and histology in titanosaurian dinosaur embryos from Upper Cretaceous of Patagonia, Argentina. *Palaeontology* **53**: 335–346.
- García RA, Paulina-Carabajal A, Salgado L. 2008.** Un nuevo basicráneo de titanosaurio de la Formación Allen (Campaniano-Maastrichtiano), Provincia de Río Negro, Patagonia, Argentina. *Géobios* **41**: 625–633.
- García RA, Salgado L, Coria RA, Chiappe LM. 2010.** Osteología embrionaria de saurópodos titanosaurios de Neuquén (Argentina): aspectos ontogenéticos y evolutivos. *Ameghiniana* **47**: 409–430.
- Gauthier J. 1986.** Saurischian monophyly and the origin of birds. *Memoirs of the California Academy of Sciences* **8**: 1–55.
- Gillilan LA. 1967.** A comparative study of the extrinsic and intrinsic arterial blood supply to brains of the submammalian vertebrates. *Journal of Comparative Neurology* **130**: 175–196.
- Gilmore CW. 1933.** Two new dinosaurian reptiles from Mongolia with notes on some fragmentary specimens. *American Museum Novitates* **679**: 1–20.
- Goloboff PA. 2014.** Extended implied weighting. *Cladistics* **30**: 260–272.
- Goloboff PA, Catalano SA. 2016.** TNT version 1.5, including a full implementation of phylogenetic morphometrics. *Cladistics* **32**: 221–238.
- Goloboff PA, Farris JS, Nixon KC. 2008.** TNT: a free program for phylogenetic analysis. *Cladistics* **24**: 774–786.
- Goloboff PA, Torres A, Arias JS. 2018.** Weighted parsimony outperforms other methods of phylogenetic inference under models appropriate for morphology. *Cladistics* **34**: 407–437.
- Gomani EM. 2005.** Sauropod dinosaurs from the Early Cretaceous of Malawi, Africa. *Palaeontologia Electronica* **8**: 27A.

- González Riga BJ, Lamanna MC, Otero A, Ortíz David LD, Kellner AWA, Ibiricu LM. 2019.** An overview of the appendicular skeletal anatomy of South American titanosaurian sauropods, with definition of a newly recognized clade. *Anais da Academia Brasileira de Ciências* **91**: e20180374.
- González Riga BJ, Mannion PD, Poropat SF, Ortíz David LD, Coria JP. 2018.** Osteology of the Late Cretaceous Argentinian sauropod dinosaur *Mendozasaurus neguyelap*: implications for basal titanosaur relationships. *Zoological Journal of the Linnean Society* **184**: 136–181.
- González Riga BJ, Ortíz David L. 2014.** A new titanosaur (Dinosauria, Sauropoda) from the Upper Cretaceous (Cerro Lisandro Formation) of Mendoza Province, Argentina. *Ameghiniana* **51**: 3–25.
- Goodrich ES. 1930.** *Studies on the structure and evolution of vertebrates*. London: Macmillan & Co.
- Gorscak E, O'Connor PM. 2016.** Time-calibrated models support congruency between Cretaceous continental rifting and titanosaurian evolutionary history. *Biology Letters* **12**: 20151047.
- Haluza A, Canale JI, Otero A, Pérez LM, Scanferla CA. 2012.** Changes in vertebral laminae across the cervicodorsal transition of a well-preserved rebbachisaurid (Dinosauria, Sauropoda) from the Cenomanian of Patagonia, Argentina. *Journal of Vertebrate Paleontology* **32**: 219–224.
- Herne MC, Nair JP, Evans AR, Tait AM. 2019.** New small-bodied ornithopods (Dinosauria, Neornithischia) from the Early Cretaceous Wonthaggi Formation (Strzelecki Group) of the Australian-Antarctic rift system, with revision of *Qantassaurus intrepidus* Rich and Vickers-Rich, 1999. *Journal of Paleontology* **93**: 543–584.
- Herne MC, Nair JP, Salisbury SW. 2010.** Comment on “A southern tyrant reptile”. *Science* **329**: 1013.
- Herne MC, Tait AM, Weisbecker V, Hall M, Nair JP, Cleeland M, Salisbury SW. 2018.** A new small-bodied ornithopod (Dinosauria, Ornithischia) from a deep, high-energy Early Cretaceous river of the Australian–Antarctic rift system. *PeerJ* **5**: e4113.
- Herngreen GFW, Kedves M, Rovnina LV, Smirnova SB. 1996.** Cretaceous palynofloral provinces: a review. In: Jansonius J, McGregor DC, eds. *Palynology: principles and applications, vol. 3*. Houston: American Association of Stratigraphic Palynologists Foundation, 1157–1188.
- Hocknull S. 2005.** Trawling for the white gold. *Australian Age of Dinosaurs Museum of Natural History Annual* **3**: 26–43.
- Hocknull SA, White MA, Tischler TR, Cook AG, Calleja ND, Sloan T, Elliott DA. 2009.** New mid-Cretaceous (latest Albian) dinosaurs from Winton, Queensland, Australia. *PLoS One* **4**: e6190.
- Holland WJ. 1906.** The osteology of *Diplodocus* Marsh with special reference to the restoration of the skeleton of *Diplodocus carnegiei* [sic] Hatcher, presented by Mr. Andrew Carnegie to the British Museum, May 12, 1905. *Memoirs of the Carnegie Museum* **2**: 226–280.
- Hopson JA. 1979.** Paleoneurology. In: Gans C, ed. *Biology of the Reptilia, Vol. 9A*. London: Academic Press, 39–146.
- Huber BT, MacLeod KG, Watkins DK, Coffin MF. 2018.** The rise and fall of the Cretaceous Hot Greenhouse climate. *Global and Planetary Change* **167**: 1–23.
- Huene FV. 1929.** Los Saurisquios y Ornitisquios del Cretáceo Argentina. *Anales Museo de La Plata* **3**: 1–196.
- Huene FV, Matley CA. 1933.** The Cretaceous Saurischia and Ornithischia of the central provinces of India. *Palaeontologia Indica* **21**: 1–74.
- Ibiricu LM, Casal GA, Lamanna MC, Martínez RD, Harris JD, Lacovara KJ. 2012.** The southernmost records of Rebbachisauridae (Sauropoda: Diplodocoidea), from early Late Cretaceous deposits in central Patagonia. *Cretaceous Research* **34**: 220–232.
- Ibiricu LM, Casal GA, Martínez RD, Alvarez BN, Poropat SF. 2020.** New materials and an overview of Cretaceous vertebrates from the Chubut Group of the Golfo San Jorge Basin, central Patagonia, Argentina. *Journal of South American Earth Sciences* **98**: 102460.
- Ibiricu LM, Casal GA, Martínez RD, Lamanna MC, Luna M, Salgado L. 2013.** *Katepensaurus goicoecheai*, gen. et sp. nov., a Late Cretaceous rebbachisaurid (Sauropoda, Diplodocoidea) from central Patagonia, Argentina. *Journal of Vertebrate Paleontology* **33**: 1351–1366.
- Ibiricu LM, Casal GA, Martínez RD, Lamanna MC, Luna M, Salgado L. 2015.** New material of *Katepensaurus goicoecheai* (Sauropoda: Diplodocoidea) and its significance for the morphology and evolution of Rebbachisauridae. *Ameghiniana* **52**: 430–446.
- Jacobs LL, Winkler DA, Downs WR, Gomani EM. 1993.** New material of an Early Cretaceous titanosaurid sauropod dinosaur from Malawi. *Palaeontology* **36**: 523–534.
- Janensch W. 1914.** Übersicht über die Wirbeltierfauna der Tendaguru-Schichten, nebst einer kurzen Charakterisierung der neu aufgeführten Arten von Sauropoden. *Archiv für Biontologie* **3**: 81–110.
- Janensch W. 1929.** Die Wirbelsäule der Gattung *Dicraeosaurus*. *Palaeontographica, Supplement VII 1*: 35–133.
- Janensch W. 1935–1936.** Die Schädel der Sauropoden *Brachiosaurus*, *Barosaurus* und *Dicraeosaurus* aus den Tendaguru-Schichten Deutsch-Ostafrikas. *Palaeontographica, Supplement VII 2*: 145–298.
- Janensch W. 1936.** Über Bahnen von Hirnvenen bei Saurischiern und Ornithischiern, sowie einigen anderen fossilen und rezenten Reptilien. *Paläontologische Zeitschrift* **18**: 181–198.
- Janensch W. 1950.** Die Wirbelsäule von *Brachiosaurus brancai*. *Palaeontographica, Supplement VII 3*: 27–93.
- Janensch W. 1961.** Die Gliedmaszen und Gliedmaszengürtel der Sauropoden der Tendaguru-Schichten. *Palaeontographica, Supplement VII 3*: 177–235.
- Jensen JA. 1987.** New brachiosaur material from the Late Jurassic of Utah and Colorado. *Great Basin Naturalist* **47**: 592–608.
- Klinkhamer AJ, Mallison H, Poropat SF, Sinapius GHK, Wroe S. 2018.** Three-dimensional musculoskeletal modelling of the sauropodomorph hind limb: the effect of postural change on muscle leverage. *Anatomical Record* **301**: 2145–2163.

- Klinkhamer AJ, Mallison H, Poropat SF, Sloan T, Wroe S. 2019.** Comparative three-dimensional moment arm analysis of the sauropod forelimb: implications for the transition to a wide-gauge stance in titanosaurs. *Anatomical Record* **302**: 794–817.
- Knoll F, Lautenschlager S, Valentin X, Díez Díaz V, Pereda Suberbiola X, Garcia G. 2019.** First palaeoneurological study of a sauropod dinosaur from France and its phylogenetic significance. *PeerJ* **7**: e7991.
- Knoll F, Ridgely RC, Ortega F, Sanz JL, Witmer LM. 2013.** Neurocranial osteology and neuroanatomy of a Late Cretaceous titanosaurian sauropod from Spain (*Ampelosaurus* sp.). *PLoS One* **8**: e54991.
- Knoll F, Schwarz-Wings D. 2009.** Palaeoneuroanatomy of *Brachiosaurus*. *Annales de Paléontologie* **95**: 165–175.
- Knoll F, Witmer LM, Ortega F, Ridgely RC, Schwarz-Wings D. 2012.** The braincase of the basal sauropod dinosaur *Spinophorosaurus* and 3D reconstructions of the cranial endocast and inner ear. *PLoS One* **7**: e30060.
- Knoll F, Witmer LM, Ridgely RC, Ortega F, Sanz JL. 2015.** A new titanosaurian braincase from the Cretaceous “Lo Hueco” locality in Spain sheds light on neuroanatomical evolution within Titanosauria. *PLoS One* **10**: e0138233.
- Korasidis VA, Wagstaff BE. 2020.** The rise of flowering plants in the high southern latitudes of Australia. *Review of Palaeobotany and Palynology* **272**: 104126.
- Korasidis VA, Wagstaff BE, Gallagher SJ, Duddy IR, Tosolini A-MP, Cantrill DJ, Norvick MS. 2016.** Early angiosperm diversification in the Albian of southeast Australia: implications for flowering plant radiation across eastern Gondwana. *Review of Palaeobotany and Palynology* **232**: 61–80.
- Ksepka DT, Norell MA. 2006.** *Erketu ellisoni*, a long-necked sauropod from Bor Guvé (Dornogov Aimag, Mongolia). *American Museum Novitates* **3508**: 1–16.
- Kubo T. 2020.** Biogeographical network analysis of Cretaceous Australian dinosaurs. *Gondwana Research* **82**: 39–47.
- Kundrát M, Coria RA, Manning TW, Snitting D, Chiappe LM, Nudds J, Ahlberg PE. 2020.** Specialized craniofacial anatomy of a titanosaurian embryo from Argentina. *Current Biology* **30**: 4263–4269.e2.
- Kurzanov SM, Bannikov AF. 1983.** A new sauropod from the Upper Cretaceous of Mongolia. *Paleontological Journal* **2**: 90–96.
- Lacovara KJ, Lamanna MC, Ibiricu LM, Poole JC, Schroeter ER, Ullmann PV, Voegelé KK, Boles ZM, Carter AM, Fowler EK, Egerton VM, Moyer AE, Coughenour CL, Schein JP, Harris JD, Martínez RD, Novas FE. 2014.** A gigantic, exceptionally complete titanosaurian sauropod dinosaur from southern Patagonia, Argentina. *Scientific Reports* **4**: 6196.
- Lamanna MC, Casal GA, Martínez RDF, Ibiricu LM. 2000.** Megaraptorid (Theropoda: Tetanurae) partial skeletons from the Upper Cretaceous Bajo Barreal Formation of central Patagonia, Argentina: implications for the evolution of large body size in Gondwanan megaraptorans. *Annals of Carnegie Museum* **86**: 255–294.
- Le Loeuff J. 2005.** Osteology of *Ampelosaurus atavicus* (Titanosauria) from southern France. In: Tidwell V, Carpenter K, eds. *Thunder-lizards: the sauropodomorph dinosaurs*. Bloomington and Indianapolis: Indiana University Press, 115–137.
- Le Loeuff J, Buffetaut E, Méchin P, Méchin-Salesse A. 1989.** Un arrière crâne de dinosaure titanosauridé (Saurischia, Sauropoda) dans le Crétacé supérieur du Var (Provence, France). *Comptes Rendus de l'Académie des Sciences de Paris* **309**: 851–857.
- Leahey LG, Salisbury SW. 2013.** First evidence of ankylosaurian dinosaurs (Ornithischia: Thyreophora) from the mid-Cretaceous (late Albian–Cenomanian) Winton Formation of Queensland, Australia. *Alcheringa* **37**: 249–257.
- Lehman TM, Coulson AB. 2002.** A juvenile specimen of the sauropod dinosaur *Alamosaurus sanjuanensis* from the Upper Cretaceous of Big Bend National Park, Texas. *Journal of Paleontology* **76**: 156–172.
- Lindoso RM, Medeiros MAA, Carvalho IdS, Pereira AA, Mendes ID, Iori FV, Sousa EP, Arcanjo SHS, Silva TCM. 2019.** A new rebbachisaurid (Sauropoda: Diplodocoidea) from the middle Cretaceous of northern Brazil. *Cretaceous Research* **104**: 104191.
- Longman HA. 1933.** A new dinosaur from the Queensland Cretaceous. *Memoirs of the Queensland Museum* **10**: 131–144.
- Lü J, Xu L, Pu H, Zhang X, Zhang Y, Jia S, Chang H, Zhang J, Wei X. 2013.** A new sauropod dinosaur (Dinosauria, Sauropoda) from the late Early Cretaceous of the Ruyang Basin (central China). *Cretaceous Research* **44**: 202–213.
- Machado EB, Avilla LdS, Nava WR, Campos DdA, Kellner AWA. 2013.** A new titanosaur sauropod from the Late Cretaceous of Brazil. *Zootaxa* **3701**: 301–321.
- Madsen JH Jr, McIntosh JS, Berman DS. 1995.** Skull and atlas–axis complex of the Upper Jurassic sauropod *Camarasaurus* Cope (Reptilia: Saurischia). *Bulletin of the Carnegie Museum of Natural History* **31**: 1–115.
- Mannion PD. 2009.** A rebbachisaurid sauropod from the Lower Cretaceous of the Isle of Wight, England. *Cretaceous Research* **30**: 521–526.
- Mannion PD. 2011.** A reassessment of *Mongolosaurus haplodon* Gilmore, 1933, a titanosaurian sauropod dinosaur from the Early Cretaceous of Inner Mongolia, People’s Republic of China. *Journal of Systematic Palaeontology* **9**: 355–378.
- Mannion PD, Allain R, Moine O. 2017.** The earliest known titanosauriform sauropod dinosaur and the evolution of Brachiosauridae. *PeerJ* **5**: e3217.
- Mannion PD, Barrett PM. 2013.** Additions to the sauropod dinosaur fauna of the Cenomanian (early Late Cretaceous) Kem Kem beds of Morocco: palaeobiogeographical implications of the mid-Cretaceous African sauropod fossil record. *Cretaceous Research* **45**: 49–59.
- Mannion PD, Calvo JO. 2011.** Anatomy of the basal titanosaur (Dinosauria, Sauropoda) *Andesaurus delgadoi* from the mid-Cretaceous (Albian–early Cenomanian) Río Limay Formation, Neuquén Province, Argentina: implications for titanosaur systematics. *Zoological Journal of the Linnean Society* **163**: 155–181.
- Mannion PD, Upchurch P, Barnes RN, Mateus O. 2013.** Osteology of the Late Jurassic Portuguese sauropod dinosaur

- Lusotitan atalaiensis* (Macronaria) and the evolutionary history of basal titanosauriforms. *Zoological Journal of the Linnean Society* **168**: 98–206.
- Mannion PD, Upchurch P, Hutt S. 2011.** New rebbachisaurid (Dinosauria: Sauropoda) material from the Wessex Formation (Barremian, Early Cretaceous), Isle of Wight, United Kingdom. *Cretaceous Research* **32**: 774–780.
- Mannion PD, Upchurch P, Jin X, Zheng W. 2019a.** New information on the Cretaceous sauropod dinosaurs of Zhejiang Province, China: impact on Laurasian titanosauriform phylogeny and biogeography. *Royal Society Open Science* **6**: 191057.
- Mannion PD, Upchurch P, Schwarz D, Wings O. 2019b.** Taxonomic affinities of the putative titanosaurs from the Late Jurassic Tendaguru Formation of Tanzania: phylogenetic and biogeographic implications for eusauropod dinosaur evolution. *Zoological Journal of the Linnean Society* **185**: 784–909.
- Martinelli AG, Forasiepi AM. 2004.** Late Cretaceous vertebrates from Bajo de Santa Rosa (Allen Formation), Río Negro province, Argentina, with the description of a new sauropod dinosaur (Titanosauridae). *Revista del Museo Argentino de Ciencias Naturales* **6**: 257–305.
- Martinelli AG, Marinho TdS, Filippi LS, Borges Ribeiro LC, Ferraz MLdF, Cavellani CL, Teixeira VdPA. 2015.** Cranial bones and atlas of titanosaurs (Dinosauria, Sauropoda) from Late Cretaceous (Bauru Group) of Uberaba, Minas Gerais State, Brazil. *Journal of South American Earth Sciences* **61**: 164–170.
- Martínez R, Giménez O, Rodríguez J, Luna M, Lamanna MC. 2004.** An articulated specimen of the basal titanosaurian (Dinosauria: Sauropoda) *Epachthosaurus sciuttoi* from the early Late Cretaceous Bajo Barreal Formation of Chubut Province, Argentina. *Journal of Vertebrate Paleontology* **24**: 107–120.
- Martínez RDF, Lamanna MC, Novas FE, Ridgely RC, Casal GA, Martínez JE, Vita JR, Witmer LM. 2016.** A basal lithostrotian titanosaur (Dinosauria: Sauropoda) with a complete skull: implications for the evolution and paleobiology of Titanosauria. *PLoS One* **11**: e0151661.
- Matzke NJ. 2013.** Probabilistic historical biogeography: new models for founder-event speciation, imperfect detection, and fossils allow improved accuracy and model-testing. *Frontiers of Biogeography* **5**: 242–248.
- Matzke NJ. 2014.** Model selection in historical biogeography reveals that founder-event speciation is a crucial process in island clades. *Systematic Biology* **63**: 951–970.
- Mays C. 2014.** A Late Cretaceous (Cenomanian–Turonian) south polar palynoflora from the Chatham Islands, New Zealand. Canberra: Association of Australasian Palaeontologists.
- McPhee BW, Mannion PD, de Klerk WJ, Choiniere JN. 2016.** High diversity in the sauropod dinosaur fauna of the Lower Cretaceous Kirkwood Formation of South Africa: Implications for the Jurassic–Cretaceous transition. *Cretaceous Research* **59**: 228–248.
- Medeiros MA, Schultz CL. 2004.** *Rayososaurus* (Sauropoda, Diplodocoidea) no Meso-Cretáceo do norte-nordeste Brasileiro. *Revista Brasileira de Paleontologia* **7**: 275–279.
- Mocho P, Royo-Torres R, Ortega F. 2019.** A new macronarian sauropod from the Upper Jurassic of Portugal. *Journal of Vertebrate Paleontology* **39**: e1578782.
- Molnar RE. 1992.** Paleozoogeographic relationships of Australian Mesozoic tetrapods. In: Chatterjee S, Hotton N, eds. *New concepts in global tectonics*. Lubbock: Texas Tech University Press, 259–266.
- Molnar RE. 2001.** A reassessment of the phylogenetic position of Cretaceous sauropod dinosaurs from Queensland, Australia. In: Leanza HA, ed. *VII International Symposium on Mesozoic Terrestrial Ecosystems: Asociación Paleontológica Argentina Publicación Especial No. 7*. Buenos Aires: Asociación Paleontológica Argentina, 139–144.
- Molnar RE. 2010.** Taphonomic observations on eastern Australian Cretaceous sauropods. *Alcheringa* **34**: 421–429.
- Molnar RE. 2011a.** New morphological information about Cretaceous sauropod dinosaurs from the Eromanga Basin, Queensland, Australia. *Alcheringa* **35**: 329–339.
- Molnar RE. 2011b.** Sauropod (Saurischia: Dinosauria) material from the Early Cretaceous Grimman Creek Formation of the Surat Basin, Queensland, Australia. *Alcheringa* **35**: 303–307.
- Molnar RE, Salisbury SW. 2005.** Observations on Cretaceous sauropods from Australia. In: Tidwell V, Carpenter K, eds. *Thunder-lizards: the sauropodomorph dinosaurs*. Bloomington and Indianapolis: Indiana University Press, 454–465.
- Molnar RE, Wiffen J. 2007.** A presumed titanosaurian vertebra from the Late Cretaceous of North Island, New Zealand. *Arquivos do Museu Nacional, Rio de Janeiro* **65**: 505–510.
- Moore AJ, Mo J, Clark JM, Xu X. 2018.** Cranial anatomy of *Bellusaurus sui* (Dinosauria: Eusauropoda) from the Middle–Late Jurassic Shishugou Formation of northwest China and a review of sauropod cranial ontogeny. *PeerJ* **6**: e4881.
- Moore AJ, Upchurch P, Barrett PM, Clark JM, Xu X. 2020.** Osteology of *Klamelisaurus gobiensis* (Dinosauria, Eusauropoda) and the evolutionary history of Middle–Late Jurassic Chinese sauropods. *Journal of Systematic Palaeontology* **20**: 1299–1393.
- Mortimer N, Campbell HJ, Tulloch AJ, King PR, Stagpoole VM, Wood RA, Rattenbury MS, Sutherland R, Adams CJ, Collot J, Seton M. 2017.** Zealandia: Earth's hidden continent. *GSA Today* **27**: 27–35.
- Navarrete C, Casal G, Martínez R. 2011.** *Drusilasaura deseadensis* gen. et sp. nov., un nuevo titanosaurio (Dinosauria-Sauropoda), de la Formación Bajo Barreal, Cretácico Superior del norte de Santa Cruz, Argentina. *Revista Brasileira de Paleontologia* **14**: 1–14.
- Novas FE, Agnolín FL, Ezcurra MD, Porfiri J, Canale JI. 2013.** Evolution of the carnivorous dinosaurs during the Cretaceous: the evidence from Patagonia. *Cretaceous Research* **45**: 174–215.
- Novas FE, Agnolín FL, Rozadilla S, Aranciaga-Rolando AM, Brissón-Egli F, Motta MJ, Cerroni M, Ezcurra MD, Martinelli AG, D'Angelo JS, Alvarez-Herrera G, Gentil AR, Bogan S, Chimento NR, García-Marsà JA, Lo Coco G, Miquel SE, Brito FFV, Ezequiel I,**

- Perez Loinaze VS, Fernández MS, Salgado L. 2019.** Paleontological discoveries in the Chorrillo Formation (upper Campanian–lower Maastrichtian, Upper Cretaceous), Santa Cruz Province, Patagonia, Argentina. *Revista del Museo Argentino de Ciencias Naturales* **21**: 217–293.
- Novas FE, Aranciaga Rolando AM, Agnolín FL. 2016.** Phylogenetic relationships of the Cretaceous Gondwanan theropods *Megaraptor* and *Australovenator*: the evidence afforded by their manual anatomy. *Memoirs of Museum Victoria* **74**: 49–61.
- Novas FE, Cambiaso AV, Ambrosio A. 2004.** A new basal iguanodontian (Dinosauria, Ornithischia) from the Upper Cretaceous of Patagonia. *Ameghiniana* **41**: 75–82.
- Nowiński A. 1971.** *Nemegtosaurus mongoliensis* n. gen., n. sp. (Sauropoda) from the uppermost Cretaceous of Mongolia. *Palaeontologia Polonica* **25**: 57–81.
- Paulina Carabajal A. 2012.** Neuroanatomy of titanosaurid dinosaurs from the Upper Cretaceous of Patagonia, with comments on endocranial variability within Sauropoda. *The Anatomical Record* **295**: 2141–2156.
- Paulina Carabajal A, Calvo JO. 2015.** Nueva información sobre la neuroanatomía del saurópodo *Limaysaurus tessonei* basada en tomografías computadas. In: *V Congreso Latinoamericano de Paleontología de Vertebrados, Colonia, Uruguay, 21–23 September 2015*. 98.
- Paulina Carabajal A, Canale JI, Haluza A. 2016.** New rebbachisaurid (Sauropoda, Diplodocoidea) cranial remains from the Cretaceous of Patagonia, Argentina, and the first endocranial description for a South American representative of the clade. *Journal of Vertebrate Paleontology* **36**: e1167067.
- Paulina Carabajal A, Carballido JL, Currie PJ. 2014.** Braincase, neuroanatomy, and neck posture of *Amargasaurus cazau* (Sauropoda, Dicraeosauridae) and its implications for understanding head posture in sauropods. *Journal of Vertebrate Paleontology* **34**: 870–882.
- Paulina Carabajal A, Coria RA, Chiappe LM. 2008.** An incomplete Upper Cretaceous titanosaur (Sauropoda) braincase: new insights on the dinosaurian inner ear and endocranium. *Cretaceous Research* **29**: 643–648.
- Paulina Carabajal A, Coria RA, Currie PJ, Koppelhus EB. 2018.** A natural cranial endocast with possible dicraeosaurid (Sauropoda, Diplodocoidea) affinities from the Lower Cretaceous of Patagonia. *Cretaceous Research* **84**: 437–441.
- Paulina-Carabajal A, Filippi L, Knoll F. 2020.** Neuroanatomy of the titanosaurian sauropod *Narambuenatitan palomoi* from the Upper Cretaceous of Patagonia, Argentina. *Publicación Electrónica de la Asociación Paleontológica Argentina* **20**: 1–9.
- Paulina-Carabajal A, Salgado L. 2007.** Un basicráneo de titanosaurio (Dinosauria, Sauropoda) del Cretácico Superior del norte de Patagonia: descripción y aportes al conocimiento del oído interno de los dinosaurios. *Ameghiniana* **44**: 109–120.
- Pentland AH, Poropat SF, Tischler TR, Sloan T, Elliott RA, Elliott HA, Elliott JA, Elliott DA. 2019.** *Ferrodraco lentoni* gen. et sp. nov., a new ornithocheirid pterosaur from the Winton Formation (Cenomanian–lower Turonian) of Queensland, Australia. *Scientific Reports* **9**: 13454.
- Pereda Suberbiola X, Torcida F, Izquierdo LA, Huerta P, Montero D, Pérez G. 2003.** First rebbachisaurid dinosaur (Sauropoda, Diplodocoidea) from the Early Cretaceous of Spain: palaeobiogeographical implications. *Bulletin de la Société Géologique de France* **174**: 471–479.
- Pereira PVGdC, Veiga IMM, Ribeiro TB, Cardozo RHB, Candeiro CRdA, Bergqvist LP. 2020.** The path of giants: a new occurrence of Rebbachisauridae (Dinosauria, Diplodocoidea) in the Açú Formation, NE Brazil, and its paleobiogeographic implications. *Journal of South American Earth Sciences* **100**: 102515.
- Porfiri JD, Juárez Valieri RD, Santos DDD, Lamanna MC. 2018.** A new megaraptoran theropod dinosaur from the Upper Cretaceous Bajo de la Carpa Formation of northwestern Patagonia. *Cretaceous Research* **89**: 302–319.
- Poropat SF, Kear BP. 2013.** Photographic atlas and three-dimensional reconstruction of the holotype skull of *Euhelopus zdanskyi* with description of additional cranial elements. *PLoS One* **8**: e79932.
- Poropat SF, Mannion PD, Upchurch P, Hocknull SA, Kear BP, Elliott DA. 2015a.** Reassessment of the non-titanosaurian somphospondylan *Wintonotitan wattsi* (Dinosauria: Sauropoda: Titanosauriformes) from the mid-Cretaceous Winton Formation, Queensland, Australia. *Papers in Palaeontology* **1**: 59–106.
- Poropat SF, Mannion PD, Upchurch P, Hocknull SA, Kear BP, Kundrát M, Tischler TR, Sloan T, Sinapius GHK, Elliott JA, Elliott DA. 2016.** New Australian sauropods shed light on Cretaceous dinosaur palaeobiogeography. *Scientific Reports* **6**: 34467.
- Poropat SF, Mannion PD, Upchurch P, Tischler TR, Sloan T, Sinapius GHK, Elliott JA, Elliott DA. 2020a.** Osteology of the wide-hipped titanosaurian sauropod dinosaur *Savannasaurus elliottorum* from the Upper Cretaceous Winton Formation of Queensland, Australia. *Journal of Vertebrate Paleontology* **40**: e1786836.
- Poropat SF, Martin SK, Tosolini A-MP, Wagstaff BE, Bean LB, Kear BP, Vickers-Rich P, Rich TH. 2018.** Early Cretaceous polar biotas of Victoria, southeastern Australia—an overview of research to date. *Alcheringa* **42**: 157–229.
- Poropat SF, Nair JP, Syme CE, Mannion PD, Upchurch P, Hocknull SA, Cook AG, Tischler TR, Holland T. 2017.** Reappraisal of *Austrosaurus mckillopi* Longman, 1933 from the Allaru Mudstone of Queensland, Australia's first named Cretaceous sauropod dinosaur. *Alcheringa* **41**: 543–580.
- Poropat SF, Pentland AH, Duncan RJ, Bevitt JJ, Vickers-Rich P, Rich TH. 2020b.** First elaphrosaurine theropod dinosaur (Ceratosauria: Noasauridae) from Australia – a cervical vertebra from the Early Cretaceous of Victoria. *Gondwana Research* **84**: 284–295.
- Poropat SF, Upchurch P, Mannion PD, Hocknull SA, Kear BP, Sloan T, Sinapius GHK, Elliott DA. 2015b.** Revision of the sauropod dinosaur *Diamantinasaurus matildae* Hocknull *et al.* 2009 from the middle Cretaceous of Australia: implications for Gondwanan titanosauriform dispersal. *Gondwana Research* **27**: 995–1033.
- Poropat SF, White MA, Vickers-Rich P, Rich TH. 2019.** New megaraptorid (Dinosauria: Theropoda) remains from

- Salisbury SW. 2005.** A new vertebrate assemblage from the mid-Cretaceous (Albian–Cenomanian) Winton Formation, central-Western Queensland. In: Reed L, ed. *10th Conference on Australasian Vertebrate Evolution, Palaeontology & Systematics and Quaternary Extinctions Symposium, Naracoorte Caves World Heritage Area, South Australia, 29 March–2 April 2005*. Naracoorte: Hansen Print.
- Salisbury SW, Molnar RE, Lamanna MC. 2006.** A new titanosauriform sauropod from the mid-Cretaceous (Albian–Cenomanian) Winton Formation of central-western Queensland, Australia. *Journal of Vertebrate Paleontology* **26**: 118A.
- Salisbury SW, Molnar RE, Lamanna MC. 2007.** Sauropods from the mid-Cretaceous (Albian–Cenomanian) Winton Formation of central-western Queensland, Australia. In: Warren A, ed. *11th Conference on Australasian Vertebrate Evolution, Palaeontology and Systematics*. Sydney: Geological Society of Australia, 26–27.
- Salisbury SW, Romilio A, Herne MC, Tucker RT, Nair JP. 2017.** The dinosaurian ichnofauna of the Lower Cretaceous (Valanginian–Barremian) Broome Sandstone of the Walmadany Area (James Price Point), Dampier Peninsula, Western Australia. *Society of Vertebrate Paleontology Memoir* **16**: 1–152.
- Sallam HM, Gorscak E, O'Connor PM, El-Dawoudi IA, El-Sayed S, Saber S, Kora MA, Sertich JJW, Seiffert ER, Lamanna MC. 2018.** New Egyptian sauropod reveals Late Cretaceous dinosaur dispersal between Europe and Africa. *Nature Ecology & Evolution* **2**: 445–451.
- Santamarina PE, Barreda VD, Iglesias A, Varela AN. 2020.** Palynology from the Cenomanian Mata Amarilla Formation, southern Patagonia, Argentina. *Cretaceous Research* **109**: 104354.
- Sanz JL, Powell JE, Le Loeuff J, Martínez R, Pereda Suberbiola X. 1999.** Sauropod remains from the Upper Cretaceous of Laño (northcentral Spain), titanosaur phylogenetic relationships. *Estudios del Museo de Ciencias Naturales de Alava* **14**: 235–255.
- Schneider CA, Rasband WS, Eliceiri KW. 2012.** NIH Image to ImageJ: 25 years of image analysis. *Nature Methods* **9**: 671–675.
- Schwarz-Wings D, Böhm N. 2014.** A morphometric approach to the specific separation of the humeri and femora of *Dicraeosaurus* from the Late Jurassic of Tendaguru, Tanzania. *Acta Palaeontologica Polonica* **59**: 81–98.
- Sciutto JC, Martínez RD. 1994.** Un nuevo yacimiento fosilífero de la Formación Bajo Barreal (Cretácico Tardío) y su fauna de sauropodos. *Naturalia Patagónica, Ciencias de la Tierra* **2**: 27–47.
- Sereno PC, Beck AL, Dutheil DB, Larsson HCE, Lyon GH, Moussa B, Sadleir RW, Sidor CA, Varricchio DJ, Wilson GP, Wilson JA. 1999.** Cretaceous sauropods from the Sahara and the uneven rate of skeletal evolution among dinosaurs. *Science* **286**: 1342–1347.
- Sereno PC, Wilson JA. 2005.** Structure and evolution of a sauropod tooth battery. In: Curry Rogers KA, Wilson JA, eds. *The sauropods: evolution and paleobiology*. Berkeley: University of California Press, 157–177.
- Sereno PC, Wilson JA, Witmer LM, Whitlock JA, Maga A, Ide O, Rowe TA. 2007.** Structural extremes in a Cretaceous dinosaur. *PLoS One* **2**: e1230.
- Seton M, Müller RD, Zahirovic S, Gaina C, Torsvik T, Shephard G, Talsma A, Gurnis M, Turner M, Maus S, Chandler M. 2012.** Global continental and ocean basin reconstructions since 200 Ma. *Earth-Science Reviews* **113**: 212–270.
- Smith ND, Makovicky PJ, Agnolin FL, Ezcurra MD, Pais DF, Salisbury SW. 2008.** A *Megaraptor*-like theropod (Dinosauria: Tetanurae) in Australia: support for faunal exchange across eastern and western Gondwana in the Mid-Cretaceous. *Proceedings of the Royal Society B: Biological Sciences* **275**: 2085–2093.
- Sues H-D, Averianov A, Ridgely RC, Witmer LM. 2015.** Titanosauria (Dinosauria, Sauropoda) from the Upper Cretaceous (Turonian) Bissekty Formation of Uzbekistan. *Journal of Vertebrate Paleontology* **35**: e889145.
- Suteethorn S, Le Loeuff J, Buffetaut E, Suteethorn V, Talumbook C, Chonglakmani C. 2009.** A new skeleton of *Phuwiangosaurus sirindhornae* (Dinosauria, Sauropoda) from NE Thailand. In: Buffetaut E, Cuny G, Le Loeuff J, Suteethorn V, eds. *Late Palaeozoic and Mesozoic ecosystems in SE Asia. The Geological Society, London, Special Publications, 315*. London: Geological Society, 189–215.
- Taylor MP. 2018.** *Xenoposeidon* is the earliest known rebbachisaurid sauropod dinosaur. *PeerJ* **6**: e5212.
- Thulborn T. 2012.** Impact of sauropod dinosaurs on lagoonal substrates in the Broome Sandstone (Lower Cretaceous), Western Australia. *PLoS One* **7**: e36208.
- Thulborn T, Hamley T, Foulkes P. 1994.** Preliminary report on sauropod dinosaur tracks in the Broome Sandstone (Lower Cretaceous) of Western Australia. *Gaia* **10**: 85–94.
- Tidwell V, Carpenter K. 2003.** Braincase of an Early Cretaceous titanosauriform sauropod from Texas. *Journal of Vertebrate Paleontology* **23**: 176–180.
- Torcida Fernández-Baldor F, Canudo JI, Huerta P, Montero D, Pereda Suberbiola X, Salgado L. 2011.** *Demandsaurus darwini*, a new rebbachisaurid sauropod from the Early Cretaceous of the Iberian Peninsula. *Acta Palaeontologica Polonica* **53**: 535–552.
- Tschopp E, Upchurch P. 2019.** The challenges and potential utility of phenotypic specimen-level phylogeny based on maximum parsimony. *Earth and Environmental Science Transactions of the Royal Society of Edinburgh* **109**: 301–323.
- Tucker RT, Roberts EM, Hu Y, Kemp AIS, Salisbury SW. 2013.** Detrital zircon age constraints for the Winton Formation, Queensland: contextualizing Australia's Late Cretaceous dinosaur faunas. *Gondwana Research* **24**: 767–779.
- Upchurch P. 1995.** The evolutionary history of sauropod dinosaurs. *Philosophical Transactions: Biological Sciences* **349**: 365–390.
- Upchurch P. 1998.** The phylogenetic relationships of sauropod dinosaurs. *Zoological Journal of the Linnean Society* **124**: 43–103.
- Upchurch P. 1999.** The phylogenetic relationships of the Nemegtosauridae (Saurischia, Sauropoda). *Journal of Vertebrate Paleontology* **19**: 106–125.

- Upchurch P, Barrett PM. 2000.** The evolution of sauropod feeding mechanisms. In: Sues H-D, ed. *Evolution of herbivory in terrestrial vertebrates: evidence from the fossil record*. Cambridge: Cambridge University Press, 79–122.
- Upchurch P, Barrett PM, Dodson P. 2004.** Sauropoda. In: Weishampel DB, Dodson P, Osmólska H, eds. *The dinosauria: second edition*. Berkeley: University of California Press, 259–322.
- Upchurch P, Hunn CA, Norman DB. 2002.** An analysis of dinosaurian biogeography: evidence for the existence of vicariance and dispersal patterns caused by geological events. *Proceedings of the Royal Society B: Biological Sciences* **269**: 613–621.
- Vine RR. 1964.** *Mackunda, Queensland. 1:250 000 Geological Series Sheet SF54-11*. Canberra: Bureau of Mineral Resources, Geology and Geophysics.
- Vine RR, Casey DJ. 1967.** *Winton, Queensland. 1:250 000 geological series sheet SF54-12*. Canberra: Bureau of Mineral Resources, Geology and Geophysics.
- Wedel MJ. 2003.** The evolution of vertebral pneumaticity in sauropod dinosaurs. *Journal of Vertebrate Paleontology* **23**: 344–357.
- Weishampel DB, Grigorescu D, Norman DB. 1991.** The dinosaurs of Transylvania. *National Geographic Research & Exploration* **7**: 196–215.
- White MA, Bell PR, Cook AG, Poropat SF, Elliott DA. 2015.** The dentary of *Australovenator wintonensis* (Theropoda, Megaraptoridae); implications for megaraptorid dentition. *PeerJ* **3**: e1512.
- White MA, Benson RBJ, Tischler TR, Hocknull SA, Cook AG, Barnes DG, Poropat SF, Wooldridge SJ, Sloan T, Sinapius GHK, Elliott DA. 2013.** New *Australovenator* hind limb elements pertaining to the holotype reveal the most complete neovenatorid leg. *PLoS One* **8**: e68649.
- White MA, Cook AG, Hocknull SA, Sloan T, Sinapius GHK, Elliott DA. 2012.** New forearm elements discovered of holotype specimen *Australovenator wintonensis* from Winton, Queensland, Australia. *PLoS One* **7**: e39364.
- Whitlock JA. 2011a.** Inferences of diplodocoid (Sauropoda: Dinosauria) feeding behavior from snout shape and microwear analyses. *PLoS One* **6**: e18304.
- Whitlock JA. 2011b.** A phylogenetic analysis of Diplodocoidea (Saurischia: Sauropoda). *Zoological Journal of the Linnean Society* **161**: 872–915.
- Wilson JA. 1999.** A nomenclature for vertebral laminae in sauropods and other saurischian dinosaurs. *Journal of Vertebrate Paleontology* **19**: 639–653.
- Wilson JA. 2002.** Sauropod dinosaur phylogeny: critique and cladistic analysis. *Zoological Journal of the Linnean Society* **136**: 217–276.
- Wilson JA. 2005.** Redescription of the Mongolian sauropod *Nemegtosaurus mongoliensis* Nowinski (Dinosauria: Saurischia) and comments on Late Cretaceous sauropod diversity. *Journal of Systematic Palaeontology* **3**: 283–318.
- Wilson JA. 2012.** New vertebral laminae and patterns of serial variation in vertebral laminae of sauropod dinosaurs. *Contributions from the Museum of Paleontology, The University of Michigan* **32**: 91–110.
- Wilson JA, Allain R. 2015.** Osteology of *Rebbachisaurus garasbae* Lavocat, 1954, a diplodocoid (Dinosauria, Sauropoda) from the early Late Cretaceous-aged Kem Kem beds of southeastern Morocco. *Journal of Vertebrate Paleontology* **35**: e1000701.
- Wilson JA, D’Emic MD, Curry Rogers KA, Mohabey DM, Sen S. 2009.** Reassessment of the sauropod dinosaur *Jainosaurus* (= “*Antarctosaurus*”) *septentrionalis* from the Upper Cretaceous of India. *Contributions from the Museum of Paleontology, University of Michigan* **32**: 17–40.
- Wilson JA, D’Emic MD, Ikejiri T, Moacdieh EM, Whitlock JA. 2011.** A nomenclature for vertebral fossae in sauropods and other saurischian dinosaurs. *PLoS One* **6**: e17114.
- Wilson JA, Malkani MS, Gingerich PD. 2005.** A sauropod braincase from the Pab Formation (Upper Cretaceous, Maastrichtian) of Balochistan, Pakistan. In: Mohabey DM, ed. *Indian non-marine Late Cretaceous: advances and challenges*. Nagpur: Gondwana Geological Society, 101–109.
- Wilson JA, Mohabey DM. 2006.** A titanosauriform (Dinosauria: Sauropoda) axis from the Lameta Formation (Upper Cretaceous: Maastrichtian) of Nand, central India. *Journal of Vertebrate Paleontology* **26**: 471–479.
- Wilson JA, Pol D, Carvalho AB, Zaher H. 2016.** The skull of the titanosaur *Tapuiasaurus macedoi* (Dinosauria: Sauropoda), a basal titanosaur from the Lower Cretaceous of Brazil. *Zoological Journal of the Linnean Society* **178**: 611–662.
- Wilson JA, Sereno PC. 1998.** Early evolution and higher-level phylogeny of sauropod dinosaurs. *Journal of Vertebrate Paleontology* **18**(sup002): 1–79.
- Wilson JA, Upchurch P. 2009.** Redescription and reassessment of *Euhelopus zdanskyi* (Dinosauria: Sauropoda) from the Early Cretaceous of China. *Journal of Systematic Palaeontology* **7**: 199–239.
- Wiman C. 1929.** Die Kreide-Dinosaurier aus Shantung. *Palaeontologia Sinica (Series C)* **6**: 1–67.
- Windholz GJ, Baiano MA, Bellardini F, Garrido A. 2021.** New Dicraeosauridae (Sauropoda, Diplodocoidea) remains from the La Amarga Formation (Barremian–Aptian, Lower Cretaceous), Neuquén Basin, Patagonia, Argentina. *Cretaceous Research* **117**: 104629.
- Windholz GJ, Coria RA, Zurriaguz VL. 2020.** Vertebral pneumatic structures in the Early Cretaceous sauropod dinosaur *Pilmatueia faundezi* from northwestern Patagonia, Argentina. *Lethaia* **53**: 369–381.
- Witmer LM, Ridgely RC, Dufeu DL, Semones MC. 2008.** Using CT to peer into the past: 3D visualization of the brain and ear regions of birds, crocodiles, and nonavian dinosaurs. In: Endo H, Frey R, eds. *Anatomical imaging: towards a new morphology*. Tokyo: Springer-Verlag, 67–87.
- Xu X, Upchurch P, Mannion PD, Barrett PM, Regalado-Fernandez OR, Mo J, Ma J, Liu H. 2018.** A new Middle Jurassic diplodocoid suggests an earlier dispersal and diversification of sauropod dinosaurs. *Nature Communications* **9**: 2700.
- Zaher H, Pol D, Carvalho AB, Nascimento PM, Riccomini C, Larson P, Juarez-Valieri R, Pires-Domingues R, Silva NJd Jr, Campos Dda. 2011.** A complete skull of an Early Cretaceous sauropod and the evolution of advanced titanosaurians. *PLoS One* **6**: e16663.

SUPPORTING INFORMATION

Additional Supporting Information may be found in the online version of this article at the publisher's web-site:

Appendix. Character additions and score changes.

Figure S1. Site map of AODL 127 (the 'Alex' site).

Figure S2. Strict consensus of the Somphospondyli portion of the 171 072 trees obtained from the equal weights analysis (with ten taxa excluded a priori).

Figure S3. Strict consensus of the Somphospondyli portion of the 9261 trees obtained from the extended implied weights analysis (with eight taxa excluded a priori).

Figure S4. Agreement subtree of the Somphospondyli portion of the extended implied weights analysis.